Design, Synthesis and Functional Studies of Biomolecule Based Coordination Polymers

A Thesis

Submitted in Partial Fulfillment of the Requirements

for the Degree of

Doctor of Philosophy

by

Biplab Joarder

ID: 20103051

Indian Institute of Science Education and Research (IISER), Pune

2015

Dedicated

to my parents

Certificate

Certified that the work described in this thesis entitled "*Design, Synthesis and Functional Studies of Biomolecule Based Coordination Polymers*" submitted by *Mr. Biplab Joarder* was carried out by the candidate, under my supervision. The work presented here or any part of it has not been included in any other thesis submitted previously for the award of any degree or diploma from any other university or institution.

Date: 27th January 2015

Dr. Sujit K. Ghosh
Research Supervisor

Email: sghosh@iiserpune.ac.in | Contact no: +91 (20) 25908076

Declaration

I declare that this written submission represents my ideas in my own words and wherever other's ideas have been included; I have adequately cited and referenced the original sources. I also declare that I have adhered to all principles of academic honesty and integrity and have not misrepresented or fabricated or falsified any idea/data/fact/source in this submission. I understand that violation of the above will result in disciplinary actions by the Institute and can also evoke penal action from the sources, which have thus not been properly cited or from whom appropriate permission has not been taken when needed.

Date: 27th January 2015

Biplab Joarder

ID: 20103051

Acknowledgement

*I am deeply indebted to my research supervisor **Dr. Sujit K. Ghosh**, who guided me and continuously encouraged me in the last five years. With his inspiring guidance, I learnt to design and successfully execute of research projects in a systematic manner. Being one of the first PhD students of his research group, I got the unique opportunity to learn how to set up a new lab from scratch. His diligent effort and training was the stepping stone behind each and every success I achieved, and will undoubtedly remain the prime asset for my future research. I acknowledge Indian Institute of Science Education and Research (IISER), Pune and its director Prof. K. N. Ganesh for providing excellent research facilities and an outstanding research ambiance.*

I am also grateful to the Research Advisory Committee members Dr. Sujit K. Ghosh, Dr. R. Boomishankar and Dr. Pankaj Poddar for their invaluable advices and suggestions provided at every step of my research work.

I am thankful to Dr. Guillaume Rogez, Dr. Jinkui Tang and my dear friend Dr. Rajat Saha for giving me the opportunity to work with them in different collaborative research projects. Because of their suggestions, I gained immense working experience in diverse fields of research which indeed proved very helpful. I am also very thankful to Dr. H. N. Gopi, Dr. M. Jayakannan, Dr. Nirmalya Ballav, Dr. Pinaki Talukdar, Dr. Partha Hazra, Dr. Arnab Mukherjee, Dr. Aloke Das, Dr V. G. Anand and Dr. Sudarshana Mukherjee for their valuable suggestions during my research period. In fact, I owe

heartiest thank to every faculty of IISER-Pune who was always ready to share their knowledge and experience with me.

It was indeed a pleasure to work in such an excellent ambiance, conducive to new learning and gaining proficient wisdom. I also thank Dr. V. S. Rao, registrar at IISER-Pune for his precious support and timely help. I am also indebted to my teachers during graduation days(epecially Dr. Paritosh Biswas and Dr. Suroj Kumar Maity), during Masters period (Kalyani University) and school days for their admirable teaching and engraving the urge to pursue a career in research.

I am grateful to my syngene (A Biocon Company) senior, Dr. Pradipta Sinha and Dr. Sandipan Sarkar for their support during my stay in syngene.

I thank Dr. Umeshareddy Kacherki (deputy librarian) and Anuradha for library support and Ms. Archana for SCXRD. I thank Sachin, Koushik and Abhijeet for IT support. I thank IISER, Pune administrative staff members, especially Mayuresh, Suvarna, Nayana, Tushar, Snehal and Prabhas for their generous support.

It's my pleasure to thank all the lovable and dear members of the team, I belong to; Sanjog, Abhijeet, Biplab (Manna), Partha da, Soumya, Avishek, Aamod, Partha, Arif, Amitosh, Amrit, Yogesh, Samraj, Kriti, Arunava, Kingshuk, Naveen and Shivani, as they always maintained a very lively environment inside lab. An all time running discussion and sharing of experiences helped me to expand the horizon of knowledge and to work as a team member.

I must thank my friends, both seniors and juniors specially; Parthada (Dr. Partha Biswas, assistant professor, Scottish Church College, CU), Anupam da, Abhigyan, Sohini, Sumit, Shukla, Ramya,

Somu, Smita, Moumita, Tanmoy, Soumya, Sagar, Arundhuti, Partha P P, Arindam, Abhishek, Sudeb, Avik, Barun, Gopal, Shyama, Rajkumar, Maidul, Rahi, Sukla, Anant, Sunil, Sandeep, Padma, Wilbee, Pramod, Arvind, Sudeshna, Sayan, Koushik, Amit, Rejaul, Chandra, Amlan da, Bag, Shanku and finally all dear friends from IISER Pune.

I would like to acknowledge my childhood friends (Especially, Suvendu, Animesh, Rajkumar, Palash, Sayan, Shekhar, Priyabrata, Biplab M, Biplab B, Nentu da, Amrita Bubai, Mithu da, Bapi da, Neeta (Sameer Priti), college friends and university friends. Apart from this, I would like to thank some special NCL Pune friends especially, Pati da (Debashis), Avik, Anirudda, Mrinmoy Chini, Shankha, Anirban and Arpan Manna.

I would offer my sincere thanks to Ma'am (Dr. Sudarshana Mukherjee) for her valuable suggestions. My Best wishes to Suvan for a wonderful life ahead.

I am also thankful to all my friends outside IISER Pune for their support and help. It is indeed difficult to name out them all.

No words can ever convey my sense of gratitude felt for my parents (my father; Mr. Bimal Joarder and mother; Mrs. Alpana Joarder), sister (Mrs. Srila Joarder) and brother in low (Dr. Sujoy Barik). It is due to their unconditional trust, timely encouragement, endless patience and unstinting sacrifice; I am able to reach this position. I would like to thank a special person to whom I am really grateful over the time for her unconditional love and caring.

Finally, I am thankful to Council of Scientific and Industrial Research (CSIR), Department of Science and Technology (DST), Government of India, for my research scholarship (CSIR-SRF)

providing requisite financial support during the course of PhD.

Moreover, I would like to thank American Chemical Society (ACS), Royal Society of Chemistry (RSC), John Wiley & Sons, Elsevier Science Ltd., for publishing several research articles produced during the course of my research as well as for giving the permission to reprint the materials under copyright.

Due acknowledgments to them, whose names are unintentionally missed out, despite their unconditional help throughout the last five years.

Yours Biplab

Contents

Contents i

Synopsis iii

Glossary of Acronyms vi

List of Publications viii

1. Introduction of Coordination Polymers 1-13

1.1. History 1
1.2. Porous coordination polymers (PCPs) or metal organic frameworks (MOFs) 2
1.3. Functionalization 7
1.3.a Pre-synthetic functionalization
1.3.b Post synthetic modification
1.4. Metal biomolecule frameworks (MbioFs) 9
1.5. Dynamism in MbioFs 10
1.6. Overview of the thesis 10
1.7. References 11

2. Amino Acid Based Dynamic Metal–Biomolecule Frameworks: An Intriguing Revelation on Dynamism Aspects 14-28

2.1. Introduction 15
2.2. Experimental Section 16
2.2.1 General remarks
2.2.2 Synthesis
2.3. Result and discussions 18
2.4. Conclusion 25
2.5. References 26

3. Investigation of Isosorbide Based Cadmium Carboxylate Framework for Selective Host-Guest Inclusion 29-42

3.1. Introduction 30
3.2. Experimental Section 31
3.2.1 General remarks
3.2.2 Synthesis
3.3. Result and discussions 33
3.4. Conclusion 39
3.5. References 40

4. Amine Decorated Metal-Biomolecule Framework for Selective Sensing of Nitro Explosive 43-58

4.1. Introduction 44

4.2. Experimental Section 46
4.2.1 General remarks
4.2.2 Synthesis
4.3. Result and Discussions 48
4.4. Conclusion 55
4.5. References 55

5. **Dynamic Metal-Organic Framework with π Lewis Acidic Pore Surface Exhibiting Excellent Guest-Responsive Features** 59-73

5.1. Introduction 60
5.2. Experimental Sections 61
5.2.1 Synthesis
5.2.2 General remarks
5.3. Result and Discussions 63
5.4. Conclusion 70
5.5. References 71

Appendix 74-94

Synopsis

The main idea behind this thesis is to develop different functionalized biomolecule based metal biomolecule framework (MbioF) by following a number of synthetic protocols, and to comprehend in-depth structure-property correlation which is absolutely crucial in order to exhibit different application-oriented properties as an outcome of the strategic rationale that encompasses and determines the synthetic methodology designed for producing such materials.

During my PhD tenure, exploration of various functional properties in the domain of biomolecule based metal organic frameworks (MOFs) or coordination polymers (CPs) has taken these polymeric advanced materials to an escalating height. Newly designed biomolecule-based ligands have been used to prepare robust, as well as dynamic metal-organic frameworks of different dimensions, employing transition metal ions under solvothermal and ambient conditions. Consequently, the functional aspects of these MbioFs have been the prime focus behind the development of some target-oriented applications. Nevertheless, a deep insight is indeed required to attain the requisite understanding of the diverse correlation aspects controlling and in a way, single-handedly directing the properties as an outcome of the minute alterations in the structural nature of these materials. This structure-property correlation has been our main guiding principle throughout the work in presented in this thesis, while choosing several biologically important molecules to fervently exploit their intrinsic properties while these eventually constitute the polymeric framework.

Chapter 1. (***Introduction of Coordination Polymers***)

At the very outset, in the first chapter, the history and path-breaking discovery of porous coordination polymers (PCPs) having inimitable adsorption features and their potential applications, by exploiting the designable surface properties and tunable surface area have been briefly discussed. The concept of pre-functionalization of the porous nanospace within the coordination polymer's channels and its consequential effect on host guest interaction has been presented. Finally and intriguingly, the advantages of introducing of biomolecules as ligands / linkers in the preparation of MbioF have been discussed.

Chapter 2. (***Amino Acid Based Dynamic Metal–Biomolecule Frameworks: An Intriguing Revelation on Dynamism Aspects***)

To start with, in second chapter, the syntheses of two isostructural, homochiral Cu^{II} coordination polymers, based on chiral amino acids (d- and l-Pyroglutamic acid), acting as biomolecule components were described. Dynamic behavior evidenced by the solid-state

structural transformations in single-crystal-to-single-crystal fashion was demonstrated in case of MBioF (Figure 1). The extent of structural dynamism was revealed by guest-inclusion studies. (*Chem. Eur. J.* **2013,** *19*, 11178-11183).

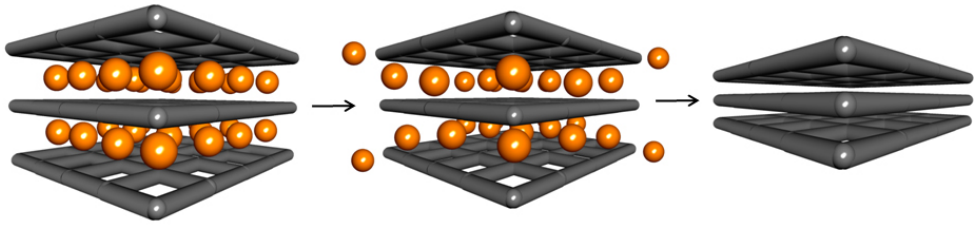

Figure 1. *Schematic representation of dynamic structural transformations of the MBioF*

Chapter 3. (***Investigation of Isosorbide Based Cadmium Carboxylate Framework for Selective Host-Guest Inclusion***)

In the 3rd chapter, we used D-isosorbide (A saccharide molecule) to design one D-isosorbide-based enantiopure dicarboxylic acid ligand, which on complexation with Cd^{II} led to a luminescent homochiral porous MbioF under solvothermal conditions (Figure **2a**). The framework consists of interconnected triple-helical chains (Figure **2b**), very similar to the triple-helical structure of a group of biologically important protein molecules called "collagen". The porous framework showed significant stability even after removal of the guest molecules, and the guest-free phase exhibited size-selective inclusion of H_2O and MeOH over other solvents (*e.g.*, THF, ethanol, benzene, and cyclohexane) inside the channels (*Inorg. Chem.*, **2012,** *51*, 4644-4649).

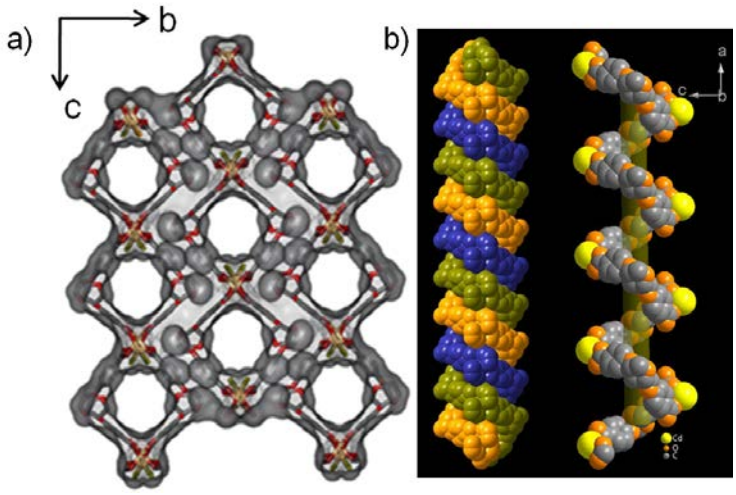

Figure 2. a) *Structural view of the 2D framework of compound **1** along a axis; b) Triple-helical chains of compound **1** (left) and space-filling views of the left handed single-helical chain (right).*

Chapter 4. (***Amine Decorated Metal-Biomolecule Framework for Selective Sensing of Nitro Explosive***)

Moving on to the fourth chapter, we used a very well known adenine (biomolecule) based MbioF and reported the unprecedented selective and sensitive aqueous-phase detection of the nitro explosive 2,4,6-trinitrophenol (TNP). Here we have used the amine-functionality of constituent adenine linker to come across an unsurpassed selective response to TNP by the hydrolytically stable MbioF compound, even in the presence of other nitro compounds in both aqueous phase and organic solution (Figure **3**). (*Chem. Eur. J.* **2014,** *21*, 965 – 969).

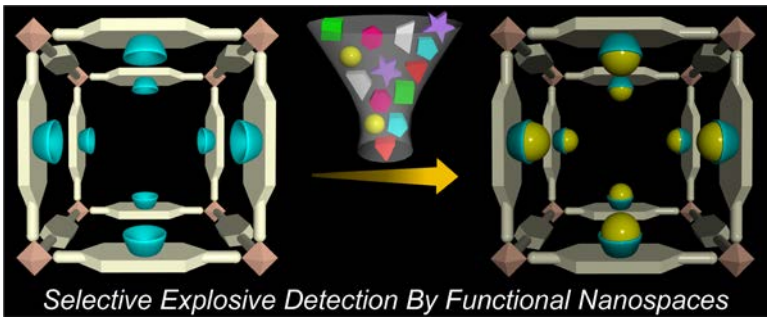

Figure 3. *Schematic representation of selective nitroexplosive sensing by amine decorated nanospace of MOF.*

Chapter 5. (***Dynamic Metal-Organic Framework with π Lewis Acidic Pore Surface Exhibiting Excellent Guest-Responsive Features***)

In the fifth and final chapter, biomolecule alanine-based flexible linker synthesis-design renders it a π-electron-deficient moiety, which was purposefully employed to synthesize a novel dynamic 3D MbioF with electron deficient pore surface, eventually giving rise to unique chemical separation phenomena based on pore surface functionalization and framework flexibility. Especially, the combination of flexible nature and polar surface present in this framework enables it to exhibit selective uptake of benzene over cyclohexane from their mixture, making it a strategically designed guest-responsive material (*Chem. Eur. J.* **2014,** *20*, 15303-15308).

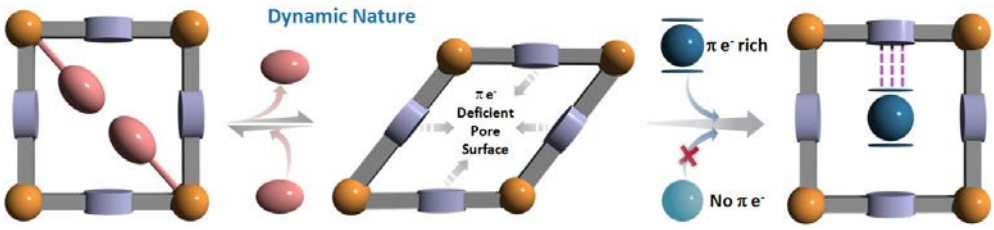

Figure 4. *Schematic representation of guest-responsive function for a dynamic MbioF.*

Glossary of Acronyms

AcOH	Acetic acid
Bio-MOF	Bio-metal organic framework
Anal.	Analysis
Calc	Calculated
CCDC	Cambridge Crystallographic Data Centre
CCD	Charge-coupled device
CD	Circular-dichroism
COF	Covalent organic framework
CP	Coordination polymer
DFT	Density functional theory
DMbioF	Dynamic metal biomolecule framework
DMF	N, N-Dimethyl formamide
DMSO-D6	Dimethyl Sulphoxide
EtOAc	Etayl acetate
EtOH	Ethanol
FE-SEM	Field emission scanning electron microscopy
FT-IR	Fourier transform infra red-spectra
gm	Gram
HOMO	Highest occupied molecular orbital
HR-TEM	High resolution transmission electron microscope
ICP	Infinite coordination particles
LUMO	Lowest unoccupied molecular orbital
MbioF	Metal biomolecule framework
MeCN	Acetonitrile
MeOH	Methanol
Mg	Milligram
MHz	Megahertz
min	Minutes
mL	Milliliter
µL	Micro liter
mM	Micro molar
mmol	Milli moles
MOF	Metal organic framework
NaOMe	Sodium Methoxide
NMR	Nuclear Magnetic Resonance
ORTEP	Oak Ridge Thermal Ellipsoid Program
PAF	Porous aromatic frameworks
PCP	Porous coordination polymer
PGA	Pyroglutamic acid
ppm	Parts per million
PSM	Post synthetic modification
PXRD	Powder X-Ray Diffraction
RT	Room Temperature
Sc-Sc	Single crystal-to-single crystal

SCXRD	Single Crystal X-Ray Diffraction
SV	Stern Volmer
TGA	Thermogravimetric Analysis
THF	Tetrahydrofuran
TMS	Tetramethylsilane
UV	Ultraviolet
TNT	2,4,6-trinitrotoluene
2,4-DNT	2,4-dinitrotoluene
2,6-DNT	2,6-dinitrotoluene
TNP	2,4,6-trinitrophenol
RDX	1,3,5-trinitro-1,3,5-triazacyclohexane
DMNB	2,3-Dimethyl-2,3-dinitrobutane
NM	Nitro-methane

Research Publications

Included in Thesis

1. A Homochiral Luminescent 2D Porous Coordination Polymer with Collagen-Type Triple Helices Showing Selective Guest Inclusion

   Biplab Joarder, Abhijeet K. Chaudhari, and Sujit K. Ghosh
   Inorg. Chem., **2012,** *51*, 4644-4649**.**

2. Amino Acid Based Dynamic Metal–Biomolecule Frameworks

   Biplab Joarder, Abhijeet K. Chaudhari, Sanjog S. Nagarkar, Biplab Manna and Sujit K. Ghosh
   Chem. Eur. J. **2013,** *19*, 11178-11183.

3. Guest-Responsive Function of a Dynamic Metal-Organic Framework with π Lewis Acidic Pore Surface

   Biplab Joarder, Soumya Mukherjee, Abhijeet K. Chaudhari, Aamod V. Desai, Biplab Manna and Sujit K. Ghosh.
   Chem. Eur. J. **2014,** *20*, 15303-15308.

4. Selective and Sensitive Aqueous Phase Detection of TNP (2,4,6-trinitro phenol) by an Amine Functionalized Metal-organic Framework

   Biplab Joarder, Aamod V. Desai, Partha Samanta, Soumya Mukherjee and Sujit K. Ghosh.
   Chem. Eur. J. **2015,** *21*, 965 – 969.

Not included in Thesis

5. Structures and Magnetic Properties of Two Analogous Dy_6 Wheels with Electron-Donation and Withdrawal Effects

   Biplab Joarder, Soumya Mukherjee, Shufang Xue, Jinkui Tang and Sujit K. Ghosh.
   Inorg. Chem. **2014**, *53*, 7554-7560.

6. A carboxylate based dinuclear dysprosium (III) cluster exhibiting slow magnetic relaxation behaviour

   Biplab Joarder, Abhijeet K. Chaudhari, Guillaume Rogez and Sujit K. Ghosh.
   Dalton Trans.**,** **2012**, *41*, 7695–7699.

7. Highly Selective Detection of Nitro-Explosive by a Luminescent Metal-Organic Framework

   Sanjog S. Nagarkar**, Biplab Joarder**, Abhijeet K. Chaudhari, Soumya Mukherjee, and Sujit K. Ghosh
   Angew. Chem. Int. Ed. **2013,** *52*, 2881-2885**.**

8. Dynamic Structural Behavior and Anion-Responsive Tunable Luminescence of a Flexible Cationic Metal–Organic Framework

Biplab Manna, Abhijeet K. Chaudhari, **Biplab Joarder**, Avishek Karmakar, and Sujit K. Ghosh
***Angew. Chem. Int. Ed.* 2013,** *52*, 998-1002.

9. Framework-Flexibility Driven Selective Sorption of p-Xylene over Other Isomers by Dynamic Metal-Organic Framework

   Soumya Mukherjee, **Biplab Joarder**, Biplab Manna, Aamod V. Desai, Abhijeet K. Chaudhari and Sujit K. Ghosh.
   ***Sci. rep. (Nature group),* 2014,** 00, 00. *(DOI:* 10.1038/srep05761*)*

10. Simultaneous Presence of Both Open Metal Sites and Free Functional Organic Sites in a Noncentrosymmetric Dynamic Metal–Organic Framework with Bimodal Catalytic and Sensing Activities

    Rajat Saha, **Biplab Joarder**, Anupam Singha Roy, Sk. Manirul Islam, and Sanjay Kumar
    Chem. Eur. J.* 2013,19*, 16607-16614.

11. Anion-Responsive Tunable Bulk Phase Homochirality and Luminescence of a Cationic Framework

    Biplab Manna, **Biplab Joarder**, Aamod V.Desai, Avishek Karmakar and Sujit K. Ghosh.
    ***Chem. Eur. J.* 2014,** *20*, 12399-12404.

12. Nitrate Bridged "Pseudo Double Propeller" Type Lanthanide (III)- Copper (II)Heterometallic Clusters: Syntheses, Structures, and Magnetic Properties

    Abhijeet K. Chaudhari, **Biplab Joarder**, Eric Rivière, Guillaume Rogez and Sujit K. Ghosh
    ***Inorg. Chem*. 2012**, *51*, 9159-9161.

13. Structural Dynamism and Controlled Chemical Blocking/Unblocking of Active Coordination Space of a Soft Porous Crystal

    Abhijeet K. Chaudhari, Sanjog S. Nagarkar, **Biplab Joarder**, Soumya Mukherjee and Sujit K. Ghosh
    ***Inorg. Chem.* 2013**, *52*, 12784-12789.

14. A Continuous π‑Stacked Starfish Array of Two-Dimensional Luminescent MOF for Detection of Nitro Explosives

    Abhijeet K. Chaudhari, Sanjog S. Nagarkar, **Biplab Joarder**, and Sujit K. Ghosh
    ***Cryst. Growth Des.* 2013**,*13*, 3716-3721.

15. Bi-Porous Metal-Organic Framework with Hydrophilic and Hydrophobic Channels: Selective Gas Sorption and Reversible Iodine Uptake Studies

    Abhijeet K. Chaudhari, Soumya Mukherjee, Sanjog S. Nagarkar, **Biplab Joarder** and Sujit K. Ghosh
    ***CrystEngComm.* 2013,** *14*, 9465-9471**.**

16. Capsule Voided Nanospace Confinement in a π-Stacked Supramolecular Organic Solid

    Abhijeet K. Chaudhari, Amitosh Sharma, Soumya Mukherjee, **Biplab Joarder** and Sujit K. Ghosh

***CrystEngComm,* 2014**, *16*, 4691-4695.

17. Slow Magnetic Relaxation in an Asymmetrically Coupled Heptanuclear Dysprosium(III)-Nickel(II) Architecture

    Soumya Mukherjee , **Biplab Joarder** , Shufang Xue , Jinkui Tang and Sujit K. Ghosh ***Proc. Indian Natl. Sci. Acad.* 2014**, A, *84*, 151-156.

18. A Dynamic Metal-organic Framework with Anion triggered Luminescence Modulation Behaviour

    Avishek Karmakar, Biplab Manna, Aamod V. Desai, **Biplab Joarder**, and Sujit K. Ghosh. ***Inorg. Chem.* 2015**, *53*, 12225−12227.

19. An Amide-Functionalized Dynamic Metal–Organic Framework Exhibiting Visual Colorimetric Anion Exchange and Selective Uptake of Benzene over Cyclohexane

    Avishek Karmakar, Biplab Manna, Aamod V. Desai, **Biplab Joarder**, and Sujit K. Ghosh. ***Chem. Eur. J.* 2015**, *21*, 7071-7076.

20. Exploiting Framework Flexibility of a Metal-Organic Framework for Selective Adsorption of Styrene over Ethylbenzene

    Soumya Mukherjee, **Biplab Joarder**, Aamod V. Desai, Biplab Manna, Rajmani Krishna, Abhijeet K. Chaudhari and Sujit K. Ghosh . ***Inorg. Chem.* 2015**, *53*, (Accepted).

Chapter 1

Introduction of Coordination Polymers

1. Introduction:

1.1. History:

The ubiquitous influence of porous materials has been a key factor for making the new-generation materials indispensable in life for a long time.[1] The development of highly porous solids began to accelerate in the wake of the industrial revolution and flourishing technological achievements in the 19th century. The era of 1950s marked the significant discovery of various procedures to synthesize zeolites which resulted in the prominent development of a whole new family of a wide range of crystalline zeolites possessing uniform porous structures.[2] The development of novel activated carbons simultaneously resulted in amazing advancement of their diverse preparative techniques in the 20th century.[3] These developments of the synthesis or preparation of porous compounds has been systematically and quite exhaustively continued in the 21st century. In the present-day scenario, we use such porous compounds in various situations for several purposes, like purification of water, air, fuel, oil, and so on.[4] The discovery of new porous compounds like porous coordination polymers (PCPs) or metal organic frameworks (MOFs), covalent organic frameworks (COFs), porous aromatic frameworks (PAFs) and porous organic cages (POCs) having unique adsorption properties has opened up numerous promising challenges in front of the scientific community to methodically address diverse scientific and technological/industrial challenges in a rather contemporary systematic manner, by exploiting the designable surface properties and tunable surface area for these materials in the porous domain.[5]

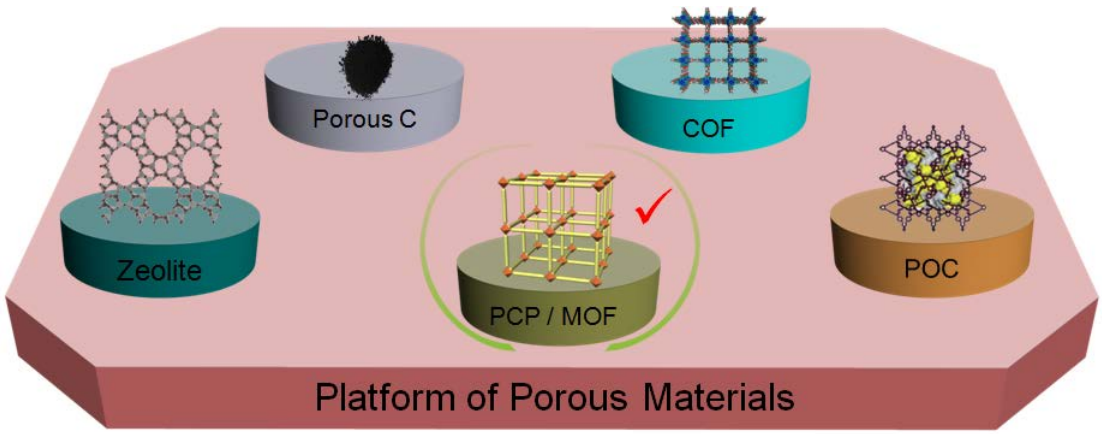

Figure 1.1. *Different types of commonly found Porous Material.*

Among all the mentioned porous materials, the class of porous coordination polymers or metal organic frameworks has emerged as the most promising candidate for the targeted applications over the last decade.[6] In an astoundingly short time, the structural chemistry of coordination polymers has attained an unmatched level. Coordination polymers have now firmly established its pivotal position in the frontiers of advanced functional porous materials.

1.2. Porous coordination polymers (PCPs) or metal organic frameworks (MOFs):

MOFs are solid crystalline materials constituted via self-assembly of single metal cations (primary building unit or PBU) or metal clusters (secondary building unit or SBU) and organic linkers containing multiple binding sites, in order to form one, two, or three dimensional extended coordination networks.[7] Since their discovery, many potential applications have been proposed[8] in strategic domains such as catalysis, separation, storage, chemosensing, magnetism and others.[9] Compared to their organic (carbons) or inorganic counterparts (zeolites, silica), one of the key advantages of MOFs is the facile option to tune their composition through changes in the metal and/or the organic linker.[10]

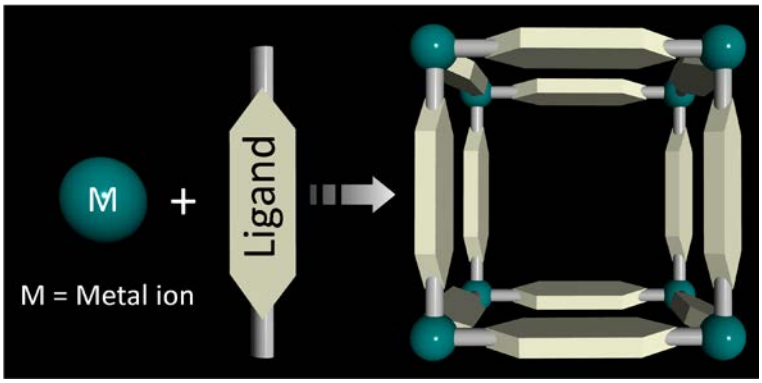

Figure 1.2. *Schematic illustration of construction of the MOF structure.*

The inherent long-range order omnipresent in these substances coupled with the unique tunable nature consequently reflects in a commanding influence on their functional behavior during comprehensive investigation of different application-oriented phenomena. In fact, the range of employed linkers is infinite, ranging from polycarboxylates, phosphonates, sulfonates, imidazolates, amines, pyridyl, phenolates etc. As compared to established regime of zeolite

materials, MOF architectures, possessing much superior chemical versatility exhibit a larger panel of pore sizes, dimensional intricacies and multifarious shapes with characteristic dissimilar sizes (tunnels, cages, etc), with sometimes a flexible porosity which eventually permits to reversibly adapt the pore size to the adsorbate. Functionalization of the organic linker comes up with a definite advantage of MOFs with the opportunity of grafting during or after the synthesis by strategic introduction of distinct organic functionalities (polar and apolar); subsequently resulting in alteration of the physicochemical properties of the solid.[11-16] Some of the potential applications are shown in the following scheme and will be discussed briefly:

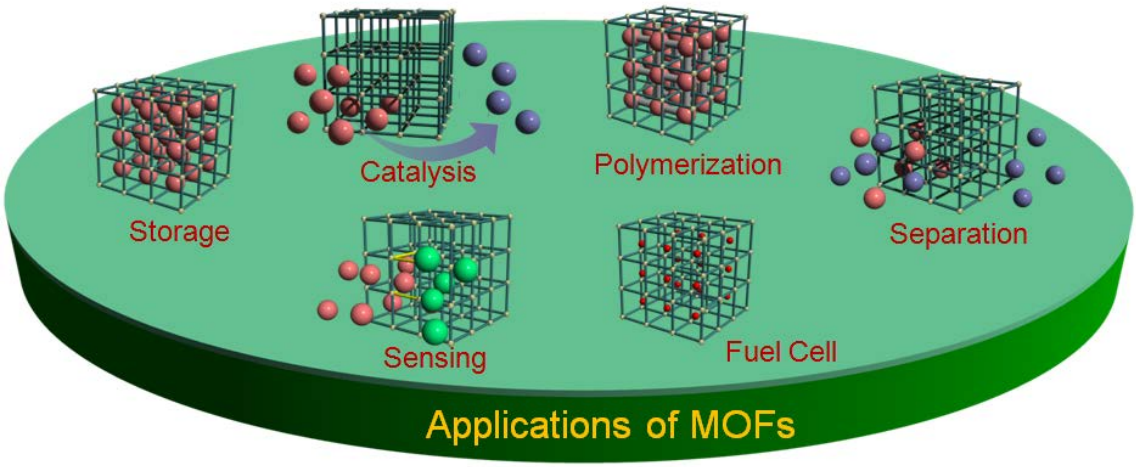

Figure 1.3. *Potential applications of MOFs.*

1.2.1. Gas storage and or separation:

Gas storage and/or separation techniques are recognized to primarily involve cryogenic distillation, membrane-based, and adsorption-based technologies.[17] Right from the path-breaking discovery of synthetic-zeolites in the 1940s, with the simultaneous emergence of various adsorbents and the development of adsorption-based separation processes, adsorption has become a key gas separation tool in industry.[18] With the syntheses of more and more new and improved adsorbent host materials with tailor-made porosity and surface features along with the urgent need for green separation procedures, adsorptive separation has been receiving the foremost importance. Hence, adsorptive separation is likely to play a key role in future energy and environmental technologies. In recent years, MOFs, owing to their stupendously high surface area and functional features allowing site-specific favorable interactions with the guest

adsorbate-species are the most promising candidates for achieving gas separation and/or storage applications.[19,20]

1.2.2. Fuel cell:

Fuel cells are one of the alternative options for energy due to the continuous increase in energy-demand, as well as limited natural energy source. So, researchers are giving attention to increase the efficiency of the fuel cells which can operate over a wide temperature range (T= 25-300 ^{0}C) and display high proton conductivity. In recent years, MOFs have been of immense significance for applications in the fields of hydrogen energy (hydrogen sorption and hydrogen generation), fuel cells, Li-ion rechargeable batteries, supercapacitors and solar cells, because of their excellent crystallinity, tunable porosity and high surface area, which play decisive role in the functional properties . Interestingly, now-a-days MOF as proton conducting materials appears to be at the heart of the fuel cell technology.[21] MOFs exhibit proton conductivity originating from either the inherent framework itself, or by including protonic charge carrier(s) in the pore surface. Proton conducting MOFs are generally classified into two categories: (1) water-assisted proton-conducting MOFs, which operate at low temperature (20–80 ^{0}C), and (2) anhydrous proton conducting MOFs, which work at intermediate temperatures (100–300 ^{0}C).

1.2.3. Polymerization:

One of the exceptional challenges in polymeric materials is the modulation-mediated development of new systems which permit a restricted array of monomers to be arranged and hence polymerized into target-based materials. All polymers existent in nature participating in biological events are basically formed as a result of enzymatic catalysis, where stereoselective, regioselective and chemoselective polymerizations continue within controlled and well-assorted molecular scale spaces. Specific nanospace effects on the reaction kinetics and selectivity of inclusion polymerization processes result out of the controlled structures of these polymers. The polymerization of monomers encapsulated inside the limited and premeditated nanospaces based on PCPs can give rise to polymeric materials with advantageous targeted structures, which can be considered as tailor-made polymerization systems.[22]

1.2.4. Catalysis:

The well-defined pores and channels in MOFs endow them with the prospective of size- and shape-selective catalysis, which is the hallmark of zeolites. The diversity of zeolites, however, is rather limited due to the sole use of SiO_4/AlO_4 tetrahedral building units. The resulting 3D

frameworks of zeolites are mostly microporous with channels/cavities of ~1.0 nm, and as a result, the catalytic applications of zeolites are restricted to relatively small organic molecules. On the contrary, MOFs can be constructed from an inestimable number of building blocks to allow for a organized fine-tuning and strategic modulation of their features. Additionally, the gentle and extremely minute reaction conditions typically employed for MOF syntheses bring about the scopes for direct incorporation of a variety of delicate functionalities into the framework motifs. The capability to fit in different functional groups into the nanospace amidst porous MOFs makes them superb candidates acting as catalysts.[23]

1.2.5. Separation:

In the chemical, petrochemical and pharmaceutical industries, separation technology is a key element behind the production of pure compounds, especially the industrially sought-after monomers. A huge portion of the production expenditures are related to purification steps, for instance using solvent extraction, adsorption, crystallization and energy-intensive distillation processes. At present, distillation accounts for more than 90% of all separation processes in the chemical industry. Because of the reactive nature or the decomposition of certain chemicals and the high costs associated with distillation, viable alternatives are required for a sustainable and energy-environment friendly chemical industry for the days of near future. An adsorbent is able to separate a mixture of chemicals into pure compounds, mostly based on the striking differences in the interactions between that particular adsorbent and the sole constituents of the mixture, sometimes isomeric in nature with extremely close physical properties. In order to realize the challenges associated with separation protocols needed for the next-generation upcoming industries, superior adsorbents are still needed. Certain MOFs which combine high degrees of chemical and thermal stability, large surface areas and tunable surface properties could be precious candidates in this regard. Consequently, well-defined pore size distributions for different adsorbent materials are obtained, making those excellent candidates for liquid phase adsorptive separations.[24]

1.2.6. Sensing:

Last decade onward, a number of investigators have started exploring the MOF materials' potential as chemical sensors. In spite of the necessity of a rather systematic approach to exploit the class of luminescent MOFs, the exceptional feature of tunability for MOF structures and unsurpassed properties has been established to be advantageous over other chemo-sensory

materials. Gas and vapor-phase detection of analytes with high degrees of sensitivity and selectivity for a spectrum of crucial applications including chemical threat detection, industrial process management, food quality control, medical diagnostics, environmental monitoring and occupational safety presents a call of the hour.[25] Since the linkers present in most of the MOF-structures include aromatic moieties which can inherently luminesce/ fluoresce following UV or visible (typically blue) excitation, it is rather anticipated that indeed quite a huge number of MOFs have been found to be photoluminescent. Molecular skeletons for MOFs those are assembled by organic linkers and inorganic nodes can, in fact, present excellent host matrices for molecular decoders. Arising of the intrinsic confinement effect within their nanopores in the concerned nanospace, which increases the framework host–guest interaction and the additional pore surface designability enables the rational incorporation of a fitting decoding component into the scaffold by virtue of strategic organic chemistry during ligand-design step or during post-synthetic modification protocol.[25]

1.3. Functionalization:

By virtue of the organic linker component(s) suitable for introducing multiple chemical moieties/functionalities, present in MOFs, principally the introduction of diverse functional groups into MOFs is much more anticipated when compared to other inorganic solids. Recent years have in fact come up with great deal of success-stories regarding the syntheses of different MOFs with more than one organic linkers, in order to involve a “mixed component” strategy.

There are two ways of chemical modification by which a MOF is rendered a functionalized one.

(a) Pre-synthetic functionalization;(b) Post-synthetic modification.

1.3.1. Pre-synthetic functionalization:

The most sought-after after approach over the years to strategically incorporate functionality in the porous nanospace has been by diverse ligand-design approaches. This involves starting from a basic precursor and rationally functionalizing it by introduction of different pendant groups, like chiral centre(s), flexible node(s), reactive or target-responsive functional moiety.[26] This approach often includes the attachment of pendant groups to the central linker of the parent molecule, such as vinyl group, chiral component(s), stilbene and a number of groups with dissimilar chemical functionalities such as alcohols, ethers, and esters. The principal advantage of this design lies in (1) the certainty of validation for the preconceived application-based properties which are obvious outcome of the functionalized linker, and (2) the relative ease of

characterization for these crystalline materials. Investigation of host-guest interactions can be also well-monitored with superior control and anticipation, owing to the prior definitive knowledge on the linker functionality residing in the porous nanoregime.

1.3.2. Postsynthetic modification:

Postsynthetic methods (PSM) have been heavily used to achieve the chemical modification of many organic and inorganic substrates. In this case, suitably conceived chemical modification is performed on the fabricated MOF material, rather than on the monomeric molecular species, i.e. the actual precursors behind the MOF. Following this procedure, the newly introduced functional groups (and the reaction conditions involved to incorporate those groups) solely need to find appropriate compatibility with the final material, and any incompatibility with the synthetic methods needed to yield the material are carefully circumvented. However, the preparation of predetermined functionalized MOFs has been a rarity indeed, limited by the rigorous solvothermal synthetic methods used to prepare most MOFs. Under commonly adopted solvothermal syntheses protocol, usually the ligands cannot contain functional groups which are thermally labile, result in problematic solubility, or can further coordinate metal ions. In fact, PSM has established itself as the most promising way-out in recent times for investigating new-generation application-oriented properties of synthetically modified MOFs.[27]

The work described in this thesis involves proficient pre-functionalization mediated chemical modification, and there are three different way-outs those have been followed for the

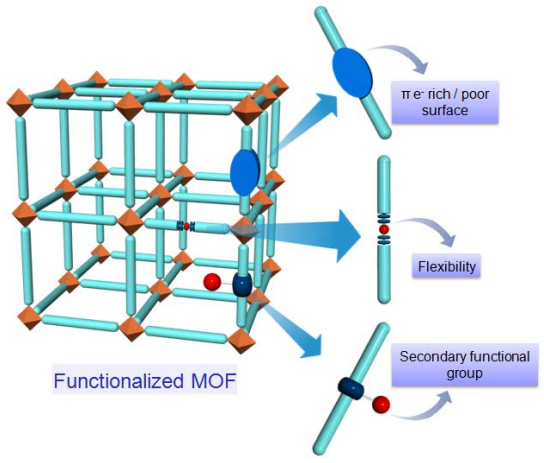

Figure 1.4. *MOF functionalization for proper host guest interactions.*

eventual accomplishment of the target-directed applications of the synthesized porous coordination polymers.

1.4. Metal biomolecule frameworks (MbioFs):

Many prospective applications of MOFs need construction from biomolecule-based building blocks, compatible from biological and environmental standpoints. For example, the majority of biological applications, including site-specific drug delivery or intracellular imaging, would require MOF materials which are non-toxic and non-hazardous in nature. Additionally, several proposed applications will require bulk amounts of MOFs. Easy recyclability and environmental compatibility of the bulk MOF materials are two essential features to reduce their environmental impact. Keeping the focus streamlined enough to address their environmental and biological compatibility, new generations of MOF materials should be designed and synthesized.[28]

In recent years, biomolecules have come up as apt building blocks for constructing Metal–Biomolecule Frameworks (MBioFs). MBioFs are defined as MOFs constituted from at least one biomolecule which serves as an organic ligand. Biomolecules present more than a few advantages as building blocks, which are described as following:[29]

(a) Simple biomolecules, including amino acids, nucleobases, sugars, and others, are easily available in large quantities and at amenable prices for preparing bulk quantities of materials.

(b) Biomolecules can form biologically-compatible MOFs.

(c) Biomolecules are indeed structurally diverse. They can be structurally rigid or flexible. These aspects are the ones having a direct influence on functional nature of the resulting MBioF.

(d) Biomolecules can possess many dissimilar metal-binding sites. As a result, they can exhibit multiple probable coordination modes, a feature that enhances the potential structural diversity of MBioFs.

(e) Inherent self-assembly properties which can be employed to direct the structure-property functional correlation of MBioFs make them an unique class apart in the MOF domain itself.

(f) Finally, quite a few biomolecules are chiral. Therefore, to create chiral MBioFs, which might yield interesting recognition, separation, and catalytic properties involving the chiral biomolecules as synthons seems a clear rationale.

1.5. Dynamism in MbioF:

Dynamic MOFs hold extreme importance because of their unpredictable and intriguing responses towards external stimuli.[31] With the changes of their reactivity-modes, solid-state structural transformations are feasible in such dynamic MOFs. Due to their intrinsic dynamic behaviour, in a short span of time, these type of MOFs have yielded unparalleled exciting properties, like selective and hysteretic sorption, magnetic bistability, reversible photochemical responses, selective sensing, etc.[30d]

Barring only a few reports on rigid MBioFs, the dynamism aspect in MBioFs has not been discovered much until now.[31] Hence, by achieving the amalgamation of dual features namely, biocompatibility coupled with dynamism it should be principally possible to develop dynamic MbioFs (DMBioF), which might turn up with fascinating properties, like soft-giant biomolecules. A dipeptide-linker-based MbioF with adaptable porosity was reported in recent times.[31] The dynamic behavior of the framework was clarified and well-correlated by molecular dynamics simulations, the results of which has presented the manner in which torsions and displacements of the peptides open the pore volume accompanied with guest loading phenomena.[31] Taking into account the flexible nature of biomolecules, MBioFs have excellent prospective to show characteristic signs of dynamic behavior. Importantly enough, the solid-state structural transformation study of DMbioFs by single crystal-to-single crystal mode is an exceedingly significant technique for studying their structure–property correlation. The functional behavior of DMBioFs can be proficiently clarified by this new consolidated approach of providing solid-state structural information of different forms of dynamic frameworks, existent in actuality. Many biologically vital systems, *e.g.* the structure-function correlation of the ribosome, have been elucidated from solid-state structural analyses. But, due to the awfully brittle character of these single crystals, it is intricate to carry out structural studies of dynamic frameworks subsequent to structural transformations, particularly for very soft DMbioFs.

Our primary object in this thesis has been to develop the structure property correlation of different functionalized biomolecule based metal biomolecule framework.

1.6. Overview of the thesis:

In chapter 2, first approach involving amide group employment to attain intensive hydrogen bonding network in plausible metal biomolecule submicron nanostructure in coordination

polymer self assembly as well as effect of hydrophobic interaction on guest inclusion by SC-SC fashion and sorption experiment have been extensively discussed .

Ligand design in incorporation of flexibility within the framework has been carefully dealt with in the following chapter by employing ether nodes in the isosorbide based dicarboxylate linker.

In chapter 4, the hydrolytically stable MbioF has been used for selective and sensitive aqueous phase detection of TNP. The rationale behind the use of the amine functionalized MbioF has been a key factor in such unsurpassed selection response to TNP in aqueous phase.

Finally in our 5th chapter, strategic design in the constitution of π e$^-$ deficient surface of a MOF has been a befitting approach in this chapter to end up with an excellent host-guest responsive phenomenon based on pore favorable electronic interaction with π e$^-$ rich guest species.

1.7. References:

(1) Schüth, F.; Sing, K. S. W.; Weitkamp, J. *Handbook of Porous Solids, Volume 1*; WILEY-VCH: Weingeim, **2002**.

(2) Breck, D. W. *Zeolite Molecular Sieves*; Wiley & Sons: New York, **1984**.

(3) Bruce, D. W.; Hare, D. O.; Walton, R. I. *Porous Materials*; John Wiley & Sons, Ltd **2011**.

(4) Canivet, J.; Fateeva, A.; Guo, Y.; Coasnecd, B.; Farrusseng, D. *Chem. Soc. Rev.*, **2014**, *43*, 5594-5617.

(5) (a) Xu, R.; Pang, W.; Yu, J.; Huo, Q.; Chen, J. *Chemistry of Zeolites and Related Porous Material – Synthesis and Structure*, John Wiley & Sons: Asia, **2007**. (b) Uribe-Romo, F. J.; Hunt, J. R.; Furukawa, H.; Klöck, C.; O'Keeffe, M.; Yaghi, O. M. *J. Am. Chem. Soc.* **2009**, *131*, 4570-4571. (c) Zhang, G.; Presly, O.; White, F.; Oppel, I. M.; Mastalerz, M. *Angew. Chem. Int. Ed.* **2014,** *53*, 1516-1520. (d) Jones, J. T. A.; Hasell, T.; Wu, X.; Bacsa, J.; Jelfs, K. E.; Schmidtmann, M.; Chong, S. Y.; Adams, D. J.; Trewin, A.; Schiffman, F.; Cora, F.; Slater, B.; Steiner, A.; Day, G. M.; Cooper, A. I. *Nature* **2011**, *474*, 367-371.

(6) Tranchemontagne, D. J.; Mendoza-Corte´ s, J. L.; Keeffe, M.; Yaghi, O. M. *Chem. Soc. Rev.*, **2009**, *38*, 1257–1283.

(7) (a) Hagrman, P. J.; Hagrman, D.; Zubieta, J. *Angew. Chem., Int. Ed.* **1999**, *38*, 2638-2684. (b) Robson, R. *J. Chem. Soc., Dalton Trans.* **2000**, 3735-3744. (c) Moulton, B.; Zaworotko, M. J. *Chem. Rev.* **2001**, *101*, 1629-1658. (d) Eddaoudi, M.; Moler, D. B.; LI, H.; Chen, B.; Reineke, T. M.; O'Keeffe, M.; Yaghi, O. M. *Acc. Chem. Res.* **2001**, *34*, 319-330. (e) Yaghi,

O. M.; O'Keeffe, M.; Ockwig, N. W.; Chae, H. K.; Eddaoudi, M.; Kim, J. *Nature* **2003**, *423*, 705-714. (f) Cote, A. P.; Shimizu, G. K. H. *Coord. Chem. Rev.* **2003**, *245*, 49-64. (g) Kim, K. *Chem. Soc. Rev.* **2002**, *31*, 96-107; h) James, S. L. Chem. Soc. Rev. **2003**, *32*, 276-288.

(8) Hoskins, B. F.; Robson, R. *J. Am. Chem. Soc.* **1990**, *112*, 1546.

(9) (a) Special issue on MOF *Chem. Soc. Rev*. **2009**, *38*, 1201–1508. (b) Special issue on MOF *Chem. Rev*. **2012**, *112*, 673-–1268. (c) Special issue on MOF *Chem. Soc. Rev*. **2014**, *43*, 5866 – 6172.

(10) (a) Ferey, G.; Serre, C. *Chem. Soc. Rev*. **2009**, *38*, 1380-1399. (b) Horcajada, P.; Gref, R.; Baati, T.; Allan, P. K.; Maurin, G.; Couvreur, P.; Ferey, G.; Morris, R. E.; Serre, C. *Chem. Rev*. **2012**, *112*, 1232-1268.

(11) (a) Eddaoudi, M.; Kim, J.; Rosi, N.; Vodak, D.; Wachter, J.; O'Keeffe, M.; Yaghi, O. M. *Science* **2002**, *295*, 469-472.

(12) Li, J.-R.; Tao, Y.; Yu, Q.; Bu, X.-H.; Sakamoto, H.; Kitagawa, S. *Chem. Eur. J.* **2008**, *14*, 2771-2776.

(13) Devic, T.; Horcajada, P.; Serre, C.; Salles, F.; Maurin, G.; Moulin, B.; Heurtaux, D.; Clet, G.; Vimont, A.; Gren_eche, J.-M.; Le Ouay, B.; Moreau, F.; Magnier, E.; Filinchuk, Y.; Marrot, J.; Lavalley, J.-C.; Daturi, M.; Ferey, G. *J. Am. Chem. Soc.* **2010**, *132*, 1127-1136.

(14) Wang, Z.; Tanabe, K. K.; Cohen, S. M. *Inorg. Chem,*. **2009**, *48*, 296-306.

(15) Kaye, S. S.; Long, J. R. *J. Am. Chem. Soc*. **2008**, *130*, 806-807.

(16) Hwang, Y. K.; Hong, D.-Y.; Chang, J. S.; Jhung, S. H; Seo, Y.-K; Kim, J.; Vimont, A.; Daturi, M.; Serre, C.; Ferey, G. *Angew. Chem., Int. Ed.* **2008**, *47*, 4144-4148.

(17) King, C. J. *Separation Progress*, McGraw-Hill, New York, *2nd edn*, **1980**.

(18) Rouquerol, F.; Rouquerol, I.; Sing, K. *Adsorption by Powders and Porous Solids- rinciples Methodology and Applications*, Academic Press, London, **1999**.

(19) Li, J. -R.; Kuppler, R. J.; Zhou, H. -C. *Chem. Soc. Rev.*, **2009**, *38*, 1477–1504.

(20) Li, J. -R.; Sculley, J.; Zhou, H. -C. *Chem. Rev*. **2012**, *112*, 869–932.

(21) Ramaswamy, P.; Wong. N. E.; Shimizu, G. K. H. *Chem. Soc. Rev.*, **2014**, *43*, 5913-5932.

(22) Uemura, T.; Yanaia, N.; Kitagawa, S. *Chem. Soc. Rev.*, **2009**, *38*, 1228–1236.

(23) Yoon, M.; Srirambalaji, R.; Kim, K. *Chem. Rev*. **2012**, *112*, 1196–1231.

(24) Voorde, B. V.; Bueken, B.; Denayer, J.; Vos, D. D. *Chem. Soc. Rev.*, **2014**, *43*, 5766-5788.

(25) Hu, Z.; Deibert, B. J.; Li, J. *Chem. Soc. Rev.*, **2014**, *43*, 5815-5840.

(26) Kiang, Y.-H.; Gardner, G. B.; Lee, S.; Xu, Z.; Lobkovsky, E. B. *J. Am. Chem. Soc*. **1999**, *121*, 8204-8215.

(27) Cohen, S. M. *Chem. Rev*. **2012**, *112*, 970–1000.

(28) (a) Gould, J. A.; Jones, J. T. A.; Bacsa, J.; Khimyak, Y. Z.; Rosseinsky, M. J. *Chem. Commun*. **2010**, *46*, 2793–2795. (b) An, J.; Geib, S. J.; Rosi, N. L. *J. Am. Chem. Soc*. **2009**, *131*, 8376–8377.

(29) Imaz, I.; Rubio, -M. M.; An, J.; Sole,-F. I.; Rosi, N. L.; Maspoch, D. *Chem. Commun*.**2011**, ***47***, 7287-7302.

(30) (a) Bradshaw, D.; Warren, J. E.; Rosseinsky, M. J. *Science* **2007**, 315, 977-980. (b) Zhang, J.-P.; Chen, X. -M. *J. Am. Chem. Soc*. **2008**, *130*, 6010–6017. (c) Chen, C. -L.; Beatty, A. M. *J. Am. Chem. Soc*. **2008**, *130*, 17222–17223. (d) Horike, S.; Shimomura, S.; Kitagawa, S. *Nat. Chem*. **2009**, *1*, 695-704. (e) Platero-Prats, A. E.; Shea, V. A. de la Pena'O.; Snejko, N.; Monge, A.; Gutierrez-Puebla, E. *Chem. Eur. J.* **2010**, *16*, 11632 – 11640. (f) Park, H. J.; Lim, D.-W.; Yang, W. S.; Oh, T. -R.; Suh, M. P. *Chem. Eur. J*. **2011**, *17*, 7251–7260.

(31) Rabone, J.; Yue, Y.-F.; Chong, S. Y.; Stylianou, K. C.; Bacsa, J.; Bradshaw, D.; Darling, G. R.; Berry, N. G.; Khimyak, Y. Z.; Ganin, A. Y.; Wiper, P.; Claridge, J. B.; Rosseinsky, M. J. *Science* **2010**, *329*, 1053-1057.

Chapter 2

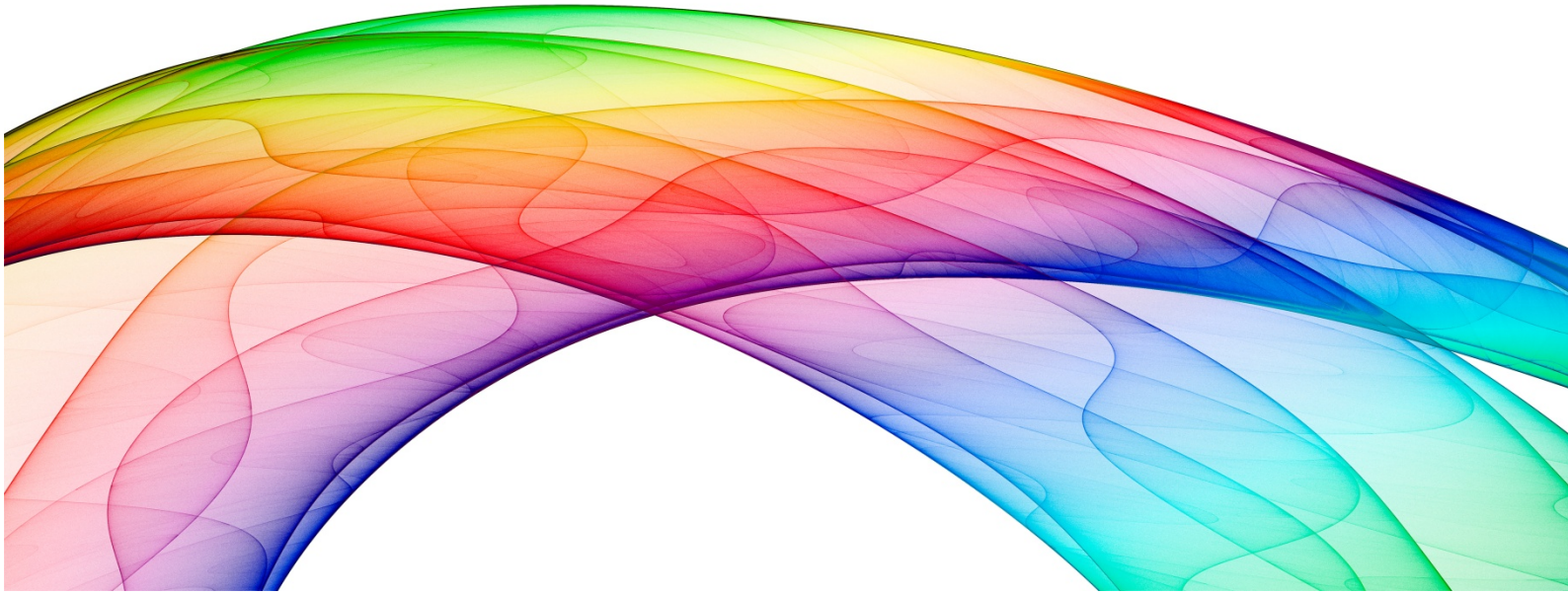

Amino Acid Based Dynamic Metal-Biomolecule Frameworks: An Intriguing Revelation on Dynamism Aspects

2.1. Introduction:

Metal–organic frameworks (MOFs) or porous coordination polymers (PCPs) are gaining more importance due to the versatility of their structural design and enormous potential applications in the field of materials science. Many highly porous rigid MOFs have been reported for gas storage, chemical separation, catalysis, sensing, etc.[1] Apart from these rigid MOFs, dynamic MOFs are of extreme importance due to their variable responses towards external stimuli.[2] These dynamic MOFs are also regarded as soft porous crystals.[2g] Solid-state structural transformations are possible in such dynamic MOF structures with changes in their modes of reactivity.[3] These are the porous materials of advanced generation. Owing to their dynamic nature, these type of MOFs have yielded unique interesting properties, like selective and hysteretic sorption, magnetic bistability, reversible photochemical responses, selective sensing, etc.[2g]

MOFs synthesized from biomolecular linkers, termed metal–biomolecule frameworks (MBioFs) are receiving increasing attention, owing to their biocompatible nature and low environmental impact.[1d, 4–8] The use of biomolecules has many advantages, like easy availability, structural and functional diversity, self-assembly, and most importantly, multiple coordination modes.[5] In this regard, biologically essential amino acids, peptides, nucleobases and carbohydrates have gained immense importance in coordination chemistry due to their strong metal-coordinating tendency with their available donor sites.[4, 5] Especially, amino acids are excellent candidates to be used as linkers, because of their various coordination modes via carboxylate and amine functionalities. Different amino-acid-derived materials reported in the literature have played helpful roles behind understanding their reactivity towards various metal ions and their framework-formation abilities. The MBioFs also offer unique properties, like drug delivery, storage and delivery of gasotransmitter gases and bioimaging.[8]

Although there are some reports of rigid MBioFs, the dynamism in MBioFs has not been explored much so far. So, combining biocompatibility with dynamism should lead to dynamic DMBioFs with interesting properties, like soft-giant biomolecules. Very recently, a dipeptide-linker-based MbioF with adaptable porosity was reported.[6] The dynamic behavior of the framework was explained by molecular dynamics simulations, with which it was shown how torsions and displacements of the peptides opened the pore volume with guest loading.[6] Considering the flexible nature of biomolecules, MBioFs present good potential to exhibit

dynamic behavior. In this regard, the solid-state structural transformation study of DMbioFs by single crystal-to-single crystal (SC-SC) fashion is a very important technique for studying their structure–property correlation. Solid-state structural information on different forms of dynamic frameworks can explain their functional behavior. Many important biological systems, like the structure and function of ribosome, have been explained from solid-state structural analysis. But, due to the very fragile nature of single crystals, it is difficult to perform structural studies of dynamic frameworks accompanying structural transformations, especially for very soft DMbioFs.

In this chapter, we report two isostructural D- and L-pyroglutamic-acid and Cu^{II}-based MBioFs and studies related to their dynamic behavior (***Scheme 2.1***).

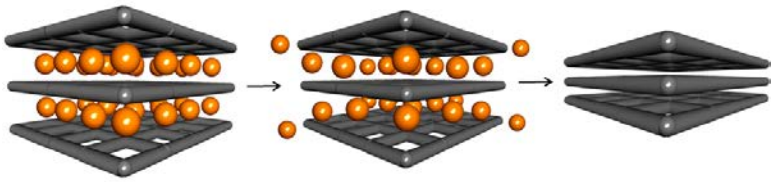

Scheme 2.1. *Schematic representation presenting dynamic structural transformations of the DMBioF (spheres represent guest molecules).*

2.2. Experimental Section:

2.2.1. General remarks:

2.2.1.1. Materials: All the reagents and solvents were commercially available and used without further purification.

2.2.1.2. Physical measurements: Powder X-ray diffraction (PXRD) patterns were measured on Bruker D8 Advanced X-Ray diffractometer at room temperature using Cu-Kα radiation (λ= 1.5406 Å) with a scan speed of 0.5° min^{-1} and a step size of 0.01° in 2 *theta*. Thermogravimetric analyses (TGA) was obtained in the temperature range of 30-600 ºC on Perkin-Elmer STA 6000 analyzer under a N_2 atmosphere at a heating rate of 10 ºC min, The Fourier transform (FT-IR) infra red-spectra ware recorded on NICOLET 6700 FT-IR Spectrophotometer using KBr Pellets. Solid state circular-dichroism (CD) spectra were measured in JASCO J815 spectrometer from 600 nm – 200 nm. The structure and morphology of the gel samples were characterized using a high resolution transmission electron microscope (HR-TEM) JEOL model 1200 EX instrument operated at an accelerating voltage of 120 kV and Field emission scanning electron microscopy

(FE-SEM). Transmission electron microscopy (TEM) samples were prepared by placing a drop of the gel sample well dispersed in acetonitrile onto a carbon-coated Cu grid (3 nm thick, deposited on a commercial copper grid for electron microscope), dried overnight in air, and was loaded into the electron microscopic chamber. FE-SEM samples were prepared by placing a drop of the gel sample well dispersed in acetonitrile onto a silicon wafer, dried in air for overnight, and were loaded into the electron microscopic chamber.

2.2.1.3. X-ray Structural Studies: Single-crystal X-ray data were collected at 200 K on a Bruker KAPPA APEX II CCD Duo diffractometer (operated at 1500 W power: 50 kV, 30 mA) with graphite-monochromated Mo Kα radiation (λ = 0.71073 Å). Crystals were placed on nylon Cryo-Loops (Hampton Research) with Paraton-N (Hampton Research). The data integration and reduction were processed with SAINT[9] software. A multi-scan absorption correction was applied to the collected reflections. The structures were solved by direct method using SHELXTL[10] and was refined on F^2 by full matrix least-squares technique using the SHELXL-97[11] program package within the WINGX[12] programme. All non-hydrogen atoms were refined anisotropically. All hydrogen atoms were located in successive difference Fourier maps and they were treated as riding atoms using SHELXL default parameters. The structures were examined using the *Adsym* subroutine of PLATON,[13] to assure that no additional symmetry could be applied to the models.

2.2.1.4. Low Pressure Sorption Measurements: Low pressure gas sorption measurements were performed using BelSorpmax (Bel Japan). All of the gases used were of 99.999% purity. As-synthesized compound was heated at 150 °C under vacuum for 3 hrs to get guest free compound **1h** and **2h**. Prior to adsorption measurement the guest free samples **1h** and **2h** ware pretreated at 120 °C under vacuum for 2 hrs using Bel-PrepvacII and purged with N_2 on cooling.

2.2.2. Synthesis:

2.2.2.a. Synthesis of $\{[Cu_2(L\text{-}PGA)_4]\cdot 4CH_3CN\}_n$ (1): L-pyroglutamic acid (L-PGA) (161.40 mg, 1.25 mmol) was taken in 15 mL of methanol and 10 mL acetonitrile mixture in a 50 mL conical flask. To this solution, sodium hydroxide (50 mg, 1.25mmol) was added for deprotonation. This mixture was sonicated for 2 minutes and to this, 2 mL methanolic solution of $Cu(NO_3)_2\cdot 3H_2O$ (120.2mg, 0.5 mmol) was added. Furthermore the mixture was sonicated for 1 min, and kept in undisturbed condition. After two days fully grown blue colored rod shaped crystals suitable for single crystal X-ray diffraction study were obtained.

2.2.2.b. Synthesis of $\{[Cu_2(D\text{-}PGA)_4]\cdot 4CH_3CN\}_n$ (2): Compound **2** was synthesized by using same method as for **1**, but using D-pyroglutamic acid (D-PGA) instead of L-pyroglutamic acid (L-PGA). Similarly after two days blue rod shaped crystal suitable for single-crystal X-ray diffraction study grew steadily.

2.2.2.c. Synthesis of $\{[Cu_8(L\text{-}PGA)_{16}]\}_n$ (1a): Compound **1** was taken out from the mother liquor, and allowed to stand at room temperature for a day in N_2 atmosphere. Compound **1** loses the non-coordinated acetonitrile molecules, upon taking out from the solution and transformed to compound **1a**. Suitable crystal was found for single-crystal X-ray diffraction study.

2.2.2.d. Synthesis of metallogel (1-8): When L-pyroglutamic acid (L-PGA) (161.40 mg, 1.25 mmol) and sodium hydroxide (50 mg, 1.25mmol) were allowed to react with $Cu(NO_3)_2$ (60.1mg, 0.25 mmol) in methanol/MeCN (2:1, 3 mL); a darkish blue colored solution formed immediately, which on sonication for about 10 minutes, gave a transparent gel (**1**) (**Appendix 2.4**). Similarly, gel **2-4** synthesized using $CuCl_2\cdot 2H_2O$ and $Cu(ClO_4)_2\cdot 6H_2O$ and $CuSO_4\cdot 5H_2O$ instead of $Cu(NO_3)_2\cdot 3H_2O$ and gel **5-8** were synthesized by using D-pyroglutamic acid (D-PGA) instead of L-pyroglutamic acid (L-PGA) with $Cu(NO_3)_2$, $CuCl_2$, $Cu(ClO_4)_2$ and $CuSO_4$ respectively (**Appendix 2.5**).

2.3. Result and discussions:

Both compounds **1** and **2** showed selective guest inclusion based on the hydrophobic and hydrophilic nature of the pore channels and guest molecules. Structure–property correlation studies were shown by the solid-state characterization of porous and nonporous phases of one DMbioFs. Both compounds also form metallogels under very similar reaction conditions, at room temperature. Interestingly, metallogel formation is found to be very sensitive to the metal/ligand concentration ratio and reveals concentration-dependent reversible sol-gel formation. Cu^{II} salts of different anions (NO_3^-, Cl^-, ClO_4^- and SO_4^{2-}) formed similar metallogels with fibrous networks but each having different patterns.

The DMBioF $\{[Cu_2(L\text{-}PGA)_4]\cdot 4CH_3CN\}_n$ (**1**) was obtained as blue crystals by treating L-PGA, $Cu(NO_3)_2\cdot 3H_2O$ and sodium hydroxide in MeOH/MeCN (MeOH=methanol, MeCN=acetonitrile) at room temperature (**Appendix 2.1**). Single-crystal X-ray diffraction (SC-XRD) analysis revealed that the compound crystallizes in orthorhombic crystal system with chiral space group $P22_12_1$ and flack parameter +0.034. The asymmetric unit of **1** consists of two

copper(II) and four PGA ligands forming a paddle-wheel unit. The two paddlewheel units are attached together via the PGA ligand in head-to-tail fashion to form a tetranuclear subunit. The tetranuclear subunit is further connected with another tetranuclear subunit through PGA ligand to extend the network (**Figure 2.1**), which results in the formation of a left-handed helix (**Figure 2.1.d**). The 1D helix chains are connected from both sides via the PGA moiety, and

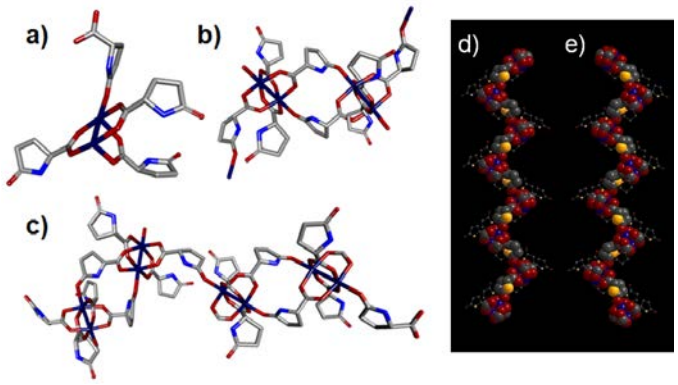

Figure 2.1. (*a) Asymmetric unit of the compound **1**; (b) Tetranuclear unit formed by two binuclear Cu units through two PGA ligands in head and tail fashion; and (c) view of two tetranuclear units connected via one PGA moiety. (Copper: navy blue; Carbon: grey; Nitrogen: blue; Oxygen; red. Hydrogen atoms and disordered solvents are omitted for clarity); (d) and (e) two types for helical chains of **1** and **2**.*

form an extended 2D network. (**Figure 2.2**). The resultant 2D framework is porous and forms 1D channel along the *a* axis (**Figure 2.3**), which is filled with disordered MeCN molecules. PLATON analysis revealed that the 2D porous structure was composed of large voids of 1282.9 $Å^3$, which represents 37.2% per unit cell volume.[14] It is clear (see **Appendix 2.2**), that along the

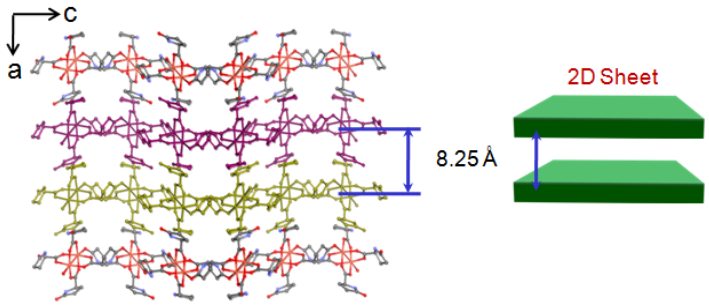

Figure 2.2. *Perspective view of the 2D framework of compound **1** along b axis.*

b axis, the 2D sheets form two different types of channels: channel A, surrounded by methylene groups of PGA ligands, being hydrophobic in nature, and channel B with carbonyl groups of

PGA ligand, aligned towards the channel and with a hydrophilic nature. These channels are filled with disordered MeCN molecules.

The crystals of DMBioF **1** release MeCN guest molecules when kept in air, and undergo drastic structural transformation along one axis from porous homochiral **1** phase to 2D dense homochiral phase $[Cu_8(L\text{-}PGA)_{16}]_n$ (**Figure 2.3**). At the same time, along another axis the

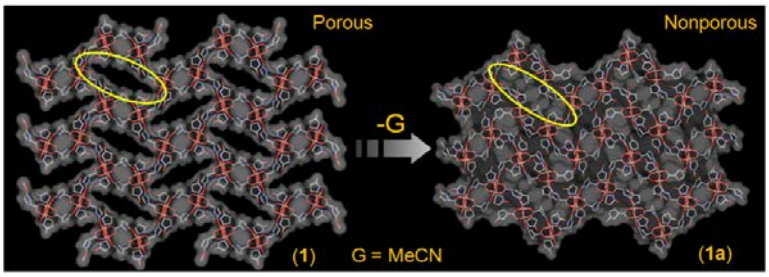

Figure 2.3. *Surface view of the compounds showing transformation of porous MBioF **1** to nonporous MBioF **1a**.*

compound shows structural transformation from a bi- to triporous framework (**Figure 2.4**). This SC-SC structural transformation is due to the slippage of 2D layers with respect to each other upon guest removal. SC-XRD analysis also confirms the structural transformation from **1** to **1a**, with change in crystal system from orthorhombic to monoclinic. PLATON analysis of **1a** revealed that the resultant 2D framework underwent shrinkage compared to **1**, after losing

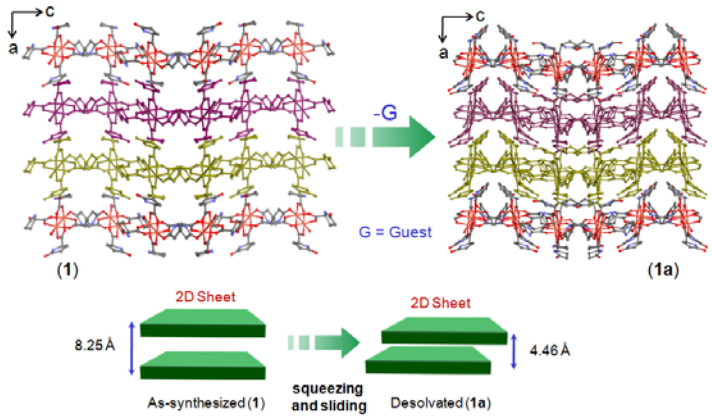

Figure 2.4. *Structural transformation where ABABA-type channels of **1** changed to ABCBA-type channels in **1a**.*

solvent molecules (void volume of 689.7 $Å^3$, 12.8% per unit cell volume). After the release of guest molecules, the framework became squeezed, and as the structural change ABABA-type

channels of **1** changed to ABCBA-type channels in **1a** (**Appendix 2.2**). Isostructural DMBioF $\{[Cu_2(D\text{-}PGA)_4]\cdot 4CH_3CN\}_n$ (**2**) was also obtained with space group $P2_12_12$ and flack parameter -0.006, when D-PGA was used instead of L-PGA, which consists of a right-handed helix. Compound **2** also showed dynamic behavior but unfortunately a desolvated structure could not be obtained even after several attempts due to its characteristic poor crystallinity.

Thermogravimetric analysis (TGA) data under N_2 atmosphere indicate that compounds **1**

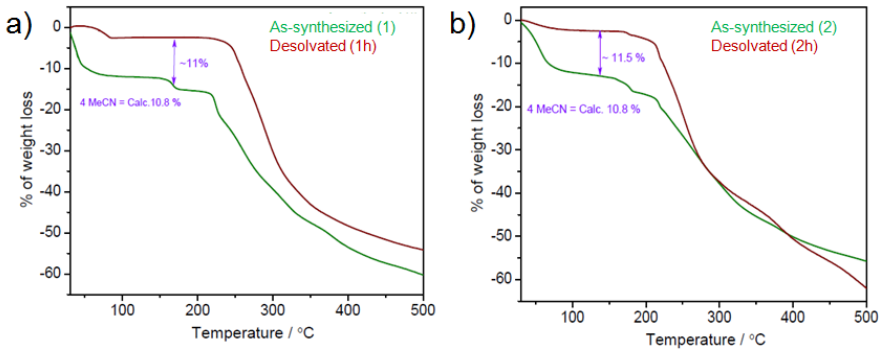

Figure 2.5. (a) *Thermogravimetric analysis (TGA) data for the as-synthesized (**1**; blue color) and de-solvated after 150°C (**1h;** wine red color) compounds;* b) *Thermogravimetric analysis (TGA) data for the as-synthesized (**2**; blue color) and de-solvated after 150°C (**2h;** wine red color) compounds.*

and **2** are stable up to 250 °C with approximately 10% weight-loss, which corresponds to four MeCN molecules present in the pore (**Figure 2.5**). Time dependent powder X-ray diffraction

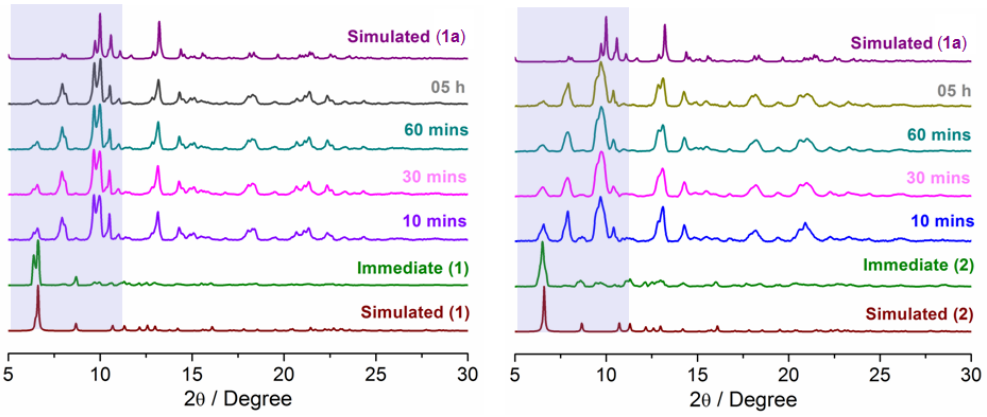

Figure 2.6. *Powder X-ray diffraction (PXRD) patterns of compound **1** (left) and **2** (right), on several time intervals.*

(PXRD) was carried out for **1** and **2,** which revealed that both compounds loose free MeCN molecules, even at room temperature. The PXRD pattern of **1** changed over time and finally

matched the simulated PXRD of compound **1a** (**Figure 2.6**). Similar structural transformations were obtained for DMBioF **2** to **2a** (**Figure 2.6**).

As mentioned above, compounds **1** and **2** crystallize in chiral space groups $P22_12_1$ and $P2_12_12$ with flack parameters of +0.034 and -0.006, respectively. Therefore, to confirm the enantiopure nature of the bulk compounds (**1** and **2**), solid state circular-dichroism (CD) spectral measurements were performed. The bulk crystals of compound **1** showed a positive Cotton effect at 211 nm, whereas the bulk crystals of compound **2** showed the opposite Cotton effect at the same wavelength. These chiral features originate from the parent chiral ligand to the framework, which were also confirmed by the CD spectra, as in both cases ligands and complexes have the similar Cotton effects (**Figure 2.7**). The significant blue-shift in the Cotton effect is due to the amide and/ or carboxylate to Cu^{II} charge transfer.[15]

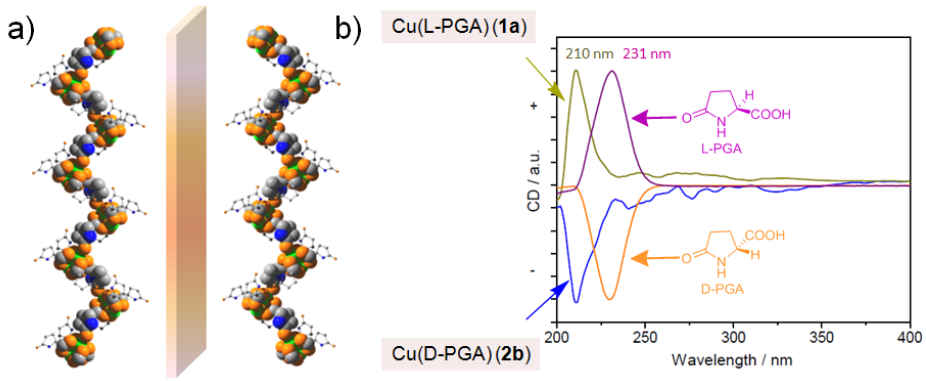

Figure 2.7. (a) *Two types of helical chains of **1** (left) and **2** (right) with mirror symmetry; (b) CD spectra of the ligands and homochiral samples at room temperature.*

To explore the dynamic behavior of the 2D frameworks, gas and solvent sorption measurements were carried out. Both compounds **1** and **2** were heated at 150 °C for 3 h before adsorption measurement to obtain guest-free phase **1h** and **2h**, respectively (h=heated form). The adsorption isotherms for N_2 (kinetic diameter =3.6 Å) and CO_2 (kinetic diameter=3.3 Å) reveal no uptake at 77 and 195 K, respectively (**Figure 2.8**); this indicates that N_2 and CO_2 molecules cannot open the channels of the desolvated phase **1h**. We also examined the solvent sorption properties of **1h** and **2h** at 298 K. The MeCN sorption isotherm indicates continuous opening of the closed channels of the frameworks, with increasing pressure. The sorption amount of MeCN molecules was found to be 47.22 and 22.76 mL g^{-1} for **1h** and **2h**, respectively, which correspond

to 2.96 and 1.42 MeCN molecules per formula unit (**Figure 2.9**). These values are lower than the actual number of MeCN molecules (4MeCN molecules per formula unit) accommodated in the as-synthesized frameworks **1** and **2**. Surprisingly, EtOH with three non-hydrogen atoms, like MeCN and of similar size (kinetic diameter of EtOH=4.3–4.53 Å and MeCN=4.3 Å),[16] failed to enter

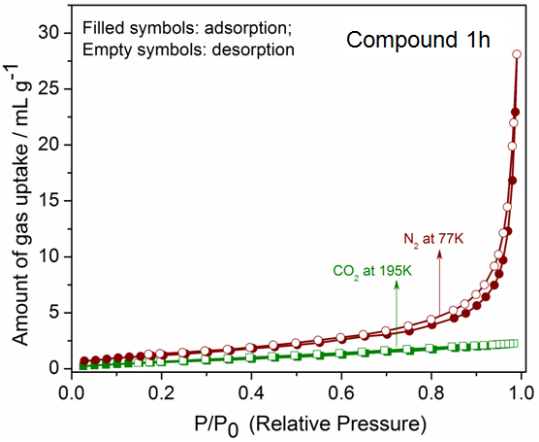

Figure 2.8. *CO_2 (blue color) and N_2 (wine color) sorption isotherms of compound **1h** at 195K and 77K respectively.*

into the channels. Compound **1h** was also exposed to MeCN at room temperature for 3 days; the PXRD patterns of **1h** and the MeCN-exposed sample suggest that once the guest molecules of

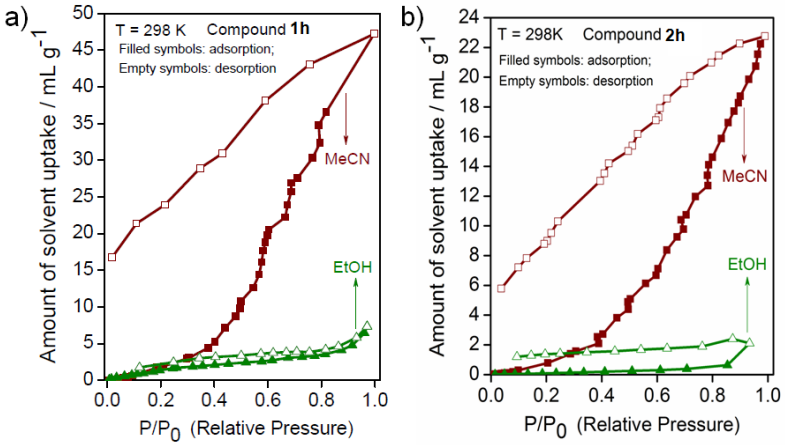

Figure 2.9. *Sorption curves for MeCN (squares) and EtOH (triangles) for **1h** (a) and **2h** (b) at 298 K; filled symbols: adsorption; empty symbols: desorption.*

the as-synthesized phase gets released, it does not return to the original framework (**Appendix 2.3**). As compared to **2h**, **1h** came up with almost double sorption-amount for guest MeCN; this

may be due to the difference of their dynamic nature, originating from the difference in their structures at the chiral centers of the framework backbone (**Figure 2.9**).

The framework of compound **1a** has three different types of channels (channel A, B and C). Channel A is hydrophilic in nature with carbonyl groups of the PGA ligands lining the walls and is nonporous. On the other hand, porous channel B has hydrophobic methylene groups of PGA ligands surrounding the channel, imparting hydrophobic nature to it. MeCN is more hydrophobic than EtOH and could open the closed framework, but the relatively hydrophilic EtOH could not. In spite of this fact, **1h** and **2h** showed different amounts of MeCN uptake. This may be due to unequal rates of opening of the channels, and indicates that the framework dynamism is Indeed related related to the chiral nature of the framework.

The development of infinite coordination particles (ICPs) are also of great interest for material scientists, due to their applications in magnetism, porosity, ion exchange, optical properties, encapsulating matrices, etc.[5,8,17,18] Importantly, coordination-polymer-based nanostructures, like nanofibers, are efficient in light harvesting purposes and could give rise to new electronically, optically and biologically active materials.[8,17,18] Specially for biological applications, use of biomolecules as building units can be a good approach. During the synthesis of compounds **1** and **2**, we observed that both D- and L-PGA ligands form nanofibers in the form of gels.[8,17,18] Gel formation was confirmed by tube-inversion method (**Figure 2.10**).

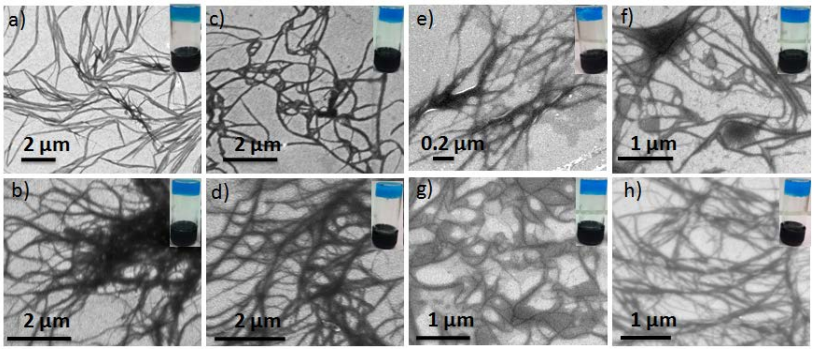

Figure 2.10. *SEM images of metallogels formed from different Cu^{II} salts and PGA ligand. (a) Gel **1** [L-PGA+Cu $(NO_3)_2$]; (b) gel **2** [L-PGA+$CuCl_2$]; (c) gel **3** [L-PGA+$Cu(ClO_4)_2$]; (d) gel **4** [L-PGA+$CuSO_4$]; (e) gel **5** [D-PGA+$Cu(NO_3)_2$]; (f) gel **6** [D-PGA+$CuCl_2$]; (g) gel **7** [D-PGA+$Cu(ClO_4)_2$]; (h) gel **8** [D-PGA+$CuSO_4$].*

Transmission electron microscopy (TEM) and field emission scanning electron microscopy (FE-SEM) were used to examine the morphology of the gel samples, which showed fibrous network structures (**Figure 2.10** and **Appendix 2.7**). The nanofibers are relatively

uniform and have a cross-sectional diameter of approximately 60–70 nm. Similar reactions with Cu^{II} salts of different anions (NO_3^-, Cl^-, ClO_4^- and SO_4^{2-}) form similar gels. Interestingly, we observed that with changing anions, we could tune the fiber morphologies as confirmed from the SEM images (**Figure 2.10**). PXRD patterns confirmed that the xerogels (dried forms of the gels) are highly crystalline materials (**Appendix 2.6**). CD spectra revealed that the nanofibers are chiral in nature and show two opposite types of Cotton effect for the L- and D-PGA gels (**Appendix 2.8**). The CD spectra of the gels are similar to the corresponding ligands and crystalline materials (**1** and **2**), and therefore confirm the chiral coordination spheres of the metal ions present in the nanofibers (**Appendix 2.8**). The observed band in the 208–213 nm region arises due to ligand-to-metal charge transfer.[8a, 15] Interestingly, gel formation is very much dependent on the ligand-to-metal ratio and exhibits reversible sol-gel transformation (**Figure 2.11**). When the ratio of deprotonated ligand/metal is 1:0.5, a characteristic gel is formed, but on adding more metal ions to an equimolar ratio (1:1), the solution becomes turbid. The gels are unstable in water; and also in higher amounts of methanol, probably due to strong polarity of the solvent, breaking the gel by forming strong H-bonds with the PGA ligands.

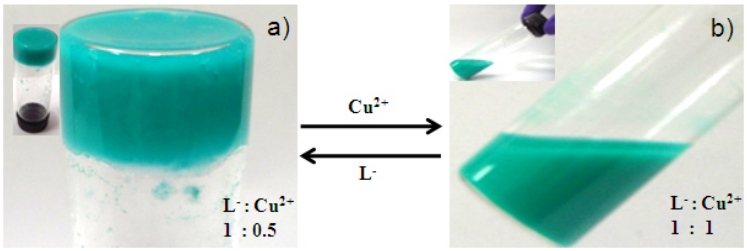

Figure 2.11. *Sol-gel reversibility experiments of gel **1** [L-PGA+Cu(NO$_3$)$_2$].*

2.4. Conclusion:

In summary, we have demonstrated a rare example of dynamic behavior of MBioFs by solid-state structural transformations in SCSC fashion. The two isostructural homochiral Cu^{II} coordination frameworks based on chiral amino acid ligands (D- and L-PGA) exhibit porous to nonporous solid-state structural transformations. The extent of structural dynamism was shown by guest-inclusion studies, which is very much dependent on chiral nature of the frameworks and of the guest molecules (hydrophobicity or hydrophilicity). Under similar reaction conditions, coordination-polymer-based chiral nanofibers were obtained, which were characterized by FE-

SEM and TEM studies. The reversible sol-gel formation of the coordination polymers and their morphology tuning by using different anions were also demonstrated. The present study will be useful for further development of dynamic MBioFs, and may help to understand the structural dynamics and functional behavior of soft giant biomolecules.

2.5. References:

(1) (a) Yaghi, O. M.; O'Keeffe, M.; Ockwig, N.W.; Chae, H. K.; Eddaoudi, M.; Kim, J. *Nature* **2003**, *423*, 705-714. (b) Dinca, M.; Long, J. R. *Angew. Chem. Int. Ed.* **2008**, *120*, 6870-6884. (c) Li, G.; Yu, W.; Cui, Y. J. *J. Am. Chem. Soc.* **2008**, *130*, 4582-4583. (d) An, J.; Geib, S. J.; Rosi, N. L. *J. Am. Chem. Soc.* **2009**, *131*, 8376–8377. (e) Moggach, S. A.; Bennett, T. D.; Cheetham. A. K. *Angew.Chem. Int. Ed*. **2009**, *48*, 7087-7089. (f) Ma, L.; Falkowski, J. M.; Abney, C.; Lin, W. *Nat. Chem*. **2010**, *2*, 838-846. (g) Lan, J.; Li, K. H.; Wu, H. H.; Olson, D. H.; Emge, T. J.; Ki, W.; Hong, M. C.; Li, J. *Angew. Chem. Int. Ed.* **2009**, *121*, 2370-2374. (h) Furukawa, H.; Ko, N.; Go, Y. B.; Aratani, N.; Choi, S. B.; Choi, E.; Yazaydin, A. O.; Snurr, R. Q.; O'Keeffe, M.; Kim, J.; Yaghi, O. M. *Science* **2010**, 239, 424-428. (i) Farha, O. K.; Yazaydın, A. O.; Eryazici, I.; Malliakas, C. D.; Hauser, B. G.; Kanatzidis, M. G.; Nguyen, S. T.; Snurr, R. Q.; Hupp, J. T. *Nat. Chem*. **2010**, *2*, 944-948. (j) Iremonger, S. S.; Liang, J.; Vaidhyanathan, R.; Shimizu, G. K. H. *Chem. Commun*.**2011**, *47*, 4430-4432. (k) Q. Lin, Q.; Wu, T.; Zheng, S. -T.; Bu, X.; Feng, P. *Chem. Commun.* **2011**, *47*, 11852-11854. (l) Zheng, B.; Bai, J.; Duan, J.; Wojtas, L.; Zaworotko, M. J. *J. Am. Chem. Soc*. **2011**, *133*, 748–751. (m) Zhou, H. –C.; Long, J. R.; Yaghi, O. M. *Chem. Rev*. **2012**, *112*, 673-674. (n) Wu, H.; Gong, Q.; Olson, D. H.; Li, J. *Chem. Rev*. **2012**, *112*, 836–868. (o) Nagarkar, S. S.; Joarder, B.; Chaudhari, A. K.; Mukherjee, S.; Ghosh S. K. *Angew. Chem. Int. Ed.* **2013**, *52*, 2881-2885.

(2) (a) Suh, M. P.; Ko, J. W.; Choi, H. J. *J. Am. Chem. Soc*. **2002**, *124*, 10976-10977. (b) Biradha, K.; Fujita, M. *Angew. Chem. Int. Ed.* **2002**, *41*, 3392-3395. (c) Nagarathinam, M.; Vittal, J. J. *Angew. Chem. Int. Ed*. **2006**, *45*, 4337–4341. (d) Bradshaw, D.; Warren, J. E.; Rosseinsky, M. J. *Science* **2007**, 315, 977-980. (e) Zhang, J.-P.; Chen, X. -M. *J. Am. Chem. Soc*. **2008**, *130*, 6010–6017. (f) Chen, C. -L.; Beatty, A. M. *J. Am. Chem. Soc*. **2008**, *130*, 17222–17223. (g) Horike, S.; Shimomura, S.; Kitagawa, S. *Nat. Chem*. **2009**, *1*, 695-704. (h) Platero-Prats, A. E.; Shea, V. A. de la Pena'O.; Snejko, N.; Monge, A.; Gutierrez-Puebla, E.

Chem. Eur. J. **2010**, *16*, 11632 – 11640. (i) Park, H. J.; Lim, D.-W.; Yang, W. S.; Oh, T. -R.; Suh, M. P. *Chem. Eur. J.* **2011**, **17**, 7251–7260. (j) Kondo, A.; Kajiro, H.; Noguchi, H.; Carlucci, L.; Proserpio, D. M.; Ciani, G.; Kato, K.; Takata, M.; Seki, H.; Sakamoto, M.; Hattori, Y.; Okino, F.; Maeda, K.; Ohba, T.; Kaneko, K.; Kanoh, H. *J. Am. Chem. Soc.*, **2011**, *133*, 10512–10522. (k) Yanai, N.; Kitayama, K.; Hijikata, Y.; Sato, H.; Matsuda, R.; Kubota, Y.; Takata, M.; Mizuno, M.; Uemura, T.; Kitagawa, S. *Nat. Mater.* **2011**, *10*, 787–793. (l) Manna, B.; Chaudhari, A. K.; Joarder, B.; Karmakar, A.; Ghosh, S. K. *Angew. Chem. Int. Ed*. **2013**, *52*, 998-1002.

(3) (a) Ranford, J. D.; Vittal, J. J.; Wu, D.; Yang, X. *Angew. Chem.Int.Ed.* **1999**, *38*, 3498-3501. (b) Iordanidis, L.; Kanatzidis, M. G. *J. Am. Chem. Soc.* **2000**, *122*, 8319-8320. (c) Barbour, L. J. *Aust. J. Chem*. **2006**, *59*, 595–596. (d) Vittal, J. J. *Coord. Chem. Rev.* **2007**, *251*, 1781-1795. (e) Zhang, Y.; Zhang, B.; Zhu, D. *J. Am. Chem. Soc.*, **2009**, *131*, 6934–6935. (f) Liu, T. -F.; Chen, Y. -P.; Yakovenko, A. A.; Zhou, H. -C. *J. Am. Chem. Soc.*, **2012**, *134* , 17358–17361. (g) He, Y. -C.; Yang, J.; Yang, G. –C.; Kana, W. –Q.; Ma, J. -F. *Chem. Commun*.**2012**, *48*, 7859–7861.

(4) (a) Schveigkardt, J. M.; Rizzi, A. C.; Piro, O. E.; Castellano, E. E.; De Santana, R. C.; Calvo, R.; Brondino, C. D. *Eur. J. Inorg. Chem*. **2002**, 2913-2919. (b) Anokhina, E. V.; Bok Go, Y.; Lee, Y.; Vogt, T.; Jacobson, A. J. *J. Am. Chem. Soc*. **2006**, *128*, 9957-9962. (c) Gould, J. A.; Jones, J. T. A.; Bacsa, J.; Khimyak, Y. Z.; Rosseinsky, M. J. *Chem. Commun*. **2010**, *46*, 2793–2795. (d) An, J.; Geib, S. J.; Rosi, N. L. *J. Am. Chem. Soc*. **2009**, *131*, 8376-8377.

(5) Imaz, I.; Rubio-Martı´nez, M.; An, J.; Sole´-Font, I.; Rosi, N. L.; Maspoch, D. *Chem. Commun*. **2011**, *47*, 7287-7302.

(6) Rabone, J.; Yue, Y.-F.; Chong, S. Y.; Stylianou, K. C.; Bacsa, J.; Bradshaw, D.; Darling, G. R.; Berry, N. G.; Khimyak, Y. Z.; Ganin, A. Y.; Wiper, P.; Claridge, J. B.; Rosseinsky, M. J. *Science* **2010**, *329*, 1053-1057.

(7) (a) Mart-Gastaldo, C.; Warren, J. E.; Stylianou, K. C.; Flack, N. L. O.; Rosseinsky, M. J. *Angew. Chem. Int. Ed*. **2012**, *51*, 11044–11048. (b) An, J.; Farha, O. K.; Hupp, J. T.; Pohl, E.; Yeh, J. I.; Rosi, N. L. *Nat.Comm*. **2012**, *3*, 1-6.

(8) Horcajada, P.; Gref, R.; Baati, T.; Allan, P. K.; Maurin, G.; Couvreur, P.; Ferey, G.; Morris, R. E.; Serre, C. *Chem. Rev*. **2012**, *112*, 1232–1268.

(9) *SAINT Plus*, version 7.03; Bruker AXS Inc.: Madison, WI, 2004.

(10) Sheldrick, G. M. *SHELXTL, Reference Manual*, version 5.1; Bruker AXS Inc.: Madison, WI, *1997*.

(11) Sheldrick, G. M. *Acta Crystallogr., Sect. A* **2008**, 112.

(12) Farrugia, L. *WINGX*, version 1.80.05; University of Glasgow: Glasgow, Scotland, 2009.

(13) Spek, A. L. *PLATON, A Multipurpose Crystallographic Tool*; Utrecht University: Utrecht, The Netherlands, **2005**.

(14) Spek, A. L. *Acta Crystallogr. Sect. A* **1990**, *46*, C34.

(15) (a) Sigel, H.; Martin, R. B.; *Chem. Rev.* **1982**, *82*, 385-426*;* (b) Tegoni, M.; Dallavalle, F.; Santos, M. A.; *J. Inorg. Biochem.* **2004**, 209-218; (c) Dong, J.; Canfield, J. M.; Mehta, A. K.; Shokes, J. E.; Tian, B.; Childers, W. S.; Simmons, J. A.; Mao, Z.; Scott, R. A.; Warncke, K.; Lynn, D. G.; *PNAS* **2007**,*104*, 13313-13318.

(16) Sadakiyo, M.; Yamada, T.; Kitagawa, H. *J. Am. Chem. Soc*. **2011**, *133*, 11050–11053.

(17) Hamilton, T. D.; Bu_car, D.-K.; Baltrusaitis, J.; Flanagan, D. R.; Li, Y.; Ghorai, S.; Tivanski, A. V.; MacGillivray, L. R. *J. Am. Chem. Soc*. **2011**, *133*, 3365–3371.

(18) Lee, H.; Lee, J. H.; Kang, S.; Lee, J. Y.; John, G.; Jung, J. H. *Chem. Commun*. **2011**, *47*, 2937-2939.

Chapter 3

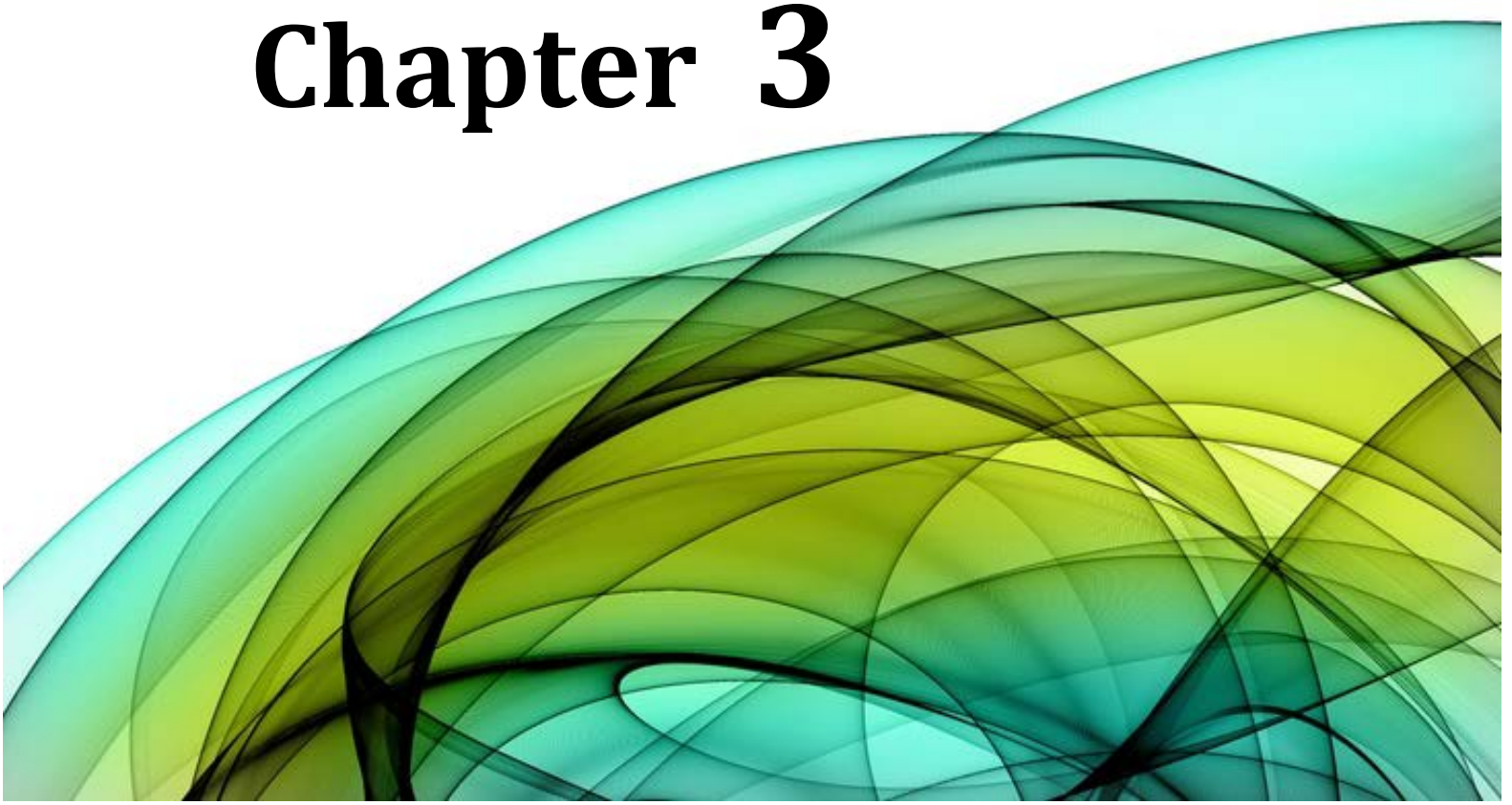

Investigation of Isosorbide Based Cadmium Carboxylate Framework for Selective Host-Guest Inclusion

3.1. Introduction:

Homochirality and helicity are ubiquitous in nature and are essential to various biological functions. Helices are also the central structural motifs in biological molecules, like α-helical protein, DNA, and collagens are with single-, double-, and triple-helix structures, respectively. All these helical biopolymers are composed of either the D or L form of basic units and always acquire either left- or right-handedness. Structural studies of helicate compounds with chiral building blocks may help to understand such kinds of unique structural behavior of naturally occurring chiral helical biopolymers.[1,2]

Among different types of chiral compounds, in recent years, homochiral porous coordination polymers or metal−organic frameworks (MOFs)[3] have attracted much attention because of their potential applications in enantioselective catalysis and separation[4-6] and the importance of chirality in biological processes.[2] Because of the lack of chiral porous zeolites, homochiral porous coordination polymers (PCPs) are particularly very attractive materials for industrial applications targeted at the separation of chiral mixtures and as heterogeneous asymmetric catalysts for the economical production of optically active organic compounds. Although numerous examples of porous, achiral PCPs with extremely high surface areas are reported,[7,8] the rational design and synthesis of homochiral porous materials still remains a challenge. Such materials are generally prepared by self-assembly process using three synthetic strategies: (1) spontaneous resolution, (2) chiral induction, and (3) use of enantiopure ligands. In the first method, achiral or racemic ligands form homochiral materials by spontaneous resolution during the self-assembly process, but mostly bulk racemates result with only a few exceptions.[9] In the second method, an auxiliary chiral ligand induces homochirality into the framework without direct involvement in structure formation.[3b,10] These two methods are quite unpredictable since their mechanisms are not yet very clear. The use of enantiopure ligands, on the other hand, is a direct and effective method for synthesis of homochiral porous materials, whereas the use of enantiopure ligands leads to generation of a single enantiomeric product.[11] D-Isosorbide is an easily accessible enantiopure small molecule derived from glucose, and it along with its different derivatives have therapeutic uses. Like many other moieties containing hydroxyl groups, modifying the hydroxyl groups of D-isosorbide by organic moieties containing proper functional groups can be one of the most effective ways to obtain enantiopure organic ligands.

In this chapter, by attaching a para substituted benzoic acid group with the hydroxyl groups of D-isosorbide, a biomolecule-based dicarboxylic acid ligand LH_2 have been synthesized. A porous two dimensional (2D) homochiral compound $[Cd(L)\text{-}(H_2O)]\cdot 3H_2O$ (**1**) was obtained by the self-assembly of LH_2 with cadmium (II) by solvothermal method. To the best of our knowledge, D-isosorbide-based enantiopure ligands have not yet been used to synthesize coordination polymers.

3.2. Experimental Section:

3.2.1. General remarks:

3.2.1.1. Materials: All the starting reagents and solvents were commercially available and used without further purification. Synthesized compounds were well purified and characterized by various instrumental technique.

3.2.1.2. Physical measurements: Powder X-ray diffraction (PXRD) patterns were measured on Bruker D8 Advanced X-Ray diffractometer at room temperature using Cu-Kα radiation (λ= 1.5406 Å) with a scan speed of 0.5° min^{-1} and a step size of 0.01° in 2 *theta*. Thermogravimetric analyses were obtained in the temperature range of 30-600 ºC on Perkin-Elmer STA 6000 analyzer under N_2 atmosphere, at a heating rate of 10 ºC min^{-1}. The Fourier transform (FT-IR) infra red-spectra were recorded on NICOLET 6700 FT-IR Spectrophotometer, using KBr Pellets. Solid state CD spectra were measured in JASCO J815 spectrometer in the range 600 nm – 200 nm.

3.2.1.3. X-ray Structural Studies: Single-crystal X-ray data were collected at 200 K on a Bruker KAPPA APEX II CCD Duo diffractometer (operated at 1500 W power: 50 kV, 30 mA) with graphite-monochromated Mo-Kα radiation (λ = 0.71073 Å). Crystals were mounted on nylon Cryo-Loops (Hampton Research) with Paraton- N (Hampton Research). The data integration and reduction were processed with SAINT[12] software. A multi-scan absorption correction was applied to the collected reflections. The structures were solved by the direct method using SHELXTL[13] and was refined on F^2 by full matrix least-squares technique, using the SHELXL-97[14] program package within the WINGX[15] programme. All non-hydrogen atoms were refined anisotropically. All hydrogen atoms were located in successive difference Fourier maps and they were treated as riding atoms using SHELXL default parameters. The structures

were examined using the *Adsym* subroutine of PLATON,[16] to assure that no additional symmetry could be applied to the models.

3.2.1.4. Low Pressure Sorption Measurements: Low pressure gas sorption measurements were performed using BelSorpmax (Bel Japan). All of the gases used, were of 99.999% purity. As-synthesized compound was heated at 160 °C under vacuum for 16 h to get guest free compound **1D**. Prior to adsorption measurement, the guest free samples **1D** was pretreated at 120 °C under vacuum for 2h, using BelPrepvacII and purged with N_2 on cooling.

3.2.2. Synthesis:

3.2.2.1. Synthesis of Ligand L′ : D-Isosorbide (10 g, 0.0684 mol) and NaH (3.45 g, 0.1436 mol) were mixed in N,N-dimethylformamide (DMF; 120 mL) solvent under N_2 atmosphere. Then the reaction mixture was stirred at 75 °C for 10 min. After that, 4-(fluoroethyl)benzoate (23.01 g, 0.1368 mol) was added dropwise. The reaction was continued for 3h. After cooling to RT, excess NaH was quenched with ice and ethyl acetate. A maximum amount of DMF was removed by rotary evaporation under reduced pressure, and the mixture was extracted with EtOAc (2 × 250 mL). The combined organic layer was washed with 150 mL of brine, dried over anhydrous sodium sulfate, and concentrated under reduced pressure to get a crude product, which was purified on silica gel (100 and 200 mesh) column chromatography. Yield: 15.28 g, 50.52% (**Scheme 3.1**).

^{1}H NMR (400 MHz, $CDCl_3$): δ 1.39 (dt, J = 1.36 and 7.32 Hz, 6H), 4.06 (d, J = 5.48 Hz, 2H), 4.10 (d, J = 10.52 Hz, 1H), 4.20 (dd, J = 4.12 and 10.56 Hz, 1H), 4.35 (q, J = 7.18 Hz, 4H), 4.67 (d, J = 5.04 Hz, 1H), 4.29−4.87 (m, 2H), 5.04 (t, J = 5.26 Hz, 1H), 6.95−7.01 (m, 4H), 8.00−8.03 (m, 4H) (**Appendix 3.1**).

^{13}C NMR (100 MHz, $CDCl_3$): δ = 14.02, 70.93, 73.13, 81.31, 85.97, 114.41, 123.48, 131.36, 161.16, 165.62 (**Appendix 3.1**).

Anal. Calcd (found) for L' : C, 65.15 (65.12); H, 5.92 (5.96).

3.2.2.2. Synthesis of Ligand LH_2: L′ (15.28 g, 0.035 mol) was dissolved in 250 mL of methanol (MeOH) and 150 mL of water (H_2O). Thereafter, $LiOH·H_2O$ (8.82 g, 0.21 mol) was added at 0 °C. The reaction mixture was stirred overnight. Excess MeOH was removed under

reduced pressure, and acidified with diluted HCl to get the desired product. The product was filtered, washed with fresh H_2O, and dried under vacuum. Yield: 9.28 g, 69.8% (**Scheme 3.1**).

^{1}H NMR (400 MHz, DMSO-d_6): δ 3.90−3.93 (m, 2H), 4.005 (dd, J = 4.16 and 11 Hz, 2H), 4.58 (d, J = 4.12 Hz, 1H), 5.01−5.05 (m, 3H), 7.04 (d, J = 8.24 Hz, 2H), 7.09 (d, J = 8.68 Hz, 2H), 7.86 (d, J = 8.68 Hz, 2H), 7.91 (d, J = 8.72 Hz, 2H) (**Appendix 3.2**).

^{13}C NMR (100 MHz, $CDCl_3$): δ= 77.19, 80.91, 85.97, 115.19, 123.89, 131.66, 160.41, 161.60 (**Appendix 3.2**).

Anal. Calcd (found) for L' : C, 62.18 (62.24); H, 4.70 (4.63).

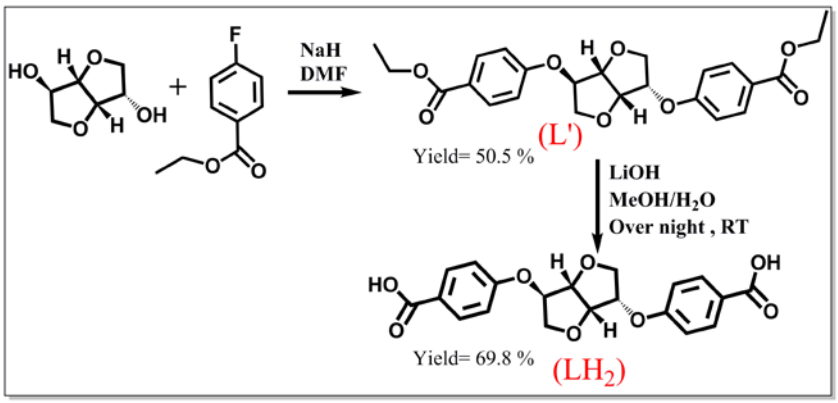

Scheme 3.1. *Schematic representation of ligand synthesis.*

3.2.2.3. Synthesis of {[Cd(L)(H$_2$O)]·3H$_2$O}$_n$ (1): Single crystals of **1** were prepared by reacting 0.125 mmol of $Cd(NO_3)_2·4H_2O$, 0.125 mmol of ligand (LH_2), and 0.2 mmol of NaOMe in 3 mL of H_2O and 2 mL of tetrahydrofuran (THF) by a solvothermal technique, in a Teflon-lined autoclave. The autoclave was heated under autogenous pressure at 160 °C for 3 days, and then cooled to RT for a 24 h period. Upon cooling to RT, the desired product appeared in ~ 45% yield.

3.3. Result and discussions:

Compound **1** was synthesized by a solvothermal reaction of LH_2 and $Cd(NO_3)_2·4H_2O$ in a THF/H_2O mixture solvent and characterized by a single-crystal X-ray diffraction (SC-XRD) technique. The phase purity of as-synthesized compound **1** was confirmed by PXRD measurement. SC-XRD analysis revealed that compound **1** crystallizes into a chiral

orthorhombic crystal system, space group $C222_1$ with a Flack parameter of 0.00(6), indicating enantiomeric purity of the single crystals. The asymmetric unit of **1** consists of one L, two Cd^{II} ions with half-occupancy, and four H_2O molecules (one-coordinated and three-non coordinated). One cadmium (Cd1) has an octahedral coordination environment with an O6 donor set from two coordinated H_2O molecules and four carboxylate O atoms from four different ligands. The other cadmium (Cd2) also has an octahedral geometry, but in distorted shape with an O6 donor set from two monodentate and two bidentate carboxylate groups from four different ligands (**Figure 3.1**). Cd−O distances are in the ranges of 2.242−2.276 Å for Cd1, and 2.259−2.427 Å for Cd2. One of the two O atoms amongthe bidentate carboxylate groups coordinated to Cd2 is bridged

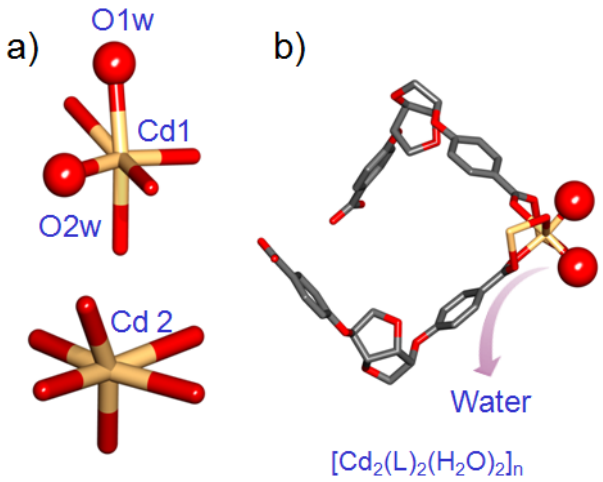

Figure 3.1. (*a) Coordination environment of two types cadmium in [$Cd_2L_2(H_2O)_2$]; (b) Structural motifs found in the single-crystal structure.*

with the other cadmium (Cd1) from both sides, thus extending the metal carboxylate chain along the *a* axis. Because of the roof-type arrangement of the D-isosorbide core and the flexibility in the ether moiety, the dicarboxylate ligand could arrange itself into a V shape. This V-shaped ligand coordinated to the cadmium ions at both its ends with carboxylate O atoms, and this subsequently resulted in a 2D porous coordination framework (**Figure 3.2** and **Appendix 3.4**).

The most interesting feature of the structure is its triple-helical[17] arrangement of the framework, very similar to the triple-helical structure of a group of biologically important protein molecules, called collagen. Each of the V-shaped dicarboxylate based ligand connected to Cd^{II} at

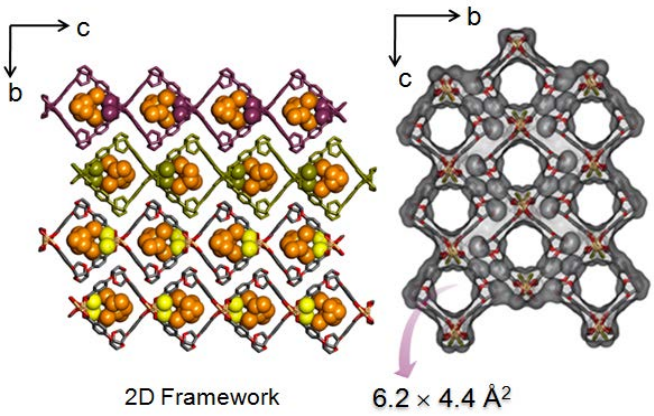

Figure 3.2. *Structural view of the 2D framework of compound **1** along a axis (Space filled ball correspond for water molecule)(left). The hydrogen atoms and solvent molecules are omitted for clarity.*

both ends has resulted in a left-handed helical strand with a pitch of 14.632 Å with a width of *ca*. 13 Å. It is noteworthy that the pitch of this helix is even greater than the pitch for the most

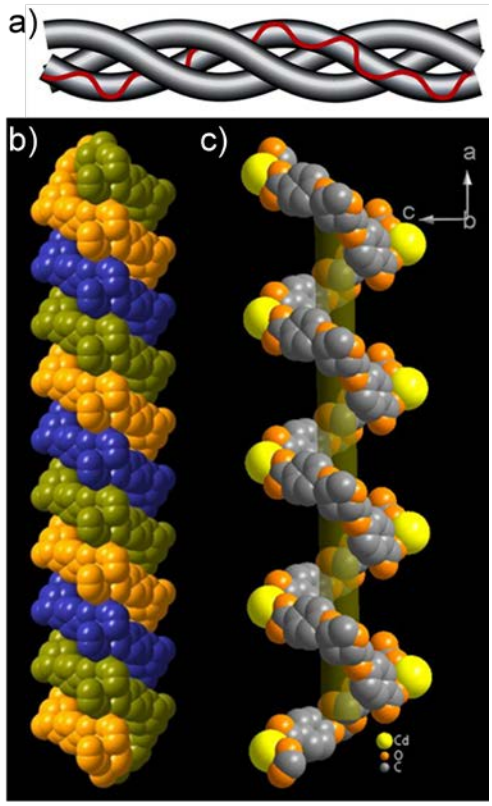

Figure 3.3. (*a) Structure of collagen; (b) Triple-helical chains of compound **1**; and (c) Space-filling view of the left handed single-helical chain.*

open protein helices, i.e., polyproline (9.36 Å).[18] Three such identical helical chains are extended along *a* axis to form a left-handed triple-helical structure (**Figure 3.3**). This structure has a very good resemblance to the structures of collagen types II, III, VII, VIII, and X, whereas the threeidentical α chains (homotrimers) form right-handed triple-helical supramolecular structures.[19] These helices interconnect each other, and also by both sides edge sharing at Cd^{II} with two identical triple helices result in the 2D homochiral framework.

The results of solid-state CD spectral measurements in the wavelength range 400−250 nm confirmed the enantiopure nature of the ligand LH_2 and compound **1**. As shown in **Figure 3.2**, the ligand and bulk crystals of **1** in powder form show positive Cotton effects at 297.95 and 291.03 nm respectively, revealing their homochiral nature. The enantiopure nature of compound **1** also supports the SC-XRD structure with chiral space group $C222_1$ and a Flack parameter

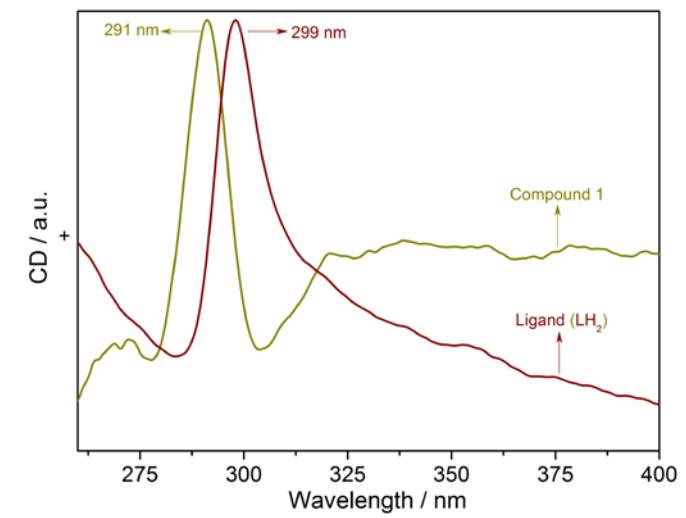

Figure 3.4. *Solid-state CD spectra of compound 1 and ligand LH_2.*

value of 0.00(6). These results also indicate that there is no racemization of the ligand during solvothermal synthesis, and the chiral feature transfers from the original chiral ligand to the framework.

The resultant 2D framework is a porous sheet-like architecture and forms a 1D channel along the a axis within the 2D sheets, with maximum channel dimensions ~6.2 × 4.4 $Å^2$ (the channel size is measured by considering the van der Waals radii for constituent atoms). The

cavities of the framework are occupied by disordered H_2O molecules. PLATON[20] analysis revealed that the 2D porous structure contains voids of 1035.5 $Å^3$, , which accounts for 22% per unit cell volume.

TGA analysis revealed that the framework is stable up to 400 °C (**Figure 3.5a**). The desolvated phase (**1D**) was generated by heating the compound for 16 h at 160 °C under reduced pressure. TGA data confirms the removal of guest H_2O molecules. Very similar PXRD data of **1D** with the as-synthesized compound **1,** suggest that the framework is quite rigid after removal of coordinated H_2O molecules. A slight flexible behavior of the framework was observed after removal of the guest H_2O molecules, as we can see from the slight variations in the PXRD pattern for **1D**. To test the reversibility of the transformation, **1D** was exposed to H_2O vapor for 3 days; the desolvated phase transformed to its original structure, which was confirmed by PXRD data (**Figure 3.5b**).

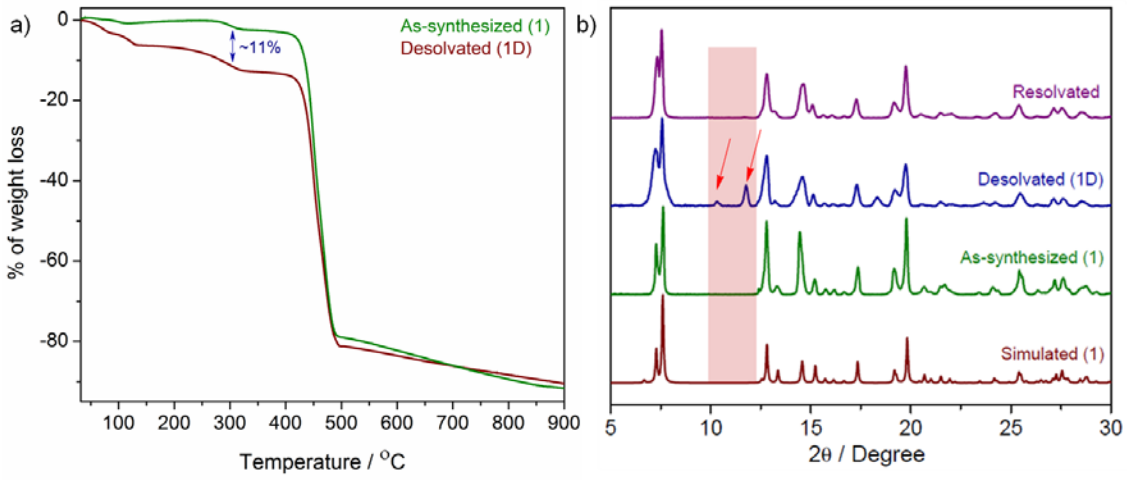

Figure 3.5. *(a) Thermogravimetric analysis (TGA) data for the as-synthesized and de-solvated compound; (b) PXRD patterns of the simulated, as-synthesized (**1**), desolvated (**1D**) and resolvated compounds.*

To check the porous properties of the 2D chiral framework (**1D**), gas and solvent sorption measurements were carried out. It shows no uptake of N_2 (1.62 cm^3/g), but some uptake for CO_2 (13.54 cm^3/g) (**Figure 3.6**). The pore size of the as-synthesized compound is 6.2 × 4.4 $Å^2$, but the PXRD pattern (**Figure 3.5b**) of the desolvated compound is little different from that of the as-synthesized compound. This indicates that the desolvated structure is not exactly the same as

the as-synthesized compound, and most probably the pore size is squeezing after removal of the guest molecules. It is well-known in the literature and have recently been observed in one of our compounds that it is not only the pore size, but also the host–guest interactions which decides the amount of adsorbate taken by the MOF.[21,22] CO_2 has a smaller kinetic diameter and a larger quadrupole moment value than N_2, so it can interact more strongly with the pore surface

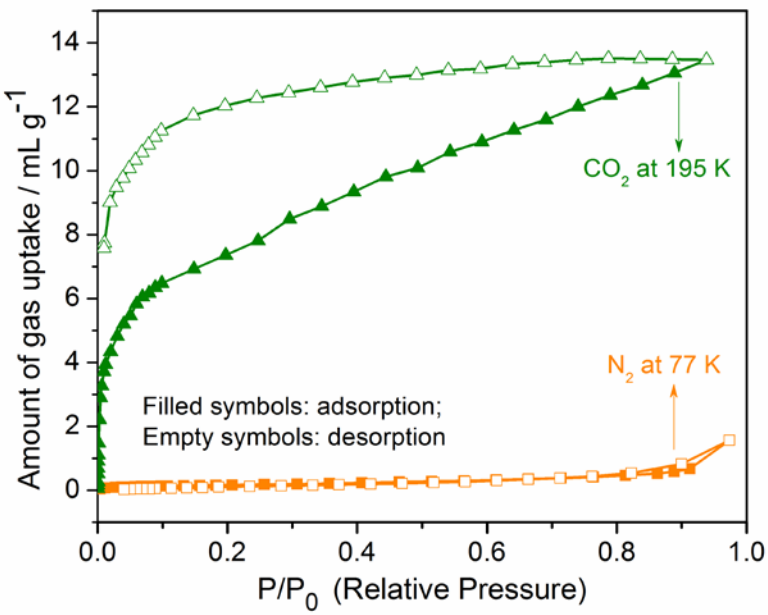

Figure 3.6. *(a) CO_2 (olive) and N_2 (orange) sorption isotherms of compound **1D** at 195K and 77K respectively.*

of the host framework, thus showing little uptake and hysteresis behavior. Interesting phenomena were observed in solvent sorption experiments at 298 K. Selective sorption of H_2O[23–27] and MeOH were observed over several other organic solvents [namely, EtOH, THF, benzene, and cyclohexane; **Figure 3.7**]. Very small sorption amounts for other organic solvents, as compared to H_2O and MeOH are desirable for removal of H_2O and MeOH from organic solvents. After removal of coordinated H_2O molecules, the framework now has open metal sites and the concerned pore is hydrophilic in nature, because of the presence of several O atoms on the pore surface. Although the pore size of the desolvated phase may not be big enough to allow the entry of guest molecules into the pore (as we can see from PXRD, the structure changed with anticipated squeezing, after removal of the coordinated guest molecules present in the pore) but

because of the hydrophilic nature of the pore surface and open metal sites, H_2O and MeOH molecules strongly interact with the surface and hence enter into the pore, which is also supported by flexible nature of the ligand.

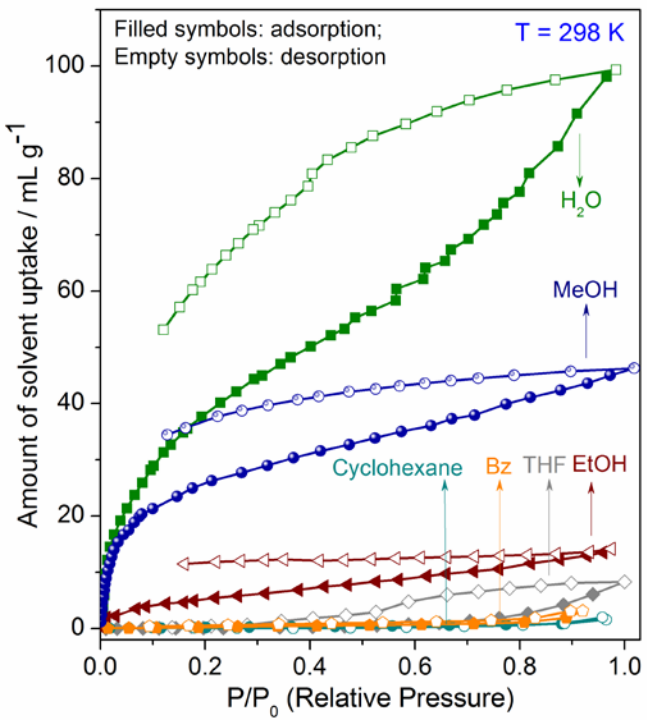

Figure 3.7. (*a) Solvent sorption graphs of compound **1D** at 298K. (Color code: H_2O, olive; MeOH, royal blue; EtOH, wine; THF, gray; cyclohexane, dark cyan; benzene, orange).*

Also, because of the strong interaction of H_2O and MeOH guests with the pore surface, desorption becomes very difficult and therefore hysteresis sorption profiles are observed.[28]

3.4. Conclusion:

In conclusion, we have designed one D-isosorbide-based enantiopure biomolecule based dicarboxylic acid as ligand, and with Cd^{II}, a homochiral porous framework has been synthesized solvothermally and characterized. The framework consists of interconnected triple-helical chains, very similar to the triple-helical structure of a group of biologically important protein molecules called "collagen". Enantiopurity of the new ligand and the newly reported cadmium(II) framework has been checked by CD measurements. The porous framework is very

stable even after removal of the guest molecules, which shows size-selective inclusion of H_2O and MeOH over other solvents (*e.g.*, THF, EtOH, benzene, and cyclohexane) inside the channels.

3.5. References:

(1) (a) Albrecht, M. *Chem. Rev*. **2001**, *101*, 3457 - 3498. (b) Meurer, K. P.; Vogtle, F. *Top. Curr. Chem.* **1985**, *127*, 1 - 76.

(2) (a) Wu, H.-C. H.; Sarko, A. *Carbohydr. Res.* **1978**, *61*, 270 . (b) Watson, J. D.; Crick, F. C. H. *Nature* 1953, 171, 737 - 738.

(3) (a) Liu, Y.; Xuan, W.; Cui, Y. *Adv. Mater*. **2010**, *22*, 4112 - 4135. (b) Morris, R. E.; Bu, X.-H. *Nat. Chem*. **2010**, *2*, 353 - 361. (c) Ma, L.; Abney, C.; Lin, W. *Chem. Soc. Rev*. **2009**, *38*, 1248 - 1256. (d) Bradshaw, D.; Claridge, J. B.; Cussen, E. J.; Prior, T. J.; Rosseinsky, M. J. *Acc. Chem. Res*. **2005**, *38*, 273 - 282.

(4) (a) Seo, J. S.; Whang, D.; Lee, H.; Jun, S. I.; Oh, J.; Jeon, Y. J.; Kim, K. *Nature* **2000**, *404*, 982 - 986. (b) Hu, A. G.; Ngo, H. L.; Lin, W. *J. Am. Chem. Soc*. **2003**, *125*, 11490 - 11491.

(5) Li, G.; Yu, W.; Cui, Y. *J. Am. Chem. Soc*. **2008**, *130*, 4582 - 4583.

(6) (a) Rowsell, J. C.; Yaghi, O. M. *J. Am. Chem. Soc*. **2006**, *128*, 1304 − 1315. (b) Zhang, J. P.; Chen, X. M. *J. Am. Chem. Soc*. **2008**, *130*, 6010 − 6017.

(7) (a) Férey, G.; Serre, C. *Chem. Soc. Rev*. **2009**, *38*, 1380 - 1399. (b) Kitagawa, S.; Matsuda, R. *Coord. Chem. Rev*. **2007**, *251*, 2490 - 2509. (c) Murray, L. J.; Dinca, M.; Long, J. R. *Chem. Soc. Rev*. **2009**, *38*, 1294 - 1314.

(8) (a) Li, J.-R.; Kuppler, R. J.; Zhou, H.-C. *Chem. Soc. Rev*. **2009**, *38*, 1477 - 1504. (b) An, J.; Rosi, N. L. *J. Am. Chem. Soc*. **2010**, *132*, 5578 - 5579. (c) Huang, X.-C.; Lin, Y.-Y.; Zhang, J.-P.; Chen, X. M. *Angew. Chem., Int. Ed*. **2006**, *45*, 1557 - 1559. (d) Wang, B.; Cote, A. P.; Furukawa, H.; O'Keeffe, M.; Yaghi, O. M. *Nature* **2008**, *453*, 207 - 211. (e) Cheon, Y. E.; Suh, M. P. *Chem. Commun*. **2009**, 2296 - 2298.

(9) (a) Garcíaa, L. P.; Amabilino, D. B. *Chem. Soc. Rev*. **2002**, *31*, 342 - 356. (b) Wang, M.-X.; Long, L.-S.; Huang, R.-B.; Zheng, L.-S. *Chem. Commun*. **2011**, *47*, 9834 - 9836.

(10) (a) Dang, D.; Wu, P.; He, C.; Xie, Z.; Duan, C. *J. Am. Chem. Soc*. **2010**, *132*, 14321 - 14323. (b) Zhang, J.; Chen, S.; Wu, T.; Feng, P.; Bu, X.-H. *J. Am. Chem. Soc* **2008**, *130*, 12882 - 12883.

(11) (a) Zhang, J.; Chen, S.; Valle, H.; Wong, M.; Austria, C.; Cruz, M.; Bu, X.-H. *J. Am. Chem. Soc.* **2007**, *129*, 14168 - 14169. (b) Dybtsev, D. N.; Nuzhdin, A. L.; Chun, H.; Bryliakov, K. P.; Talsi, E. P.; Fedin, V. P.; Kim, K. *Angew. Chem., Int. Ed.* **2006**, *45*, 916 - 920.

(12) SAINT Plus, version 7.03; Bruker AXS Inc.: Madison, WI, **2004**.

(13) Sheldrick, G. M. SHELXTL, Reference Manual, version 5.1; Bruker AXS: Madison, WI, **1997**.

(14) Sheldrick, G. M. *Acta Crystallogr., Sect. A* **2008**, 112 − 122.

(15) Farrugia, L. WINGX, version 1.80.05; University of Glasgow: Glasgow, **2009.**

(16) Spek, A. L. PLATON, A Multipurpose Crystallographic Tool; Utrecht University: Utrecht, The Netherlands, **2005**.

(17) (a) Grosshans, P.; Jouaiti, A.; Bulach, V.; Planeix, J.-M.; Hosseini, M. W.; Nicoud, J.-F. *Chem. Commun*. **2003**, 1336. (d) Cui, Y.; Ngo, H. L.; Lin, W. *Chem. Commun*. **2003,** 1388.

(18) Dickerson, R. E.; Geis, I. The Structure and Action of Proteins; Harper & Row: Evanston, IL, 1969.

(19) Gelse, K.; Poschl, E.; Aigner, T. *Adv. Drug Delivery Rev*. **2003**, *55*, 1531.

(20) Spek, A. L. Acta Crystallogr., Sect. A **1990**, *46*, C34.

(21) Nagarkar, S. S.; Chaudhari, A. K.; Ghosh, S. K. *Inorg. Chem*. **2012**, *51*, 572 - 576.

(22) Maji, T. K.; Matsuda, R.; Kitagawa, S. *Nat. Mater*. ***2007***, *6*, 142 - 148.

(23) (a) Kitagawa, S.; Kitaura, R.; Noro, S. I. *Angew. Chem., Int. Ed.* **2004**, *43*, 2334 - 2375. (b) Uemura, K.; Matsuda, R.; Kitagawa, S. J. Solid State Chem. 2005, 178, 2420 - 2429. (c) Kitagawa, S.; Uemura, K. *Chem. Soc. Rev*. **2005**, *34*, 109 - 119.

(24) Serre, C.; Millange, F.; Thouvenot, C.; Nogues, M.; Marsolier, G.; Louer, D.; Férey, G. *J. Am. Chem. Soc.* **2002**, *124*, 13519 - 13526.

(25) Gu, J.-Z.; Lu, W.-G.; Jiang, L.; Zhou, H.-C.; Lu, T.-B. *Inorg. Chem*. **2007**, *46*, 5835 - 5837.

(26) Kita, H.; Horii, K.; Ohtoshi, Y.; Tanaka, K.; Okamoto, K. *J. Membr. Sci. Lett*. **1995**, *14*, 206 - 208.

(27) Uchida, S.; Mizuno, N. *J. Am. Chem. Soc*. **2004**, *126*, 1602 − 1603.

(28) Ghosh, S. K.; Sareeya, B.; Kitagawa, S. *Angew. Chem., Int. Ed*. **2008**, *47*, 3403 − 3406.

Chapter 4

Amine Decorated Metal-Biomolecule Framework for Selective Sensing of Nitro Explosive

4.1. Introduction:

The reliable and accurate detection of explosives has become a major concern in the perspective of the rapidly growing explosive-deployment behind international terrorist attacks.[1] The ingredients used in most of the industrial explosives are based on nitroaromatics, nitroaliphatics and organic peroxide compounds such as 2,4,6-trinitrotoluene (TNT), 2,4-dinitrotoluene (2,4-DNT), 2,4,6-trinitrophenol (TNP) and 1,3,5-trinitro-1,3,5-triazacyclohexane (RDX), 2,3-Dimethyl-2,3-dinitrobutane (DMNB), nitro-methane (NM) etc.[1,2] Considering all nitro explosives, TNP is one of the powerful explosives in its class being expansively used in the landmines for decades together.[3] Moreover, the mutagenic activities of TNP lead to severe health issues, resulting into catastrophic environmental pollution.[4] As a relevant fact, TNP-usage in chemical industries, especially leather, pharmaceutical, and dye industries or in explosive devices and rocket fuels drastically affects the soil and aquatic system by uncontrolled contamination, causing strong irritation and allergic reactions.[3] The wide use of this compound has made it a significant environmental contaminant. Hence, rapid and selective detection of trace amounts of TNP present in soil and aquatic systems adjacent to chemical industries, or in an explosive-affected area is a pressing challenge targeted at appropriate environmental monitoring. However, selective and sensitive detection of aqueous contaminant TNP from other nitro compounds is a daunting task, considering the analyte's pronounced electron affinity resulting in false response.[5]

Recent years have witnessed quite a few new detection technologies and sophisticated instruments to be employed for serving the explosive-detection purpose, but these techniques are undoubtedly expensive and have serious accessibility issues. Thus, fluorescence-based chemosensors have been of immense importance and have several advantages over other approaches because of their high sensitivity, portability, short response time and compatibility in both solid and solution media.[6] A wide variety of luminescent materials including small organic molecules, supramolecular polymers, carbon nanotubes, conjugated organic polymers, nanocrystals, dendrimers and metal complexes have been used for fluorescence-based explosive-sensors.[7] Remarkable lack of stability, obnoxious toxicity and inability to control the specific molecular recognitions for such materials are the common limitations for explosive sensing applications.

Detection of trace amounts of nitro explosive-content in aqua and soil presents a stupendous challenge because of the extreme scarcity of a suitable sensor compound to perform the task. In actuality, the precedence of any suitable material functioning as explosive-sensor in the desired aqueous medium is indeed rare.[8] In the last few years, metal organic frameworks (MOFs) or coordination polymers (CPs) have undergone a remarkable upsurge, in view of designable crystalline solids in the microporous domain for their potential applications ranging from gas storage/separations, catalysis, optoelectronics, sensing, clean energy etc.[9] Especially, MOFs as sensory materials are excellent candidates,[10, 11] owing to their tunable host-guest interactions involving specific functionalization, letting them act as pre-concentrator for the concerned target analytes (***Scheme 4.1***).

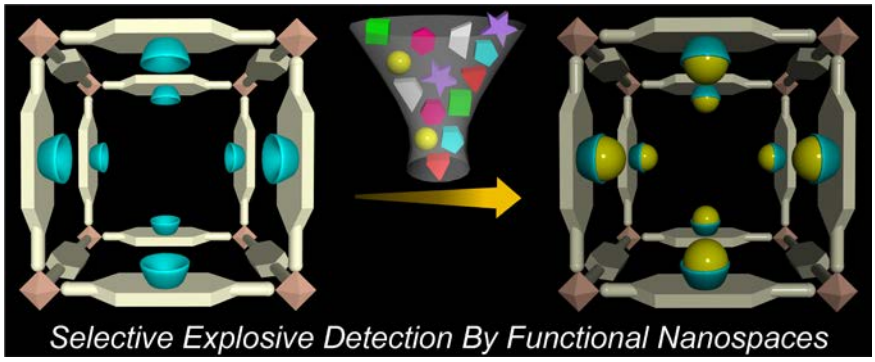

Scheme 4.1. *Schematic representation of selective nitroexplosive sensing by the amine decorated nanospace of MOF.*

The major challenge posed lies in aqueous phase selective detection of TNP, since most of the reported MOFs involve detection in organic/organic-water mixture phase.[11] Only two very recent reports came up with unprecedented fluorescence based TNP-selectivity in aqueous phase.[12] For these cases, employment of pyridyl lewis basic sites for achieving the targeted TNP selectivity in aqua was the key feature. The primary aim of the present approach was to improve the selectivity-efficiency in aqueous phase, by introduction of different preconceived functionalities in the microporous domain. In this regard, amine group appeared to be the best targeted functionality to envisage into, considering its easily conceivable maximized ionic as well as H-bonding interactions with TNP analyte. This new strategic rationale allows the comprehensive investigation of fluorescence-based selective TNP-sensing performance,

exploiting the seemingly favorable interactions those might take place between the free functional amines decorating the MOF-pore surface and the TNP analyte. In this chapter, bio-MOF-**1** have been envisioned as the probe, considering its excellent features, including a rare combination of porosity, water stability, luminescence property and free functional amine groups having a characteristic blue emission signature.[13] The free amine groups in the porous architecture should ideally facilitate a facile diffusion of TNP (**Figure. 4.1b**), plausibly owing to the desired H-bonding interactions, as previously mentioned. Notably, all other pyridyl nitrogens are coordinated to the Zn-centres, maximizing the interaction-allowance for the free amine group (**Figure. 4.1b**). Moreover, excellent hydrolytic stability allows it to be used in water, where as significantly large pore windows can allow easy diffusion of analytes inside the MOF channels.

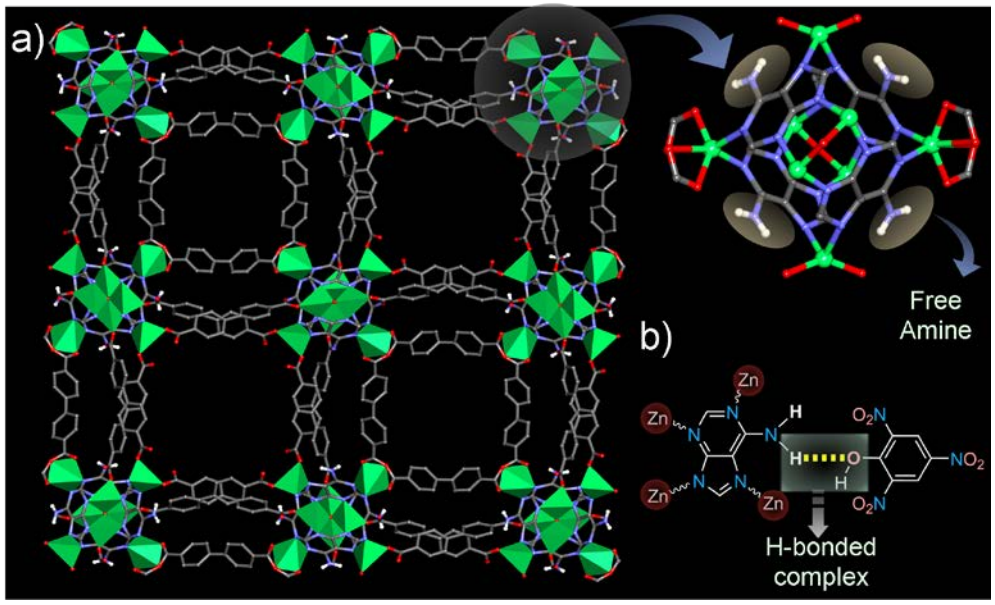

Figure 4.1. *(a) The crystal structure of bio-MOF-1 showing 1D channels along the crystallographic c direction. Highlighted portion is Zn- adeninate chain, in which free amine groups are exposed to the nanospace; (b) Plausible H-bonding interactions between adenine and TNP.*

4.2. Experimental Section:

4.2.1. General remarks:

4.2.1.1. ***Caution!*** TNT, RDX and TNP are highly explosive and should be handled carefully and in small amounts. The explosives were handled as dilute solutions and with safety measures to avoid explosion.

4.2.1.2. Materials: TNT and RDX were obtained from HEMRL Pune (India). TNP, 2,4-DNT, 2,6-DNT, DMNB, NM were purchased from Aldrich, 1,3-DNB, NB from local company and used as received. Dry solvents were used during complete analysis and were obtained Aldrich.

4.2.1.3. Physical measurements. X-ray powder pattern was recorded on Bruker D8 Advanced X-ray diffractometer at room temperature using Cu Kα radiation (λ = 1.5406 Å). Thermogravimetric analyses were obtained in the temperature range of 30−800 °C on PerkinElmer STA 6000 analyzer under a N_2 atmosphere at a heating rate of 10 °C min^{-1}. Fluorescence measurements were done using Horiba FluoroMax 4, with stirring attachment. The UV-Vis measurements were performed using Chemito SPECTRASCAN UV-2600.

4.2.1.4. X-ray Structural Studies: Single-crystal X-ray data were collected at 200 K on a Bruker KAPPA APEX II CCD Duo diffractometer (operated at 1500 W power: 50 kV, 30 mA) with graphite-monochromated Mo Kα radiation (λ = 0.71073 Å). Crystals ware on nylon CryoLoops (Hampton Research) with Paraton-N (Hampton Research). The data integration and reduction were processed with SAINT[14] software. A multi-scan absorption correction was applied to the collected reflections. The structures ware solved by the direct method using SHELXTL[15] and was refined on F^2 by full-matrix least-squares technique using the SHELXL-97[16] program package within the WINGX[17] programme. All non-hydrogen atoms were refined anisotropically. All hydrogen atoms were located in successive difference Fourier maps and they were treated as riding atoms using SHELXL default parameters. The structures were examined using the *Adsym* subroutine of PLATON,[18] to assure that no additional symmetry could be applied to the models. CCDC-1021375 (cocrystal **1, Appendix 4.2**) contains the supplementary crystallographic data for this compound. These data can be obtained free of charge from The Cambridge Crystallographic Data Centre via www.ccdc.cam.ac.uk/data_request/cif.

4.2.1.5. Fluorescence study: 1 mg of desolvated Bio MOF **1 (1D)** is weighed and added to a fluorescence cuvette (path length of 1cm) containing 2 mL of water under stirring. The fluorescence response upon excitation at 340 nm was measured *in-situ* in the range of 350-650 nm, after incremental addition of freshly prepared aqueous analyte solutions (1 mM or Saturated) and corresponding fluorescence intensities were monitored at 406 nm. The solution was stirred at constant rate during fluorescence measurement to maintain homogeneity of solution.

4.2.2. Synthesis:

4.2.2.1. Synthesis of Bio MOF (1): Synthesis of Bio MOF was done according to the previously reported procedure.[6] As-synthesized compound was rinsed with DMF (2X) followed by $CHCl_3$ exchange procedure to get $CHCl_3$ exchanged compound. $CHCl_3$ exchanged compound was dried at 130 ^{0}C under N_2, atm for 6-7 h to get the desolvated compound (**1D**).

4.2.2.2. Synthesis of co-crystal: A 1 mL methanolic solution of picric acid (5.7 mg, 0.025 mmol) was carefully layered over a 1 mL solution of adenine (3.4 mg, 0.025 mmol) in H_2O-MeOH (1:1) in a glass tube. Clean, pale yellow coloured crystals suitable for X-ray analysis were obtained after 5 days in 60% yield.

4.3. Result and discussions:

In the microporous domain, bio-MOF-**1**, $\{[Zn_8(ad)_4(BPDC)_6O{\cdot}2Me_2NH_2]{\cdot}G\}_n$ (G= DMF and water) possessing infinite zinc-adeninate secondary building units (SBUs), interconnected via multiple BPDC (BPDC= biphenyl dicarboxylic acid) linkers constitute a 3D extended framework.[13]

Conceivably, the two types of 1D channels present along *c*-axis (~7 X 7 and ~10 X 10 Å^2),[19] containing disordered Me_2NH_2 cations can permit facile diffusion of the analytes inside the porous architecture, resulting into the close proximity of the e^- deficient analytes to the e^- rich MOF, imperative for the feasible allowance of any favorable interactions.

The water stability as reported for bio-MOF-1 is well-established in literature.[13a] When bio-MOF-**1** was soaked in water for several weeks, retention of crystallinity was observed, as evidenced by PXRD analysis (**Figure. 4.2a**), affirming the hydrolytic stability. Moreover, simultaneous stability of bio-MOF- **1** in TNP solution was verified by PXRD analyses (**Figure. 4.2a**). The pore has free amine groups protruded inside it, making them more feasibly interact with the guest receptor(s). The desolvated phase (**1D**) of the compound was confirmed by TGA analysis (**Figure. 4.2b**). When compound 1D was dispersed in water and excited at 340 nm, it exhibited a strong emission at 405 nm (**Figure. 4.3**).

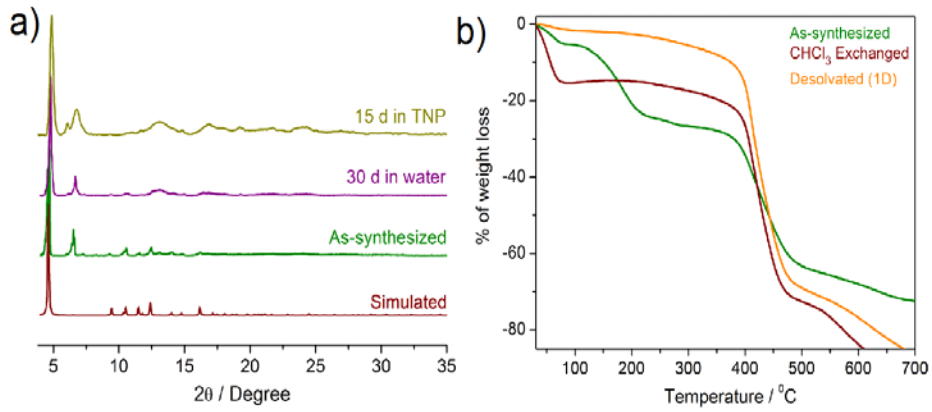

Figure 4.2. *(a) Powder X-ray diffraction (PXRD) patterns of compound **1**; (b) Thermogravimetric analysis (TGA) data for the as-synthesized (**1**; green), (CH_3Cl exchanged; wine) and desolvated (**1D;** orange color) compound.*

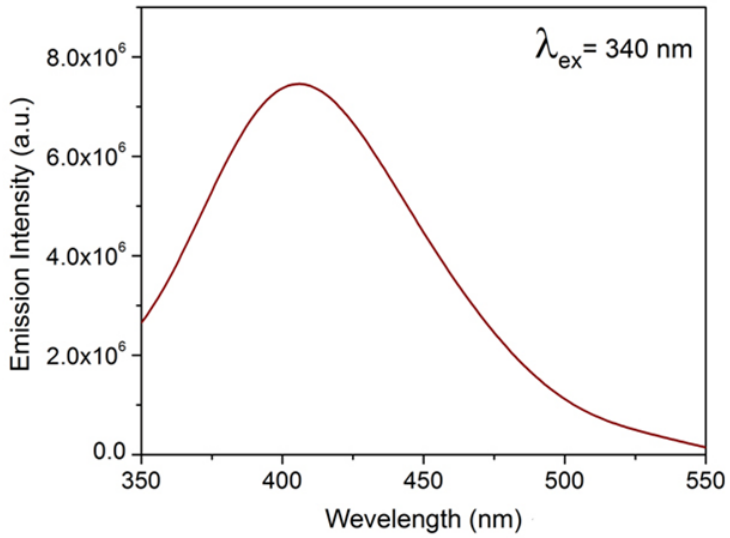

Figure 4.3. *Emission spectra of MOF (**1D**) dispersed in water, upon excitation at 340 nm.*

Benefiting from the stability issue in water, the ability of **1D** to sense trace amounts of nitroexplosives in aqueous medium was investigated. The emission response was monitored by fluorescence titration with different nitro explosives such as TNP, TNT, RDX, DMNB, NM, 2,4-DNT and 2,6-DNT (**Figure. 4.4a** and **Appendix 4.3**). The results showed fast detection and high fluorescence quenching (93%) for TNP on incremental addition of 10^{-3} M (200 µL) analyte

(**Figure. 4.4b**). On the other hand, corresponding change in fluorescence intensity for the other nitro analytes are exceedingly low (**Figure. 4.4b**). This clearly demonstrates the remarkable selectivity exhibited by bio-MOF-**1** towards TNP over all the congener nitro analytes. The compound **1D** can sense TNP at extremely low concentration, with a detection limit of 12.9 nM (2.9 ppb). This demonstrates the supersensitivity for selective TNP detection in aquatic phase, imperative for environmental applications.[8b] The change in the luminescence response for a single crystal of bio-MOF-**1** to TNP could be markedly well-distinguished under confocal microcope (Inset, **Figure. 4.4b**)

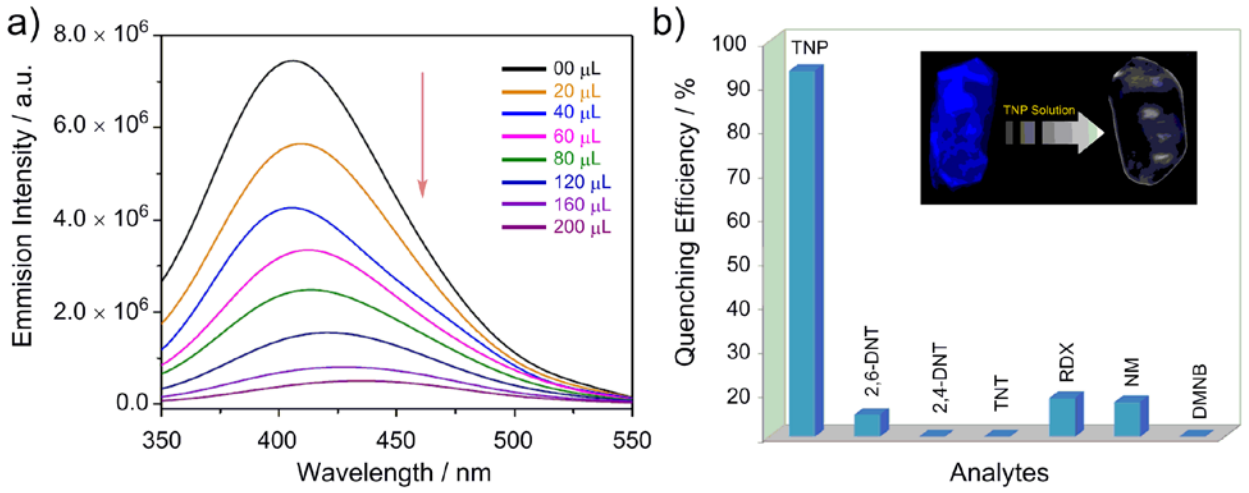

Figure 4.4. (*a) Emission spectra of MOF (**1D**) dispersed in water, upon incremental addition of TNP solution (1mM) in water; (b) Quenching efficiency of bio-MOF-**1** (**1D**) for different nitro analytes. (Inset: Confocal images showing fluorescent to nonfluroscent conversion of single crystal).*

To comprehend the underlying principle behind this observed selectivity of bio-MOF-**1** towards TNP, possible quenching mechanism was comprehensively investigated. In the absence of an unambiguous evidence of TNP loaded MOF crystal due to weak diffraction, a co-crystal of TNP and the functional co-ligand (adenine) was obtained by slow diffusion at room temperature (**Figure. 4.5c**). Single crystal x-ray (SC-XRD) studies revealed that the co-crystal crystallized in Triclinic P_{-1} space group as [(Adenine)(TNP)]·CH_3OH (**Figure. 4.5c, Appendix 4.1**). The free primary amine group of adenine forms a cooperative intermolecular hydrogen bonded complex with TNP, as anticipated from the predicted strategy (**Figure. 4.1c**).

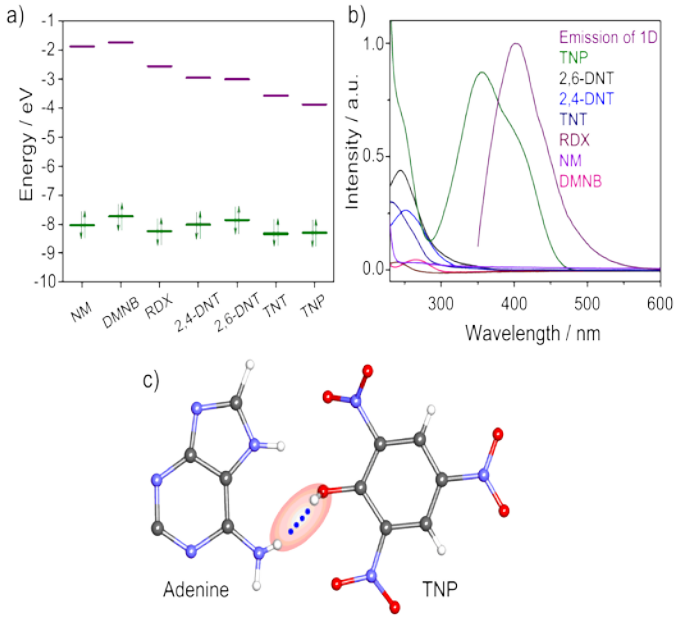

Figure 4.5. (*a) HOMO and LUMO energies of the electron deficient nitro analytes; (b) The spectral overlap-extent between the analyte's absorption band and the emission band of bio-MOF-**1** (**1D**) at rt; (c) SC-XRD structure of the co-crystal revealing intermolecular H-bonding interactions (Color code: Gray, carbon; blue, nitrogen; red, oxygen; white, hydrogen).*

The complexation process and smooth diffusion in the MOF through **1D** channelized pore magnify the host-guest interactions yielding a highly sensitive response. In addition, we sought to understand the rationale behind this extraordinary sensing ability of the compound by examining the electronic features of the concerned molecules. Usually, the conduction band of MOFs lie above those of the LUMO of analytes, allowing a possible photo-induced electron transfer to the electron deficient analytes, consequently resulting in an outstanding fluorescent quenching.[7i] The HOMO-LUMO energies for the employed analytes were calculated by density functional theory using the B3LYP/ 6-31G* method (**Figure. 4.5a, Appendix 4.5**) and the results were in good agreement, supportive of the observed maximum quenching for TNP. The high degree of fluorescence quenching efficiency, when correlated with the corresponding LUMO energies of the analytes suggests that electron transfer is not the sole mechanism behind the remarkable quenching response.

As a matter of fact, when the absorption bands of the non-emissive analytes display considerable overlap with the emission spectra of fluorophore, resonance energy transfer can

effectively occur. Now, energy transfer being a long-range process, the quenching of emission can pass on to the surrounding fluorophores. Henceforth, when energy transfer process gets involved in quenching, the quenching efficiency can undergo a radical upsurge, amplifying the detection sensitivity range as well as selectivity limits. The possibility of resonance energy transfer heavily relies on the spectral overlap-extent between the analyte's absorption band and the emission band of the luminophore. **Figure. 4.5b** presents a large overlap-extent between the absorption spectrum of TNP and the emission spectrum of **1D**, with nearly absent overlap in the cases of RDX, DMNB, NM, and other nitro explosives. To introspect into the quenching mechanism, the quenching constant was calculated and Stern-Volmer (SV) equation was utilized to analyze the quenching efficiency of the analytes. The SV plot demonstrated an upward bending upon incremental addition of TNP, while all other nitro analytes registered linear increases in their respective SV profiles (**Figure. 4.6**). This exclusive nonlinearity of the SV plot for TNP (**Appendix 4.4**) strongly corroborated for the amalgamation of static and dynamic quenching processes or energy transfer phenomena between TNP and MOF. The quenching constant (K_D) for TNP was found to be $4.6\times10^4\ M^{-1}$, as verified by linear fitting of SV plot at low

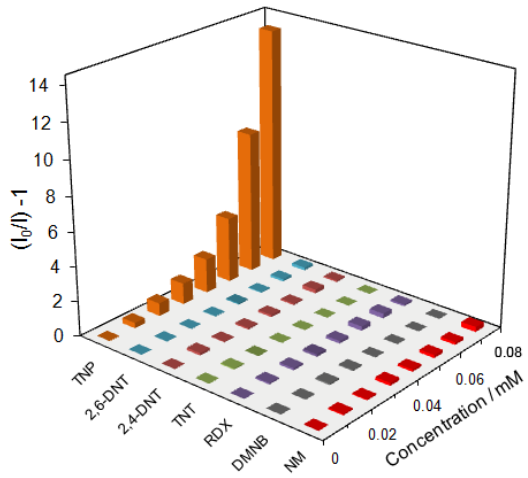

Figure 4.6. *Stern-Volmer plot of various nitro analytes in water.*

concentration range (0-0.04 mM) (**Figure. 4.7a**).[20] This gives an idea about the strong interactions occuring between TNP and bio-MOF-**1**. It is indeed mention-worthy that in the entire MOF regime, this is highest quenching constant value reported till date for selective TNP

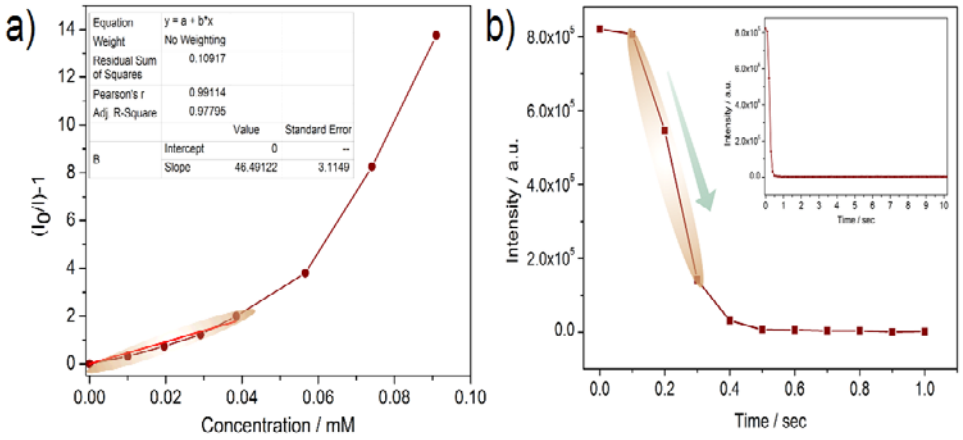

Figure 4.7. (a) *Stern-Volmer (SV) plots for TNP. The relative fluorescence intensity is linear with the PA concentration in the range of 0 – 0.04 mM, I_0/I = 1 + 46.45 ([PA]/mM) (R^2 = 0.978); (b) Fluorescence kinetics of* ***1D*** *in presence of TNP (200μL, 1mM in water) in water (λ_{em}= 405 nm, λ_{ex}= 340 nm) (Inset: Complete kinetic plot up to 10 secs).*

sensing, upholding the superquenching efficiency of **1D** towards TNP.[10f] Enthused from these interesting outcomes, TNP-selectivity in presence of other nitro explosives was thoroughly checked. In a typically designed experimental protocol, the fluorescence spectra for water-dispersed **1D** was monitored with the incremental addition of a saturated aqueous solution of TNT (40 μL in two equally divided batches), to allow high affinity basic sites in the porous channel of **1D** to get accessible to TNT, which resulted in a seemingly insignificant luminescence quenching. Notably, subsequent TNP (40 μL, 1 mM aqueous solution) addition came up with a prompt and significant fluorescence quenching, with a precisely similar trend followed in the following repeat-cycles of TNT and TNP-addition performed in the same sequential manner (**Figure. 4.8a**). Addition of aqueous solutions of the congener nitro analytes followed by TNP to **1D** also revealed an exactly matching trend. This reiterated the unmatched TNP- selectivity observed for **1D**, even in the simultaneous presence of other nitro compounds, when verified in binary analytes combinations. We also verified the sensitivity of TNP quenching in presence of all other nitro-analytes and found similar trend (**Figure. 4.8b**). Therefore, the combined influence of electron transfer and energy transfer processes render the hydrolytcally stable MOF **1D** to exhibit highly selective TNP sensing over all the congener nitro analytes.

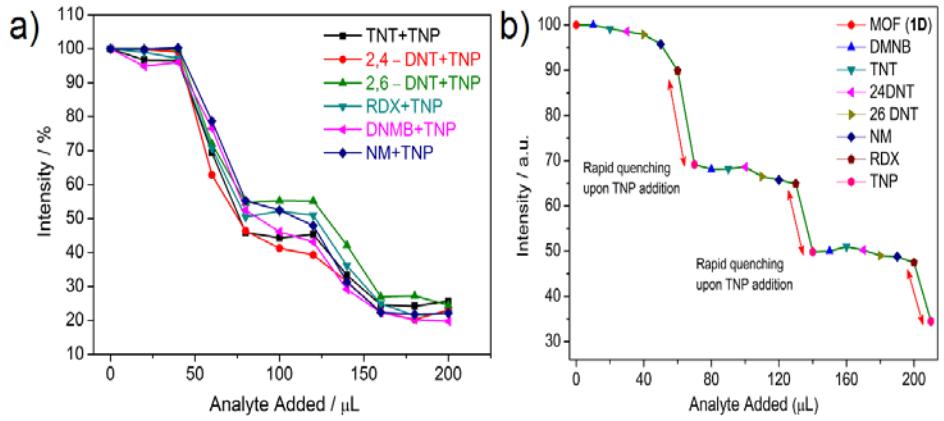

Figure 4.8. *(a) Fluorescence quenching of **1D** upon addition of aqueous solutions of different nitro compounds followed by TNP; (b) Fluorescence quenching of **1D** upon successive addition of aqueous solutions of different nitro compounds (10μL each, 1mM stock solution) in the mixture. Maximum quenching is observed for TNP, even in presence of other nitro analytes .*

Prompt detection of TNP-explosive traces is a major concern from the aspect of national security issue, forensic sciences and environmetal concerns. Furthermore, due to its electron deficient character, the degradation of TNP is very difficult in the biosystem, leading to the unavoidable environmental contamination by this industrial by-product.[8c] To propel the applicability of the compound for real-time sensing, an experiment involving the visual response of the MOF (**1D**) sprinkled on black TLC strips to various nitro-analytes was conducted. As expected, complete darkening in case of TNP was observed upon addition of 2-3 drops of 1 mM TNP solution within 1 min (**Figure. 4.9**). To extrapolate this observation, other nitro analytes

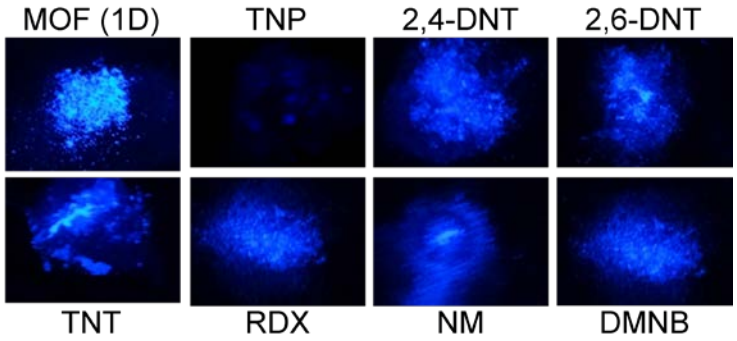

Figure 4.9. *Response of **1D** coated black strip to various analytes in water, monitored under 365 nm UV illumination.*

were added to similar MOF loaded strips. The exceptional luminescence-response of the powdered MOF **1D** towards TNP in this contact mode on black strips (**Figure. 4.9**) reaffirmed the exceptional TNP-selectivity. This fast naked eye detection under UV affords an effective way-out for the proficient detection of TNP, exploiting the presently studied activated phase of bio-MOF-**1** (**1D**) in a realistic scenario as an effective wayout against the harmful effects of this aqueous pollutant. Fluorescence kinetics of **1D** in presence of TNP also supported the prompt fluorescence quenching (**Figure. 4.7b**).

4.4. Conclusion:

In conclusion, the unique amalgamation of amine functionalized porous channels and hydrolytic constancy imparts an exclusive TNP selectivity to the strategically chosen biologically imperative bio-MOF-**1** in aqueous media, even in the concurrent presence of all other nitro analytes. The mutual occurrence of the ionic interactions between primary amine decorated pores and TNP, and favorable electron and energy transfer processes renders bio-MOF-**1** with an unprecedentedly sensitive luminescence quenching efficiency for TNP. Demonstrating the potential of fluorescent MOFs, the present work describes the best results (93% quenching for TNP) for real-time aqueous phase nitro explosive detection in MOF regime aimed at practical security and environmental applications.

4.5. References:

(1) (a) Germain, M. E.; Knapp, M. J. *Chem. Soc. Rev.* **2009**, *38*, 2543 – 2555. (b) Salinas, Y.; -Manez, R. M.; Marcos, M. D.; Sancenon, F.; Castero, A. M.; Parra, M.; Gil, S. *Chem. Soc. Rev.* **2012**, *41*, 1261 – 1296.

(2) (a) Toal, S. J.; Trogler, W. C.; *J. Mater. Chem.* **2006**, *16*, 2871 – 2883. (b) Meaney, M. S.; McGuffin, V. L. *Anal. Bioanal. Chem.* **2008**, *391*, 2557 – 2576.

(3) He, G.; Peng, H.; Liu, T.; Yang, M.; Zhang, Y.; Fang, Y. *J. Mater. Chem.* **2009**, *19,* 7347 – 7353.

(4) (a) Thorne, P. G.; Jenkins, T. F. *Field Anal. Chem.Technol.* **1997**,*1*, 165-170. (b) Wollin, K. M.; Dieter, H. H. *Arch. Environ. Contam.Toxicol.* **2005**, *49*, 18 – 26. (c) Wyman, J. F.;

Serve, M. P.; Hobson, D. W.; Lee, L. H.; Uddin, D. E. *J. Toxicol. Environ. Health Part A* **1992**, *37*, 313 – 327.

(5) Xu, B.; Wu, X.; Li, H.; Tong, H.; Wang, L. *Macromolecules*, **2011**, *44*, 5089 – 5092.

(6) (a) Xin, Y.; Wang, Q.; Liu, T.; Wang, L.; Li, J.; Fang, Y. *Lab Chip* **2012**, *12*, 4821 – 4828. (b) Salinas, Y.; Martínez-Máñez, R.; Marcos, M. D.; Sancenón, F.; Costero, A. M.; Parraad, M.; Gilad, S. *Chem. Soc. Rev.* **2012**, *41*, 1261 – 1296.

(7) (a) Andrew, T. L.; Swager, T. M. *J. Am. Chem. Soc.* **2007**, *129*, 7254 –7255. (b) Hughes, A. D.; Glenn, I. C.; Patrick, A. D.; Ellington, A.; Anslyn, E. V. *Chem. Eur. J.* **2008**, *14*, 1822 – 1827. (c) Gole, B.; Shanmugaraju, S.; Bar, A. K.; Mukherjee, P. S.; *Chem. Commun.* **2011**, *47*, 10046 – 10048. (d) Snow, E. S.; Perkins, F. K.; Houser, E. J.; Badescu, S. C.; Reinecke, T. L. *Science* **2005**, *307*, 1942 – 1945. (e) Cavaye, H.; Shaw, P. E.; Wang, X.; Burn, P. L.; Lo, S. -C.; Meredith, P. *Macromolecules* **2010**, *43*, 10253 – 10261. (f) Kartha, K. K.; Babu, S. S.; Srinivasan, S.; Ajayaghosh, A. *J. Am. Chem. Soc.* **2012**, *134*, 4834 – 4841. (g) Cavaye, H.; Smith, A. R. G.; James, M.; Nelson, A.; Burn, P. L.; Gentle, I. R.; Lo, S. C.; Meredith, P. *Langmuir* **2009**, *25*, 12800 – 12805. (h) Swarnkar, A.; Shanker, G. S.; Nag, A. *Chem. Commun.* **2014**, *50*, 4743-4746. (i) Das, S.; Bharadwaj, P. K. *Inorg. Chem.* **2006**, *45*, 5257-5259.

(8) (a) He, G.; Yan, N.; Yang, J.; Wang, H.; Ding, L.; Yin, S.; Fang, Y. *Macromolecules* **2011**, *44*, 4759–4766. (b) Li, D.; Liu, J.; Kwok, R. T. K.; Liang, Z.; Tang, B. Z.; Yu, J. *Chem. Commun.*, **2012**, *48*, 7167–7169. (c) Xu, Y.; Li, B.; Li, W.; Zhao, J.; Sun, S.; Pang, Y. *Chem. Commun.*, **2013**, *49*, 4764 - 4766. (d) Ding, L.; Bai, Y.; Cao, Y.; Ren, G.; Blanchard, G. J.; Fang, Y. *Langmuir* **2014**, *30*, 7645 −7653.

(9) (a) Keeffe, M. O.; Yaghi, O. M.; *Chem. Rev.* **2012**, *112*, 675 – 702. (b) Wang, C.; Zhang, T.; Lin, W.; *Chem. Rev.* **2012**, *112*, 1084 – 1104. (c) Horcajada, P.; Gref, T.; Baati, P.; Allan, P. K.; Maurin, G.; Couvreur, P.; Ferey, G.; Morris, R. E.; Serre, C. *Chem. Rev*. **2012**, *112*, 1232 – 1268. (d) Dinca, M.; Long, J. R.; *Angew. Chem. Int. Ed.* **2008**, *120*, 6870 – 6884. (e) Lun, D. J.; Waterhouse, G. I. N.; Telfer, S. G. *J. Am. Chem. Soc.* **2011**, *133*, 5806–5809. (f) Horike, S.; Shimomura, S.; Kitagawa, S. *Nat. Chem.* **2009**, *1*, 695 – 704. (g) Henke, S.; Fischer, R. A. *J. Am. Chem. Soc.* **2011**, *133*, 2064 – 2067. (h) Li, S. -L.; Xu, Q. *Energy Environ. Sci.* **2013**, *6*, 1656 – 1683.

(10) (a) Kreno, L. E.; Leong, K.; Farha, O. K.; Allendorf, M.; Duyne, R. P. V.; Hupp, J. T. *Chem. Rev*. **2012**, *112*, 1105 – 1125. (b) Wang, J. -H.; Li, M.; Li, D. *Chem. Sci.* **2013**, *4*, 1793 - 1801. (c) Li, H.; Shi, W.; Zhao, K.; Niu, Z.; Li, H.; Cheng, P. *Chem. Eur. J.* **2013**, *19*, 3358 – 3365. (d) Tian, D.; Li, Y.; Chen, R.-Y.; Chang, Z.; Wang, G.-Y.; Bu, X. -H. *J. Mater. Chem. A*, **2014**, *2*, 1465 – 1470. (e) Zhang, S. -R.; Du, D. -Y.; Qin, J. -S.; Bao, S. -J.; Li, S. -L.; He, W. -W.; Lan, Y. -Q.; Shen, P.; Su, Z. -M. *Chem. Eur. J.* **2014**, *20*, 3589 – 3594. (f) Hu, Z.; Deibert, B. J.; Jing, Li. *Chem. Soc. Rev.* **2014**, *43*, 5815 – 5840. (g) Wang, G. -Y.; Song, C.; Kong, D. -M.; Ruan, W. -J.; Chang, Z.; Li, Y. *J. Mater. Chem. A*, **2014**, *2*, 2213 – 2220. (h) Meilikhov, M.; Furukawa, S.; Hirai, K.; Fischer, R. A.; Kitagawa, S. *Angew. Chem. Int. Ed.* **2013**, *52*, 341 –345.

(11) (a) Nagarkar, S. S.; Joarder, B.; Chaudhari, A. K.; Mukherjee, S.; Ghosh, S. K. *Angew. Chem. Int. Ed.* **2013**, *52*, 2881 – 2885. (b) Zhao, L.; Ye, J.; Li, W.; Bogale, R. F.; Wang, B.; Gong, W.; Ning, G. *Inorg. Chem. Commun*. **2014**, *46*, 212 – 215. (c) Zhou, X. -H.; Li, L.; Li, H. -H.; Li, A.; Yang, T.; Huang, W. *Dalton Trans*. **2013**, *42*, 12403 – 12409. (d) Gong, Y. -N.; Huang, Y. -L.; Jiang, L.; Lu, T. -B. *Inorg. Chem***. 2014**, *53*, 9457 – 9459.

(12) (a) Nagarkar, S. S.; Desai, A. V.; Ghosh, S. K. *Chem. Commun.* **2014**,*50*, 8915 - 8918. (b) Song, X. -Z.; Song, S. -Y.; Zhao, S. -N.; Hao, Z. -M.; Zhu, M.; Meng, X.; Wu, L. -L.; Zhang, H. -J. *Adv. Funct. Mater*. **2014**, *24*, 4034 – 4041.

(13) (a) An, J.; Geib, S. J.; Rosi, N. L. *J. Am. Chem. Soc.* **2009**, *131*, 8376 – 8377. (b) An, J.; Shade, C. M.; Chengelis-Czegan, D. A.; Petoud, S.; Rosi, N. L. *J. Am. Chem. Soc.* **2011**, *133*, 1220 – 1223.

(14) *SAINT Plus*, version 7.03; Bruker AXS Inc.: Madison, WI, 2004.

(15) Sheldrick, G. M. *SHELXTL, Reference Manual*, version 5.1; Bruker AXS Inc.: Madison, WI, *1997*.

(16) Sheldrick, G. M. *Acta Crystallogr., Sect. A* **2008**, 112.

(17) Farrugia, L. *WINGX*, version 1.80.05; University of Glasgow: Glasgow, Scotland, 2009.

(18) Spek, A. L. *PLATON, A Multipurpose Crystallographic Tool*; Utrecht University: Utrecht, The Netherlands, 2005

(19) Yu, J.; Cui, Y.; Xu, H.; Yang, Y.; Wang, Z.; Chen, B.; Qian, G. *Nat. Comm*. **2013**, *4*, 2719.

(20) Luo, W.; Zhu, Y.; Zhang, J.; He, J.; Chi, Z.; Miller, P. W.; Chena, L.; Sua, C. -Y. *Chem. Commun.* **2014**, *50*, 11942 – 11945.

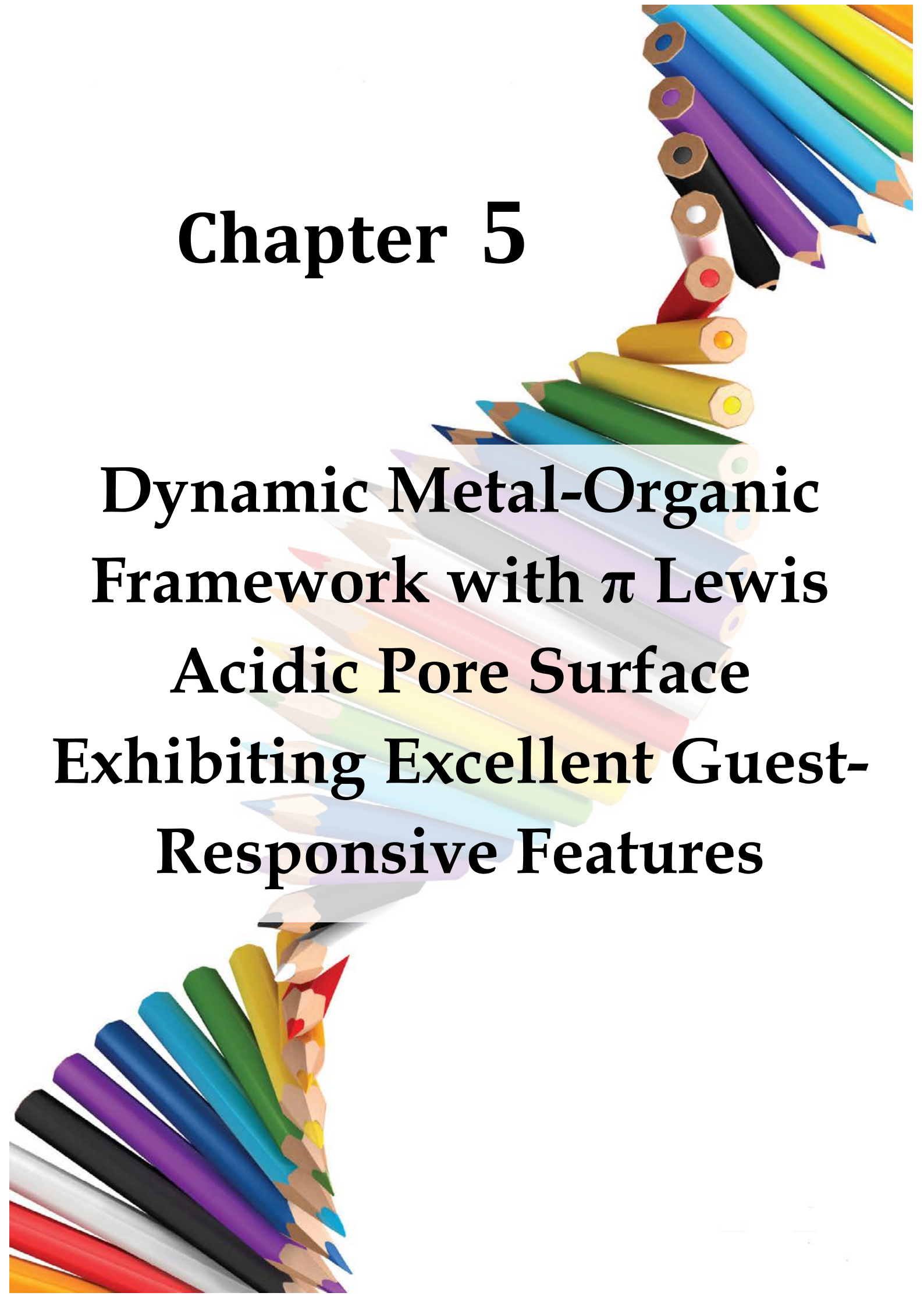

Chapter 5

Dynamic Metal-Organic Framework with π Lewis Acidic Pore Surface Exhibiting Excellent Guest-Responsive Features

5.1. Introduction:

Porous coordination polymers (PCPs) or metal–organic frameworks (MOFs) built from organic linkers and metal ions have been of immense importance for their application in a variety of fields, such as gas storage, chemical separation, drug delivery, and catalysis.[1] In the porous domain, high surface area and large pore size play significant roles. Therefore, extensive efforts have been exerted in designing large and systematically tunable pores of such promising materials. In addition to such a targeted approach, another emerging strategy is the introduction of dynamism to the porous coordination framework, which led to the development of soft porous crystals.[2] Among all types of porous crystalline materials, soft PCPs are a unique class of material, because of their guest-responsive dynamic behavior.[3] Structural flexibility has also been observed in zeolite frameworks but to a lesser extent and very rare,[4] compared to the PCPs. To improve the performance of the dynamic porous frameworks, it is necessary to add extra components to the framework. Integrating pore-surface functionalization along with the inherent bimodality (crystallinity and flexibility) of dynamic porous PCPs may lead us to intelligent host materials capable of providing rigid zeolitic porous properties as well as soft enzyme-like specificity.[5] In spite of the importance and the interest that dynamic PCPs have generated, compounds reported based on functionalized pore surfaces of dynamic PCPs for selective host–guest interaction are rare.[6] Although use of pore surface functionalization in rigid frameworks has been widely explored[7] for chemical separation and storage, examples are lacking in the case of dynamic systems,[8] probably due to the difficulties associated with the proper design and correlation of structural features with properties of such systems. The exploration of such structures is important for the further development of functional porous materials.

With this background, a dynamic coordination framework with an electron-deficient pore surface to achieve separation of structurally similar small molecules, based on a selective host–guest interaction and framework flexibility have been designed. Targeting this, we have synthesized a new ligand containing two flexible aliphatic carboxylic acid units connected by a pyromellitic diimide based electron-deficient core (electron density map, **Appendix 5.1**); this system was chosen to retain a long enough rigid central part to create porosity and flexible units to provide dynamic nature of the expected porous structure. Moreover, Zn^{II} is very cooperative

for making dynamic frameworks, as it exhibits versatile coordination chemistry and can readily adopt tetrahedral and octahedral geometries with four and six coordination numbers.

5.2. Experimental Section:

5.2.1. Synthesis:

5.2.1.1. Ligand Synthesis LH_2: 1,2,4,5- Benzene tetacarboxylic anhydride (BTCA) (2 gm, 9.16 mmol) and L-alanine (1.64 gm, 18.35 mmol) were mixed in glacial acetic acid (AcOH) (60 mL) solvent under N_2 atmosphere. Then the reaction mixture was stirred at 120 °C for overnight. Light yellow solution was concentrated to approximately 15 mL under reduced pressure and diluted with distilled water to get the product as white precipitate. Yield 2.8 gm, 84.8%

^{1}H NMR (400 MHz, DMSO-d_6): δ=1.57(d, J=7.32Hz, 6H), 4.95(q, J=7.32, Hz, 2H), 8.29(s, 2H).

^{13}C NMR (100 MHz, DMSO-d_6): δ= 14.68, 47.54, 117.99, 136.79, 165.46, 170.69. (**Appendix 5.3** and **5.4**)

Anal. Calcd (found) for LH_2 : C, 53.34 (53.30); H, 3.36 (3.39); N, 7.78 (7.76).

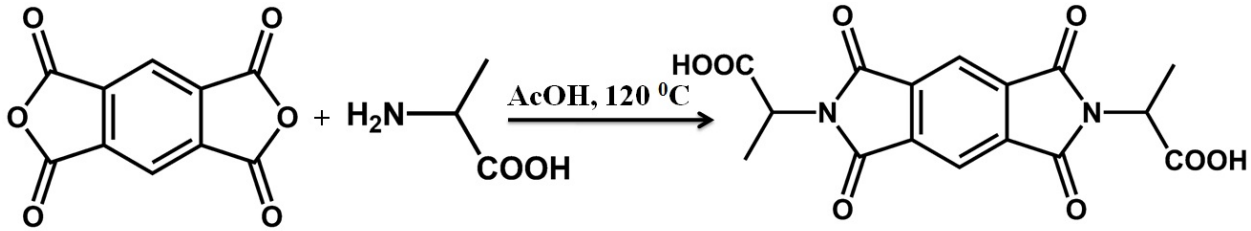

BTCA L-Alanine LH_2

5.2.1.2. Synthesis of $[Zn_2(L)_2(DMF)_2]_n$ (1): LH_2 (18 mg, 0.05 mmol), $Zn(NO_3)_2 \cdot 6H_2O$ (15 mg, 0.05 mmol), DMF (1 mL) and EtOH (1 mL) were placed in a teflon capped glass vial, which was heated at 90 °C for 48h and then cooled to room temperature. Growth of colourless crystals occurred upon cooling to RT, the desired product appeared in ~ 70% yield.

5.2.2. General remarks:

5.2.2.1. Physical measurements: Powder X-ray diffraction (PXRD) patterns were measured on Bruker D8 Advanced X-Ray diffractometer at room temperature using Cu-Kα radiation (λ= 1.5406 Å) with a scan speed of 0.5° min^{-1} and a step size of 0.01° in 2 *theta*. Thermogravimetric analysis was recorded on Perkin-Elmer STA 6000, TGA analyser under N_2 atmosphere with

heating rate of 10 °C/min. The IR-spectra were recorded on a *Thermoscientific*–Nicolet-6700 FT-IR spectrometer. FT-IR spectra were recorded on NICOLET 6700 FT-IR Spectrophotometer using KBr Pellets. Solid state UV-visible spectra were recorded on Perkin-Elmer UV visible spectrometer.

5.2.2.2. X-ray Structural Studies: Single-crystal X-ray data of compound **1** was collected at 200 K on a Bruker KAPPA APEX II CCD Duo diffractometer (operated at 1500 W power: 50 kV, 30 mA) using graphite-monochromated Mo-Kα radiation (λ = 0.7107Å[3]). Crystal was on nylon Cryo Loops (Hampton Research) with Paraton-N (Hampton Research). The data integration and reduction were processed with SAINT[9] software. A multi-scan absorption correction was applied to the collected reflections. The structure was solved by the direct method using SHELXTL[10] and was refined on *F2* by full-matrix least-squares technique using the SHELXL-97[11] program package within the WINGX[12] programme. All non-hydrogen atoms were refined anisotropically. All hydrogen atoms were located in successive difference Fourier maps and they were treated as riding atoms using SHELXL default parameters. The structures were examined using the *Adsym* subroutine of PLATON[13] to assure that no additional symmetry could be applied to the models. **Appendix 5.2** contains crystallographic data for the **1** (CCDC-964583 contains the supplementary crystallographic data for this thesis. These data can be obtained free of charge from The Cambridge Crystallographic Data Centre via www.ccdc.cam.ac.uk/data_request/cif.).

5.2.2.3. Low Pressure Gas Sorption Measurements: Low pressure gas and solvent sorption measurements were performed using BelSorpmax (Bel Japan). All of the gases used were of 99.999% purity. As-synthesized compound was heated at 180 °C under vacuum for 8 hrs to get guest free compound **1D**. Prior to adsorption measurement the guest free sample **1D** was pretreated at 150 °C under vacuum for 5 hrs using BelPrepvacII and purged with N_2 on cooling.

5.2.2.4. NMR study of Guest-included phases: Compound **1D** was exposed to vapors of different guests, digested with DCl and all the organic components were dissolved in DMSO-d_6 for ^{1}H and ^{13}C NMR experiments.

5.2.2.5. Electron density plot for Ligand (LH_2): Electrostatic potential surface calculation was performed with the *Gaussian09 Rev D* program suite using Density functional theory (DFT) with

Becke's three-parameter hybrid exchange functional and the Lee-Yang-Parr correlation functional (B3LYP) and 6-31G(d,p) basis set.

5.3. Result and discussions:

In this chapter, we report a new Zn^{II}-based three-dimensional (3D) dynamic coordination framework with a π-electron-deficient pore surface and an active metal center capable of demonstrating a selective host–guest interaction for chemical separation (especially, commercially important benzene/cyclohexane separation)[5a,16] based on pore surface functionalization and framework flexibility (*Scheme 5.1*).

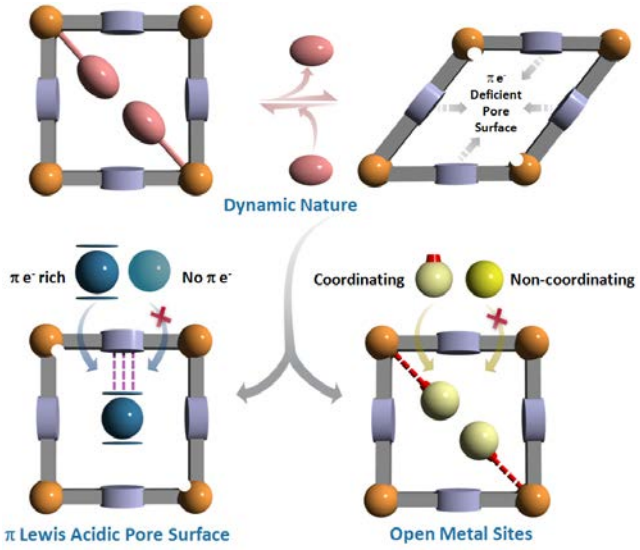

Scheme 5.1. *Schematic representation of guest-responsive function for a dynamic MOF.*

The 3D framework $[Zn_2L_2(DMF)_2]_n$ (**1**) was synthesized by solvothermal reaction of $Zn(NO_3)_2 \cdot 6H_2O$ with a newly designed ligand LH_2 in a solvent mixture of DMF/EtOH (1:1) at 90 °C for 48 h. Single crystal X-ray diffraction studies revealed that compound **1** crystallized in the monoclinic non-centrosymmetric space group $P2_1$ (**Appendix 5.2**). The asymmetric unit contains two independent Zn^{2+} ions, two L units, and two coordinated DMF molecules. The Adsym subroutine of PLATON was employed to confirm that no additional symmetry could be applied to the model. The two Zn^{2+} ions present in the asymmetric unit are entirely different in their coordination environments. Zn1 has a tetrahedral geometry with an O4 donor set from four different carboxylate groups of the ligand, whereas the other metal ion (Zn2) displays octahedral

geometry with an O6 donor set from four different carboxylate groups and two coordinated DMF molecules (**Appendix 5.3**). Zn1 and Zn2 are bridged by three carboxylate groups to give a dimeric unit, and each dimeric unit is connected on both sides to other dimeric units via carboxylate groups leading to a metal carboxylate chain along the a axis. The other side of the carboxylate group of the ligands is connected to similar metal carboxylate chains resulting in a 3D porous coordination polymer. The resultant 3D framework is nonporous in nature but if coordinated DMF solvents are omitted, then it shows narrow unsymmetrical **1D** channel along the a axis (**Figure 5.1**).

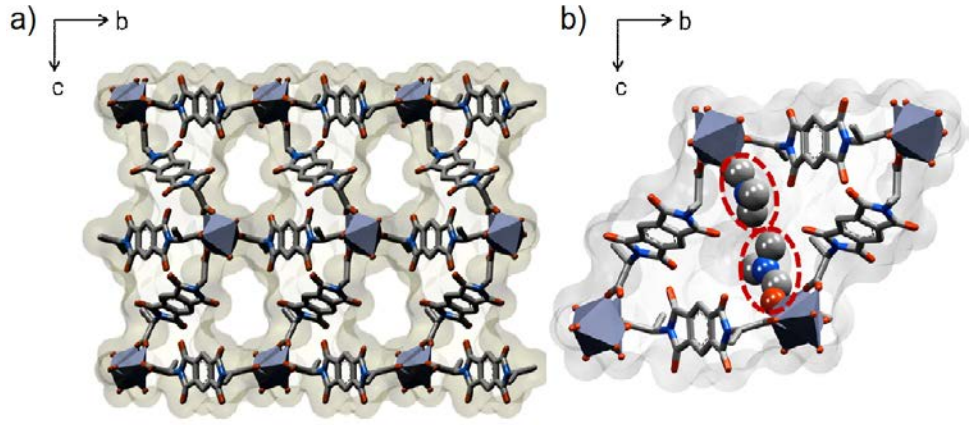

Figure 5.1. (*a) View of structural motifs found in the single-crystal structure of compound **1** along the a axis; (b) Surface view of compound **1** along the* a *axis. The hydrogen atoms and solvent molecules (for a) are omitted for clarity.*

The powder X-ray diffraction (PXRD) pattern of compound **1** matched with the simulated pattern, indicating phase purity of the bulk sample (**Figure 5.2a**). Thermogravimetric analysis (TGA) under an N_2 atmosphere indicates a weight loss of approximately 15.1% at around 220 °C, which corresponds to two coordinated DMF molecules (calcd 14.9%) per formula unit (**Figure 5.2b**). Variable-temperature powder X-ray diffraction (VT-PXRD) analysis clearly shows that compound **1** underwent a phase transition after 120 °C, with retention of crystallinity (**Appendix 5.6**). The desolvated phase of compound **1** (**1D**) was obtained by heating it at 180 °C under vacuum for 8h. The TGA curve of compound **1D** shows no significant weight loss up to 400 °C, suggesting complete loss of coordinated DMF molecules (**Figure 5.2b**). The PXRD pattern of **1D** is different from that of the as-synthesized phase **1**. The crystalline nature

from the PXRD pattern of the desolvated phase **1D** indicates that a large structural transformation occurred upon desolvation (**Figure 5.2a**).

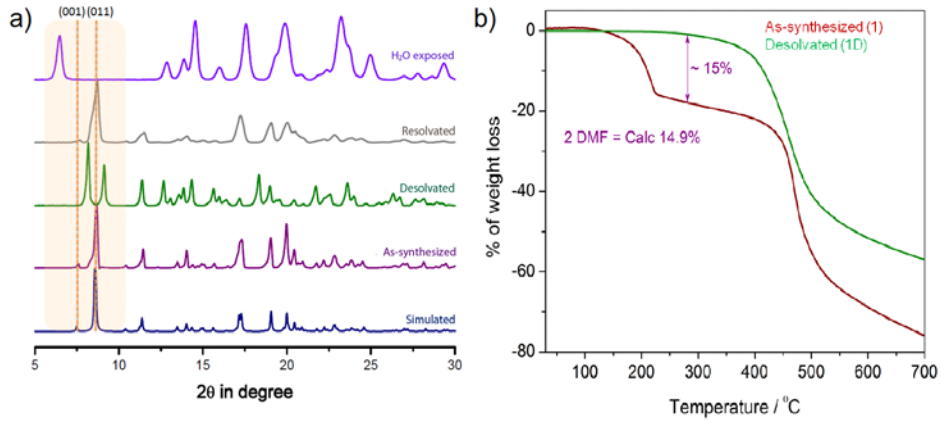

Figure 5.2. *(a) PXRD patterns of the simulated, as-synthesized (**1**), desolvated (**1D**), resolvated, and H_2O-exposed compounds; (b) Thermogravimetric analysis (TGA) data for the as-synthesized (**1**; wine colour) and de-solvated (**1D**; olive colour) compound.*

The PXRD data of **1D** was indexed with the program TREOR90 using the first twenty observed Bragg reflection patterns. The best solution indicated a monoclinic cell with a=12.98 Å, b=19.48 Å, c=4.9 Å, β=94.648 Å, and V= 1492 $Å^3$. Statistical analysis of the powder data using the FINDSPACE module of EXPO2009[15] indicated the most probable space group to be P*21/a*. The reduced unit cell parameters indicate the squeezing of the framework on desolvation. When compound **1D** was exposed to DMF vapor for two days, the original framework was restored, as confirmed from the PXRD pattern (**Figure 5.2a**). PXRD data of the resolvated sample showed significant broadening, which is attributed to the fundamental heterogeneity/disorder created by the dynamic pore opening/closing event, or might also result from loss of crystallinity. Interestingly, when the desolvated phase was exposed to air, the PXRD pattern of the desolvated phase started to change. We exposed the desolvated phase to water vapor for two days to drive the reaction to complete transformation and found a stable new phase (**1W**). The highly unstable nature of the desolvated phase in open air is indicative of the strong hydrophilic nature upon removal of the coordinated DMF solvent and consequent generation of open metal sites. Although the two new phases are highly crystalline in nature, unfortunately due to weak diffraction of the single crystals, the structures of the two new phases (**1D** and **1W**) could not be

obtained. The desolvated phase **1D** showed a similar result when it was exposed to other coordinating solvents such as MeOH and EtOH, which has been confirmed from PXRD, TGA, and solvent sorption studies (**Appendix 5.7 and 5.8**). Notably, the water sorption profile showed interesting results: after inclusion of two water molecules it showed a clear step and further inclusion of ~10 molecules of water per formula unit with a large hysteresis profile (**Appendix 5.9**). Thus, the above observations indicate that the framework is highly dynamic in nature and can exist in different crystalline phases (**1**, **1D**, **1W** and **1D**solvent).

The generation of accessible open metal sites as well as the flexibility of the framework (**1D**) impelled us to explore the host–guest interactions inside the pore.[14] Therefore, detailed sorption experiments were performed to study the effect of structural transformations with different adsorptive probes. Compound **1D** exhibited differential adsorption behavior towards N_2 (77 K), CO_2 (195 K), and CH_4 (195 K) (**Figure 5.3a**). The adsorption isotherms for N_2, CO_2, and

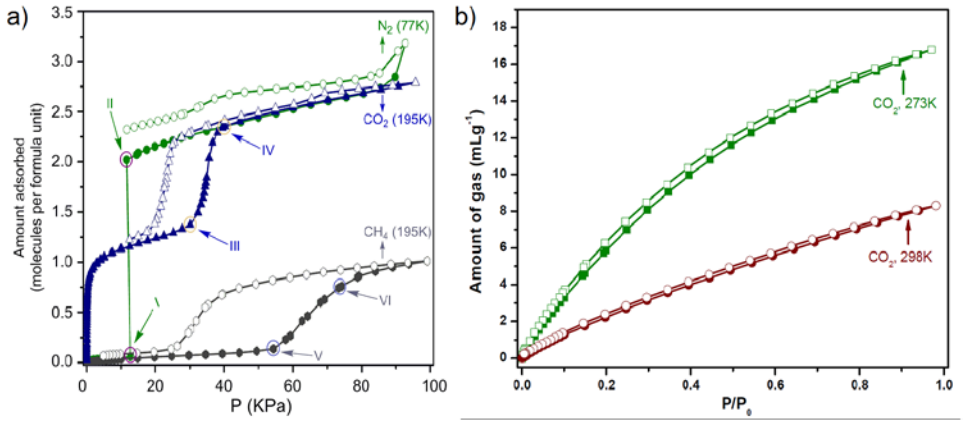

Figure 5.3. *(a) and (b) Gas sorption isotherms of **1D** at various temperatures. Closed and open symbols denote adsorption and desorption, respectively.*

CH_4 are characterized by gate-opening-type adsorption, which is a typical characteristic of a flexible framework.[2a] In the case of N_2 (kinetic diameter = 3.6 Å) adsorption at 77 K, the uptake is 85 mLg^{-1}, which corresponds to three molecules of N_2 per formula unit. Interestingly, the adsorption profile shows an opening step at a pressure P of ~13 kPa, followed by a sudden increase in uptake (Point I–II in **Figure 5.3a** corresponding to two molecules of N_2 per formula unit), and subsequently reaching a saturation limit (three molecules of N_2 per formula unit), followed by desorption with a little hysteresis. But in case of CO_2 (3.3 Å), the adsorption profile

showed a Type-I curve up to P=28 kPa (Point III) followed by a stepwise rise (via point IV, P=40 kPa followed by desorption with hysteresis. The initial one-molecule CO_2-uptake (28 mLg^{-1}) (**Figure 5.3a**) is probably due to size-dependent inclusion, whereas the consequent stepwise increase in CO_2-adsorption to finally accommodate 2.7 CO_2 molecules per formula unit (74 mLg^{-1}) is attributed to a "breathing effect".[2a] A similar gate-opening-type adsorption with a hysteresis curve was observed for CH_4 (3.76 Å) at 195 K with an adsorption of 27 mLg^{-1}, which corresponds to an uptake of one molecule of CH_4 per formula unit. The isosteric heat of adsorption for CO_2 is found to be 38.5 $kJmol^{-1}$ for low loading, as measured from CO_2 adsorption data plots at 273 K and 298 K. Due to irregular shape of the channels, the exact pore dimensions of the framework could not be ascertained.

From the application-perspective, the separation of liquid phase hydrocarbons, especially those having similar physical properties and comparable molecular sizes is highly challenging for industrial applications. In this context, separation of benzene and cyclohexane is a pressing issue, since cyclohexane is usually produced by hydrogenation of benzene in the petrochemical industry.[16] This inherent difficulty arises due to similar boiling points (benzene, 80.1 °C and cyclohexane, 80.7 °C), related molecular geometry, and comparable Lennard- Jones collision diameters.[5a] Our strategic π-electron-deficient ligand[17] designing approach was aimed at exploring the performance of **1D** for benzene/cyclohexane separation. Vapor sorption experiments for both of these solvents were carried out at 298 K. Remarkably, the sorption

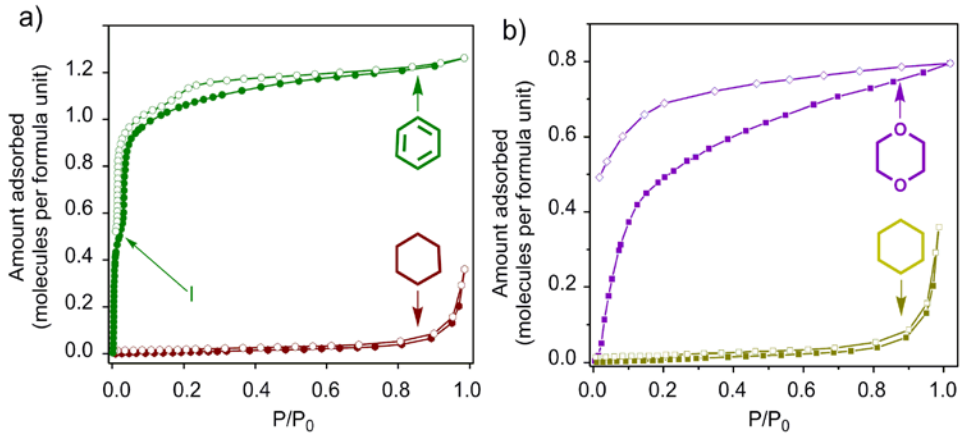

Figure 5.4. *Solvent sorption isotherms of **1D** at 298 K for (a) benzene and cyclohexane, and (b) dioxane and cyclohexane. Closed and open symbols denote adsorption and desorption, respectively.*

profile of benzene shows a gradual increase of uptake up to P/P_0=0.02 (Point I in **Figure 5.4a**)

and exhibits a small step at this point, which is related to a small structural change accompanied by an interesting structural transformation (verified from PXRD patterns of exposed samples, **Figure 5.5**). The driving force to open the structure could be the presence of higher affinity π-π interactions between the pore surface and guest molecules. The amount of benzene- uptake is 0.5 molecules per formula unit at point-I, followed by another 0.5 molecule uptake via pore-opening till it reaches saturation point. Interestingly, although cyclohexane has a similar molecular geometry and other physical properties, no adsorption of cyclohexane occurs even in the higher pressure region. This can be attributed to the favorable donor–acceptor π-π interactions occurring between the π-electron-deficient pore surface of the framework and the π-cloud of benzene along with the cooperative effect of structural flexibility. Since cyclohexane has no π electron, it cannot interact strongly with the pore surface to enter into the channels. We also performed other studies to get further support for this. In a typical experiment, when **1D** was exposed to benzene vapor and cyclohexane vapor separately at room temperature for two days, the PXRD patterns of the benzene-exposed sample and **1D** differed considerably, but the pattern for the cyclohexane-exposed sample remained the same as that of **1D** (**Figure 5.5**). These samples were digested with

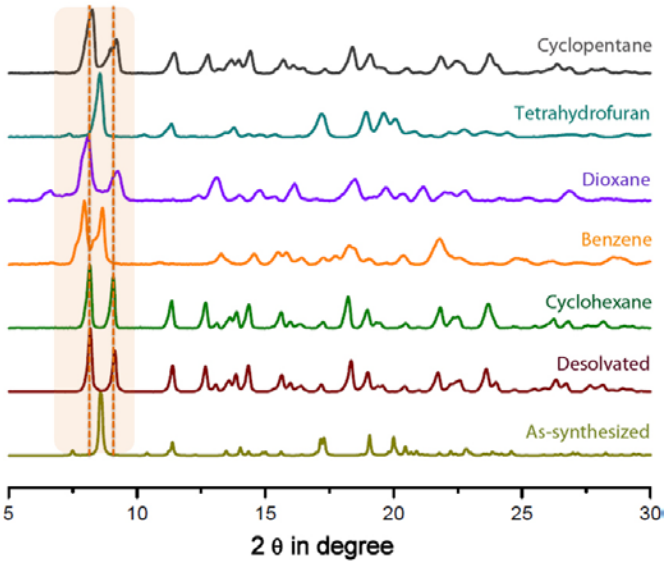

Figure 5.5. *PXRD patterns of **1**, desolvated (**1D**), and solvent vapor-exposed phases (cyclohexane, benzene, dioxane, THF, and cyclopentane) (**1D**⊃ solvent).*

DCl, and dissolved in [D_6]DMSO to confirm the presence of the respective guests, included inside the framework by NMR experiments. ^{1}H and ^{13}C NMR spectra conclusively proved the

presence of benzene molecules and simultaneously the absence of cyclohexane molecules, after vapor-exposure (**Figures 5.6**). In support to the role of π-π interactions, UV/Vis spectra for benzene, cyclohexane-exposed samples, and **1D** were recorded. The absorption spectra show a

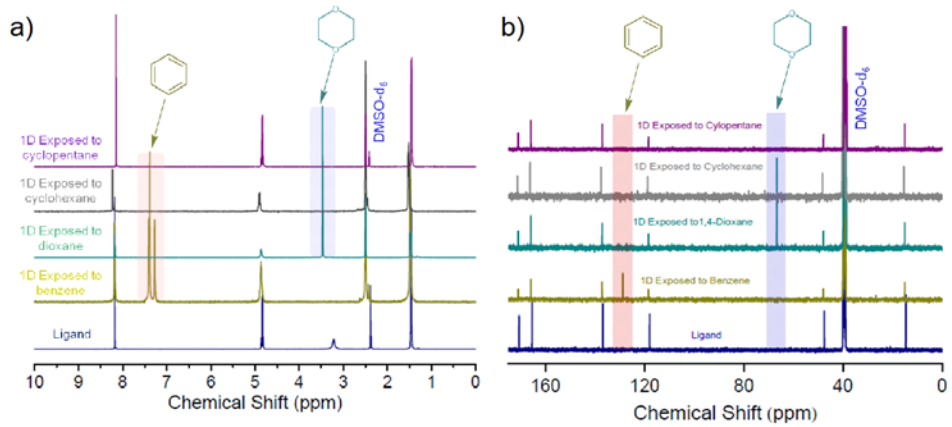

Figure 5.6. (a) *^{1}H-NMR and (b) ^{13}C-NMR spectra of various solvent vapor-exposed phases of $[Zn_2L_2]$ (**1D**). Solvent vapor was exposed for 48h to the phase **1D,** before digesting in DCl/DMSO- d_6.*

prominent shift of the absorption band due to benzene inclusion in host **1D** (**Appendix 5.11**). Notably, when we used a mixture of benzene cyclohexane vapor (ratio 1:1) it also gave the same results. Sorption experiments on toluene, *p*-xylene, *o*-xylene, and *m*-xylene were also carried out and the results reflected the inclusion of π-electron- rich guests within the pores of the framework (**Figure 5.6a** and **Appendix 5.10**).

Additionally, to check the influence of open metal sites on the sorption profiles for coordinating and non-coordinating guest probe solvents, sorption experiments on dioxane and alcohols (MeOH, EtOH, and 2-propanol) were executed at 298 K. Remarkably, 0.8 molecules of dioxane uptake per formula unit is observed in the adsorption profile of dioxane with hysteresis (**Figure 6.4b**), supporting the efficiency of **1D** for dioxane accommodation (also verified from ^{1}H and ^{13}C NMR spectroscopy, as previously done, **Figure 5.6**). This selective adsorption of dioxane over cyclohexane (although both have comparable sizes, **Appendix 5.12**) is attributed to the possible coordination of dioxane solvent molecules to the coordinatively unsaturated Zn^{2+} sites present in the host framework. The sorption for alcohols (MeOH, EtOH, and 2-propanol) at 298 K shows inclusion (adsorption of MeOH > EtOH > 2-propanol) with hysteresis (**Appendix**

5.7). This can be ascribed to the formation of adequate host–guest (Zn^{2+}···O of alcohol and O···H-O of alcohol) and guest–guest interactions coupled with favorable H-bonding interactions along with framework flexibility of the dynamic framework.

To verify this dual functionality, we further studied the sorption properties for THF and cyclopentane at 298 K (**Figure 5.6b**). Sorption profiles indicate 3.6 molecules (97 mLg^{-1}) of

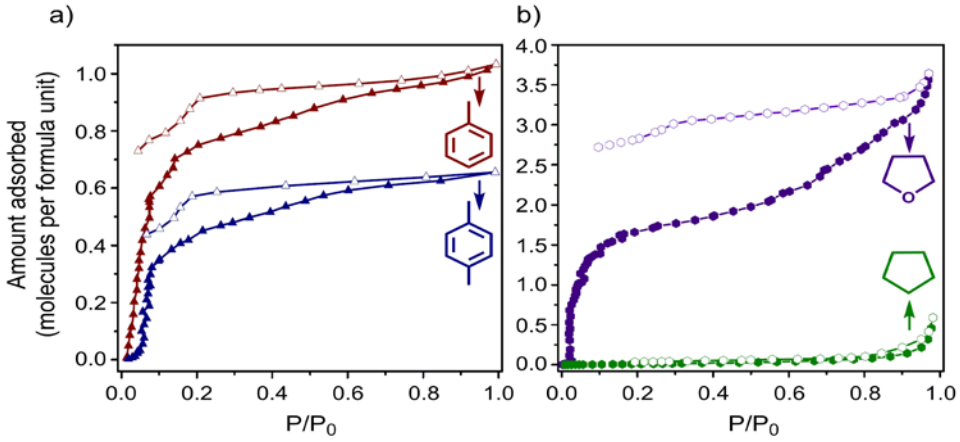

Figure 5.7. *Solvent sorption isotherms of 1D at 298 K for (a) toluene and p-xylene, and (b) THF and cyclopentane. Closed and open symbols denote adsorption and desorption, respectively.*

THF uptake per formula unit with hysteresis, but almost no uptake of cyclopentane. Irrespective of their very similar dimensions (kinetic diameter, **Appendix 5.12**), this differential response towards THF and cyclopentane can only be attributed to the presence of donor sites in THF. PXRD patterns (**Figure 5.5**) were recorded after exposing to different guest solvents reconfirmed the structural dynamism after guest inclusion. Hence, structural flexibility, favorable donor–acceptor π-π interactions, and the presence of open metal sites are three crucial factors that play individual roles in determining the selective guest accommodation inside the porous framework.

5.4. Conclusion:

In conclusion, we have successfully synthesized a dynamic 3D coordination framework with an electron-deficient pore surface using a predesigned biomolecule based diimide π-electron-deficient flexible ligand and Zn^{II} metal ions, showing chemical separations based on pore surface functionalization and framework flexibility. A combined influence of the structural flexibility, electronic interaction between guest and polar pore surface, and the effect of open metal sites resulted in selective sorption of aromatic solvents (benzene, toluene, and xylenes) of similar or

bigger size over cyclic aliphatic solvents (cyclohexane and cyclopentane) and also coordinating over non-coordinating solvents of similar size. In particular, the unique combination of flexible nature and polar surface present in this framework enables it to exhibit selective uptake of benzene over cyclohexane in mixtures of the two, making it a strategically designed guest-responsive material. Further exploration of this type of materials might result in important industrial applications for chemical separation.

5.5. References:

(1) (a) Keeffe, M. O.; Yaghi, O. M. *Chem. Rev.* **2012**, *112*, 675–702. (b) Wang, C.; Zhang, T.; Lin, W. *Chem. Rev.* **2012**, *112*, 1084–1104. (c) Nagarkar, S. S.; Joarder, B.; Chaudhari, A. K.; Mukherjee, S.; Ghosh, S. K. *Angew. Chem., Int. Ed.* **2013**, *52*, 2881-2885. (d) Suh, M. P.; Park, H. J.; Prasad, T. K.; Lim, D. –W. *Chem. Rev.* **2012**, *112*, 782–835. (e) Li, J. –R.; Sculley, J.; Zhou, H. –C. *Chem. Rev*. **2012**, *112*, 869–932. (f) Horcajada, P.; Gref, R.; Baati, T.; Allan, P. K.; Maurin, G.; Couvreur, P.; Ferey, G.; Morris, R. E.; Serre, C. *Chem. Rev*. **2012**, *112*, 1232–1268. (g) Yoon, M.; Srirambalaji, R.; Kim, K. *Chem. Rev*. **2012**, *112*, 1196–1231. (h) Furukawa, H.; Ko, N.; Go, Y. B.; Aratani, N.; Choi, S. B.; Choi, E.; Yazaydin, A. Ö.; Snurr, R. Q.; O'Keeffe, M.; Kim, J.; Yaghi, O. M. *Science*, **2010**, *329*, 424-428. (i) Ma, L.; Falkowski, J. M.; Abney, C.; Lin, W. *Nat. Chem*. **2010**, *2*, 838-846. (j) Dinca, M.; Long, J. R. *Angew. Chem. Int. Ed.* **2008**, *120*, 6870-6884. (k) Li, G.; Yu, W.; Cui, Y. J. *J. Am. Chem. Soc.* **2008**, *130*, 4582-4583. (l) Moggach, S. A.; Bennett, T. D.; Cheetham. A. K. *Angew.Chem. Int. Ed*. **2009**, *48*, 7087-7089. (m) An, J.; Geib, S. J.; Rosi, N. L. *J. Am. Chem. Soc*. **2009**, *131*, 8376–8377. (n) Xiang, S.; Zhou, W.; Gallegos, J. M.; Liu, Y.; Chen, B. *J. Am. Chem. Soc.*, **2009**, *131*, 12415–12419. (o) Zhang, J. -P.; Chen, X. –M. *J. Am. Chem. Soc*. **2008**, *130*, 6010–6017. (p) Nagarathinam, M.; Vittal, J. J. *Angew. Chem. Int. Ed*. **2006**, *45*, 4337–4341. (q) Lun, D. J.; Waterhouse, G. I. N.; Telfer, S. G. *J. Am. Chem. Soc.* **2011**, *133*, 5806– 5809.

(2) (a) Horike, S.; Shimomura, S.; Kitagawa, S. *Nat. Chem*. **2009**, *1*, 695-704. (b) Ghosh, S. K.; Bureekaew, S.; Kitagawa, S. *Angew. Chem. Int. Ed*. **2008**, *47*, 3403 –3406.

(3) (a) Rabone, J.; Yue, Y. -F.; Chong, S. Y; Stylianou, K. C.; Bacsa, J.; Bradshaw, D.; Darling, G. R.; Berry, N. G.; Khimyak, Y. Z.; Ganin, A. Y.; Wiper, P.; Claridge, J. B.; Rosseinsky,

M. J. *Science* **2010**, *329*, 1053-1057. (b) Serre, C.; Mellot-Draznieks, C.; Surblé, S.; Audebrand, N.; Filinchuk, Y.; Férey, G. *Science*, **2007**, *315*, 1828-1831.

(4) Sartbaeva, A.; Wells, S. A.; Treacy, M. M. J.; Thorpe, M. F. *Nature*, **2006**, *5*, 962-965.

(5) (a) Shimomura, S.; Horike, S.; Matsuda, R.; Kitagawa, S. *J. Am. Chem. Soc.*, **2007**, *129*, 10990–10991. (b) Yanai, N.; Uemura, T.; Inoue, M.; Matsuda, R.; Fukushima, T.; Tsujimoto, M.; Isoda, S.; Kitagawa, S. *J. Am. Chem. Soc.* **2012**, *134*, 4501−4504.

(6) (a) Sato, H.; Matsuda, R.; Sugimoto, K.; Takata, M.; Kitagawa, S. *Nat. Mater,* **2010**, *9*, 661-666. (b) Park, J.; Yuan, D.; Pham, K. T.; Li, J.-R.; Yakovenko , A.; Zhou, H. –C. *J. Am. Chem. Soc.*, **2012**, *134*, 99–102.

(7) (a) Demessence, A.; D'Alessandro, D. M.; Foo, M. L.; Long, J. R. *J. Am. Chem. Soc.* **2009**, *131*, 8784–8786. (b) Zhang, Z.; Gao, W. –Y.; Wojtas, L.; Ma, S.; Eddaoudi, M.; Zaworotko, M. J. *Angew. Chem. Int. Ed.* **2012**, *51*, 9330–9334. (c) Mulfort, K. L.; Farha, O. K.; Stern, C. L.; Sarjeant, A. A.; Hupp, J. T. *J. Am. Chem. Soc.* **2009**, *131*, 3866–3868.

(8) (a) Devic, T.; Salles, F.; Bourrelly, S.; Moulin, B.; Maurin, G.; Horcajada, P.; Serre, C.; Vimont, A.; Lavalley. J. –C.; Leclerc, H.; Clet, G.; Daturi, M.; Llewellyn, P. L.; Filinchuk, Y.; Ferey, G.; *J. Mater. Chem.* **2012,** *22*, 10266-10273. **(**b) Biswas, S.; Ahnfeldt, T.; Stock, N.; *Inorg. Chem.* **2011**, *50*, 9518–9526. (c) Wang, Z.; Cohen, S. M. *J. Am. Chem. Soc.***2009,** *131*, 16675–16677.

(9) *SAINT Plus*, version 7.03; Bruker AXS Inc.: Madison, WI, 2004.

(10) Sheldrick, G. M. *SHELXTL, Reference Manual*, version 5.1; Bruker AXS Inc.: Madison, WI, *1997*.

(11) Sheldrick, G. M. *Acta Crystallogr., Sect. A* **2008**, 112.

(12) Farrugia, L. *WINGX*, version 1.80.05; University of Glasgow: Glasgow, Scotland, 2009.

(13) Spek, A. L. *PLATON, A Multipurpose Crystallographic Tool*; Utrecht University: Utrecht, The Netherlands, 2005.

(14) (a) Chen, B.; Yang, Y.; Zapata, F.; Lin, G.; Qian, G.; Lobkovsky, E. B. *Adv. Mater.* **2007**, *19*, 1693–1696. (b) Zhang, Z.; Xiang, S.; Rao, X.; Zheng, Q.; Fronczek, F. R.; Qian, G.; Chen, B. *Chem. Commun.*, **2010**, *46*, 7205–7207. (c) Majumder, M.; Sheath, P.; Mardel, J. I.; Harvey, T. G.; Thornton, A. W.; Gonzago, A.; Kennedy, D. F.; Madsen, I.; Taylor, J. W.; Turner, D. R.; Hill, M. R. *Chem. Mater*. **2012**, *24*, 4647−4652.

(15) Altomare, A.; Giacovazzo, C.; Guagliardi, A.; Moliterni, A. G. G.; Rizzi, R.; Werner, E. J. *Appl. Crystallogr.* **2000**, *33*, 1180−1186.

(16) Bai, Y. X.; Qian, J. W.; Zhao, Q.; Xu, Y.; Ye, S. R. *J. Appl. Polym. Sci.* 2006, *102, 2832-2838.*

(17) (a) Yoshizawa, M.; Kusukawa, T.; Kawano, M.; Ohhara, T.; Tanaka, I.; Kurihara, K.; Niimura, N.; Fujita, M. *J. Am. Chem. Soc.* **2005**, *127*, 2798-2799. (b) Tanaka, D.; Masaoka, S.; Horike, S.; Furukawa, S.; Mizuno, M.; Endo, K.; Kitagawa, S. An*gew. Chem. Int. Ed.* **2006**, *45*, 4628-4631.

(18) (a) Shao, P.; Huang, R.Y.M. *Journal of Membrane Science* **2007**, *287*, 162–179; (b) Lu, J.; Liu, N.; Li, L.; Lee, R. *Separation and Purification Technology* **2010**, *72*, 203–207.

Appendix

2.6. Appendix:

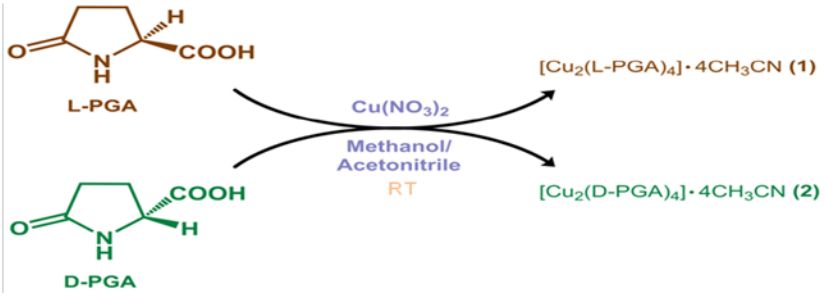

Appendix 2.1: Synthetic scheme of compounds **1** and **2**.

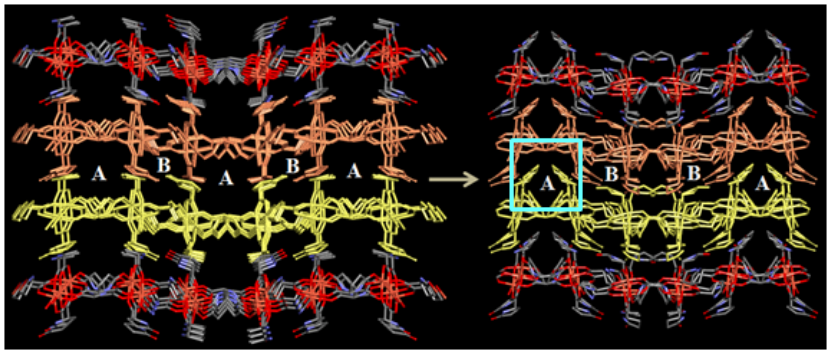

Appendix 2.2: Structural transformation from a bi- to tri-porous framework.

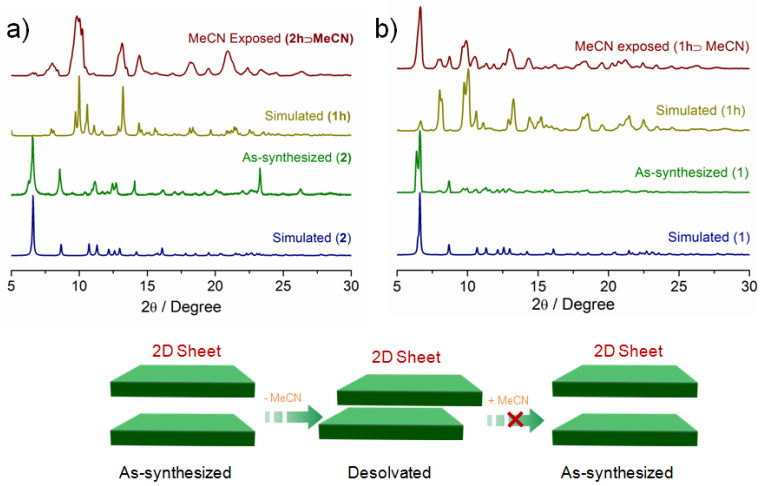

Appendix 2.3: Test for reversibility on MeCN exposure , monitored by PXRD analyses, (left) compound **1** and (right) for compound **2**.

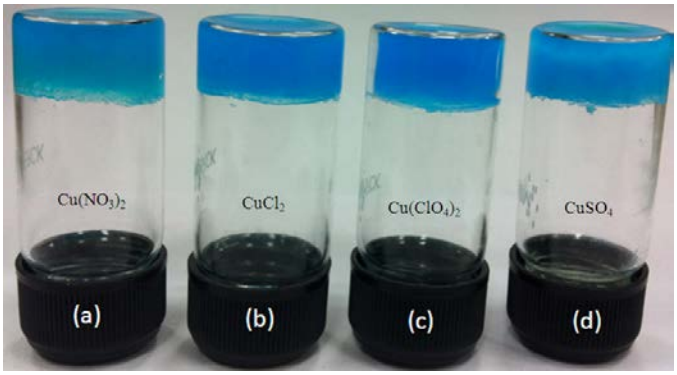

Appendix 2.4: Metallogels upon combining Cu^{II} salt and L-PGA, (a) gel **1** [L-PGA+ $Cu(NO_3)_2$]**;** (b) gel **2** [L-PGA+ $CuCl_2$]**;** (c) gel **3** [L-PGA+ $Cu(ClO_4)_2$]**;** (d) gel **4** [L-PGA+ $CuSO_4$].

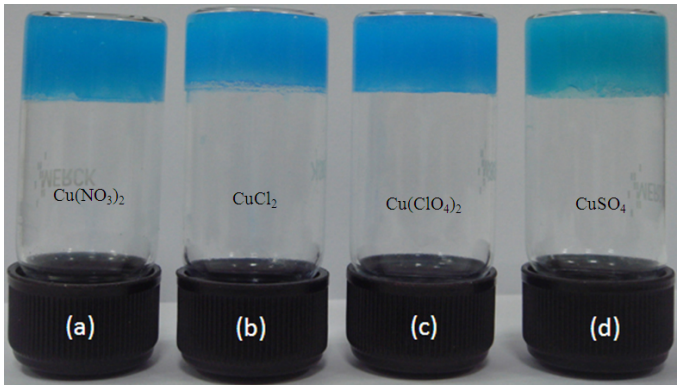

Appendix 2.5: Metallogels upon combining Cu^{II} salt and D-PGA, (a) gel **5** [D-PGA+ $Cu(NO_3)_2$]**;** (b) gel **6** [D-PGA+ $CuCl_2$]**;** (c) gel **7** [D-PGA+ $Cu(ClO_4)_2$]**;** (d) gel **8** [D-PGA+ $CuSO_4$].

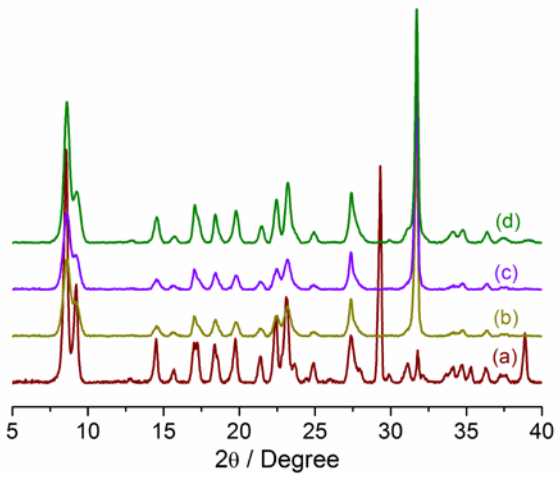

Appendix 2.6: Powder X-ray diffraction (PXRD) patterns of. a) gel **1** b) gel **2** c) gel **5** d) gel **6**.

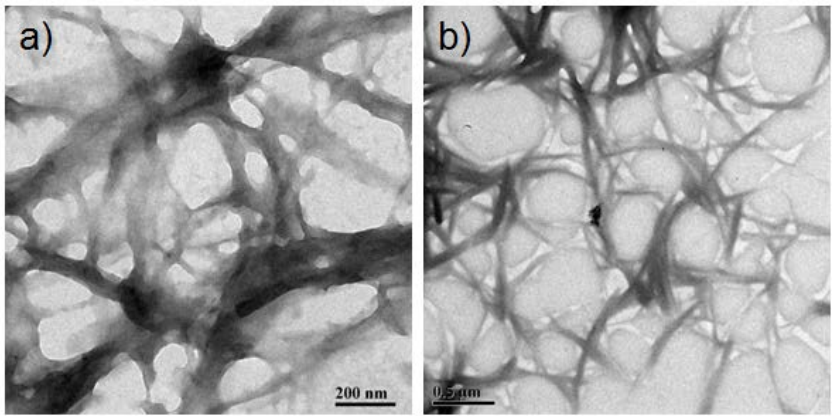

Appendix 2.7: TEM images of metallogels, formed upon combining Cu^{II} salt and L-PGA ligand; (a) gel **1** [L-PGA+ $Cu(NO_3)_2$]**;** (b) gel **2** [L-PGA+ $CuCl_2$]**.**

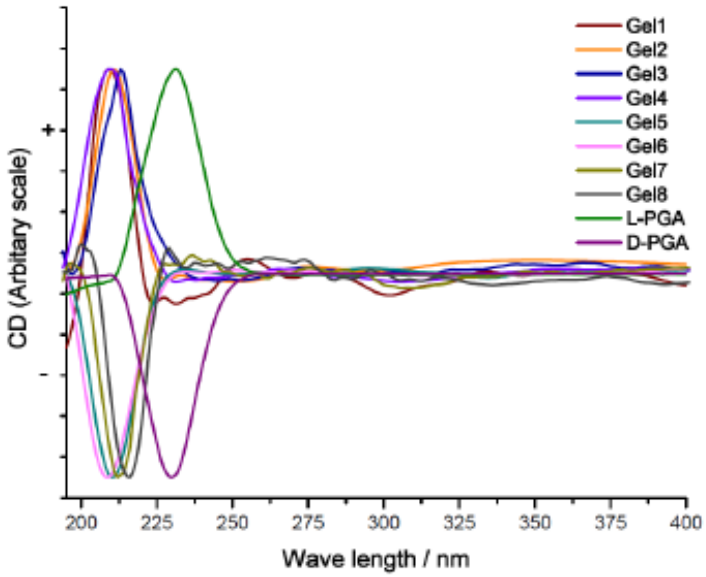

Appendix 2.8: Solid state CD spectra of the gels (Gel **1-8**).

Appendix 2.9: *Crystal data and structure refinement for compound **1**.*

Identification code	**Compound 1**
CCDC No	899203
Empirical formula	C_{54} H_{72} Cu_4 N_{15} O_{24}
Formula weight	1569.43
Temperature	200(2) K
Wavelength	0.71069 Å
Crystal system	Orthorhombic
Space group	*P 2 2_1 2_1*
Unit cell dimensions	*a* = 8.280(5) Å *b* = 15.304(5) Å *c* = 27.239(5) Å
Volume	3452(2) $Å^3$
Z	2
Density (calculated)	1.510 Mg/m^3
Absorption coefficient	1.301 mm^{-1}
F(000)	1618
Crystal size	0.10 x 0.08 x 0.06 mm^3
Theta range for data collection	2.57 to 27.00°.
Index ranges	-10<=h<=9, -17<=k<=19, -34<=l<=30
Reflections collected	15855
Independent reflections	7403 [R(int) = 0.0263]
Completeness to theta = 27.00°	99.3 %
Absorption correction	Semi-empirical from equivalents
Max. and min. transmission	0.9260 and 0.8809
Refinement method	Full-matrix least-squares on F^2
Data / restraints / parameters	7403 / 1 / 439
Goodness-of-fit on F^2	1.107
Final R indices [I>2sigma(I)]	R_1 = 0.0479, wR_2 = 0.1367
R indices (all data)	R_1 = 0.0529, wR_2 = 0.1397
Absolute structure parameter	0.034(17)
Largest diff. peak and hole	0.814 and -0.618 e.$Å^{-3}$

Appendix 2.10: *Crystal data and structure refinement for compound **1a**.*

Identification code	**Compound 1a**
CCDC No	899204
Empirical formula	C_{80} H_{96} Cu_8 N_{16} O_{48}
Formula weight	2558.05
Temperature	200(2) K
Wavelength	0.71073 Å
Crystal system	Monoclinic
Space group	*P2*
Unit cell dimensions	*a* = 24.138(6) Å *b* = 8.351(2) Å *β*= 91.586(8) deg *c* = 26.801(7) Å
Volume	5401(2) $Å^3$
Z	2
Density (calculated)	1.573 Mg/m^3
Absorption coefficient	1.640 mm^{-1}
F(000)	2608
Crystal size	1.10 x 0.80 x 0.60 mm^3
Theta range for data collection	0.76 to 28.66°.
Index ranges	-32<=h<=32, -9<=k<=11, -35<=l<=35
Reflections collected	54409
Independent reflections	23883 [R(int) = 0.1935]
Completeness to theta = 28.66°	97.8 %
Absorption correction	Semi-empirical from equivalents
Max. and min. transmission	0.4394 and 0.2656
Refinement method	Full-matrix least-squares on F^2
Data / restraints / parameters	23883 / 877 / 1369
Goodness-of-fit on F^2	0.732
Final R indices [I>2sigma(I)]	R_1 = 0.1084, wR_2 = 0.2554
R indices (all data)	R_1 = 0.2316, wR_2 = 0.2995
Absolute structure parameter	0.10(3)
Largest diff. peak and hole	1.551 and -0.855 e.$Å^{-3}$

Appendix 2.11: *Crystal data and structure refinement for compound **2**.*

Identification code	**Compound 2**
CCDC No	899205
Empirical formula	$C_{54}\ H_{72}\ Cu_4\ N_{15}\ O_{24}$
Formula weight	1569.43
Temperature	200(2) K
Wavelength	0.71073 Å
Crystal system	Orthorhombic
Space group	*P* 2_1 2_1 2
Unit cell dimensions	*a* = 15.3549(19) Å *b* = 27.269(3) Å *c* = 8.2486(10) Å
Volume	3453.7(7) $Å^3$
Z	2
Density (calculated)	1.509 Mg/m^3
Absorption coefficient	1.301 mm^{-1}
F(000)	1618
Crystal size	0.10 x 0.09 x 0.08 mm^3
Theta range for data collection	2.47 to 29.19°.
Index ranges	-11<=h<=21, -36<=k<=37, -11<=l<=6
Reflections collected	20948
Independent reflections	9143 [R(int) = 0.0527]
Completeness to theta = 29.19°	99.6 %
Absorption correction	Semi-empirical from equivalents
Max. and min. transmission	0.9031 and 0.8809
Refinement method	Full-matrix least-squares on F^2
Data / restraints / parameters	9143 / 2 / 439
Goodness-of-fit on F^2	0.539
Final R indices [I>2sigma(I)]	R_1 = 0.0433, wR_2 = 0.1284
R indices (all data)	R_1 = 0.0556, wR_2 = 0.1416
Absolute structure parameter	-0.006(14)
Largest diff. peak and hole	0.833 and -0.720 $e.Å^{-3}$

3.6. Appendix:

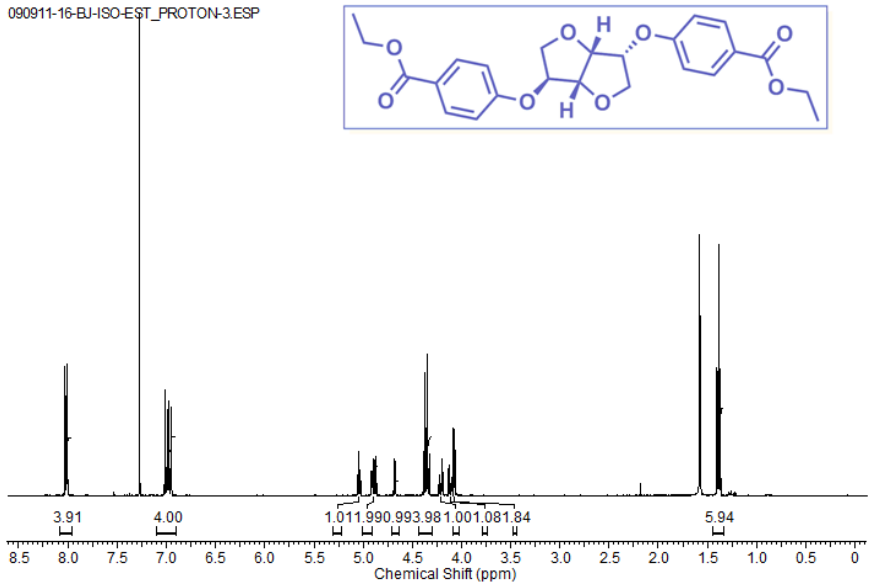

Appendix 3.1.1: *^{1}H NMR spectrum of Ligand L'.*

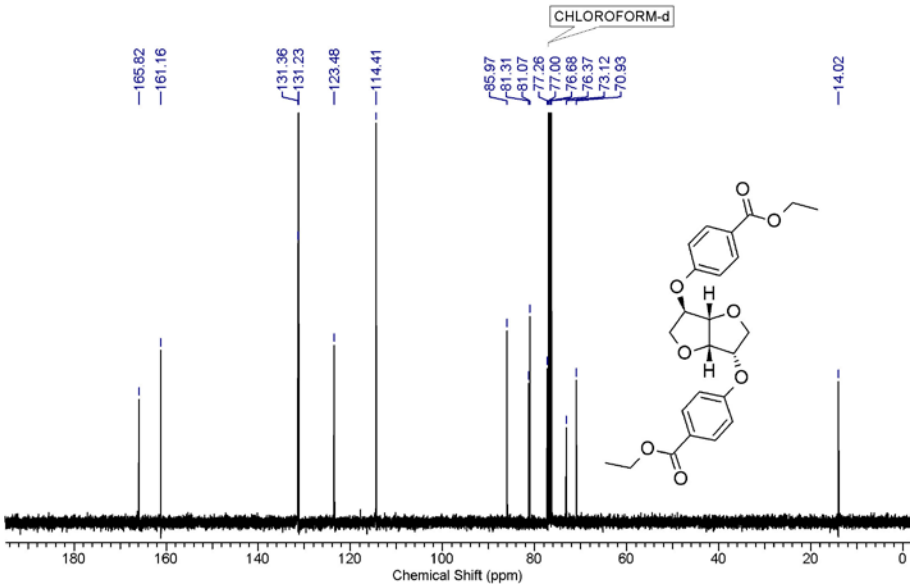

Appendix 3.1.2.: *^{13}C NMR spectrum of Ligand L'.*

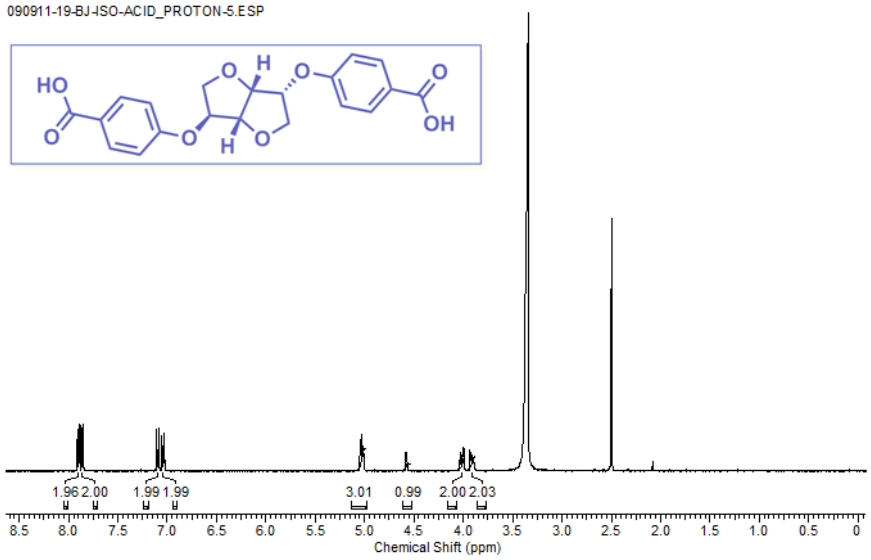

Appendix 3.2.1: *^{1}H NMR spectrum of Ligand LH_2.*

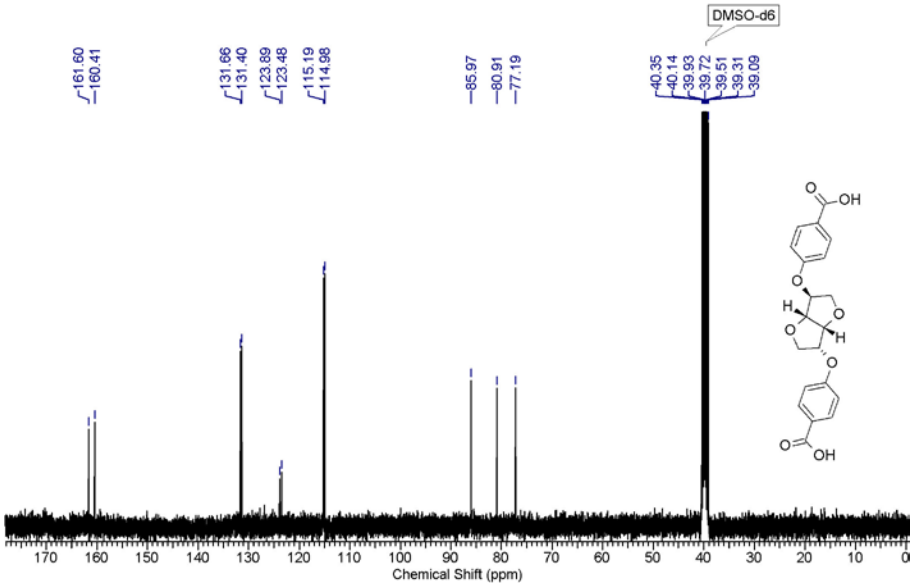

Appendix 3.2.2.: *^{13}C NMR spectrum of Ligand LH_2.*

Appendix 3.3: *Crystal data and structure refinement for compound **1**.*

Identification code	**Compound1**
CCDC	848075
Empirical formula	C_{20} H_{24} Cd O_{12}
Formula weight	568.79
Temperature	200(2) K
Wavelength	0.71073 Å
Crystal system	Orthorhombic
Space group	*C 2 2 2*$_1$
Unit cell dimensions	*a* = 7.3160(5) Å *b* = 26.4953(19) Å *c* = 24.2927(17) Å
Volume	4708.9(6) Å^3
Z	8
Density (calculated)	1.605 Mg/m^3
Absorption coefficient	0.988 mm^{-1}
F(000)	2304
Crystal size	0.15 x 0.14 x 0.10 mm^3
Theta range for data collection	1.75 to 28.69 deg
Index ranges	-7<=h<=9, -35<=k<=33, -25<=l<=32
Reflections collected	13528
Independent reflections	5550 [R(int) = 0.0658]
Completeness to theta = 28.69°	99.9 %
Absorption correction	Semi-empirical from equivalents
Max. and min. transmission	0.9077 and 0.8660
Refinement method	Full-matrix least-squares on F^2
Data / restraints / parameters	5550 / 0 / 294
Goodness-of-fit on F^2	1.125
Final R indices [I>2sigma (I)]	R_1 = 0.0659, wR_2 = 0.1695
R indices (all data)	R_1 = 0.0693, wR_2 = 0.1715
Absolute structure parameter	0.00(6)

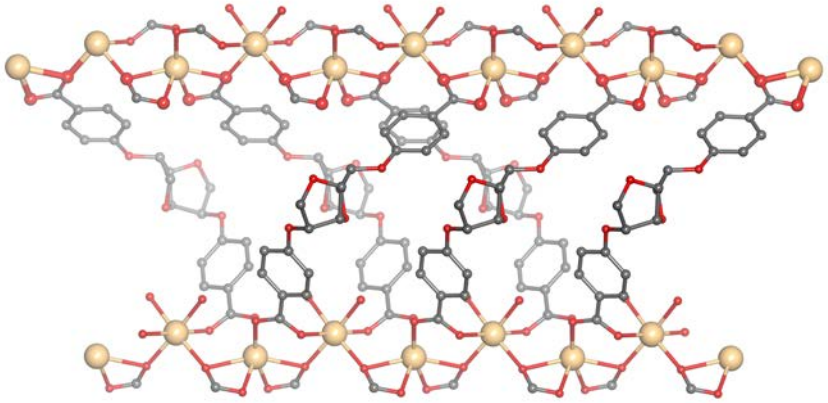

Appendix 3.4: *Metal-carboxylate chain showing coordination environment around the metal centres.*

4.6. Appendix:

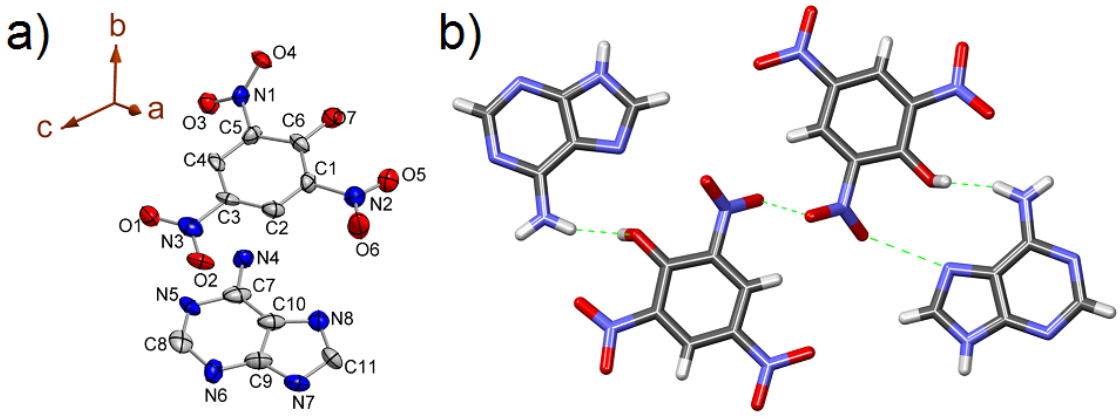

Appendix 4.1: *(a)* Ortep diagram of [(Adenine)(TNP)]· CH_3OH co-crystal structure in 50% probability. (Hydrogens are removed for clarity); (b) Hydrogen bonding interaction between amine and -OH in the co-crystal.

Appendix 4.2: *Crystal data and structure refinement for compound **1**.*

Identification code	**Co-crystal 1**	
CCDC	1021375	
Empirical formula	$C_{12}\ H_{12}\ N_8\ O_8$	
Formula weight	396.30	
Wavelength	0.71073 Å	
Crystal system	Triclinic	
Space group	P_{-1}	
Unit cell dimensions	a = 9.96(3) Å	α = 117.80(5)°.
	b = 10.03(3) Å	β = 115.33(5)°.
	c = 10.44(3) Å	γ = 91.12(5)°.
Volume	802(5) $Å^3$	
Z	2	
Absorption coefficient	0.140 mm^{-1}	
F(000)	408	
Theta range for data collection	2.35 to 27.01°.	
Index ranges	-12<=h<=11, -12<=k<=12, -13<=l<=11	
Independent reflections	3293 [R(int) = 0.2627]	
Completeness to theta = 27.01°	93.8 %	
Data / restraints / parameters	3293 / 0 / 257	
Goodness-of-fit on F^2	0.881	
Final R indices [I>2sigma(I)]	R_1 = 0.0888, wR_2 = 0.1610	
R indices (all data)	R_1 = 0.3227, wR_2 = 0.2445	

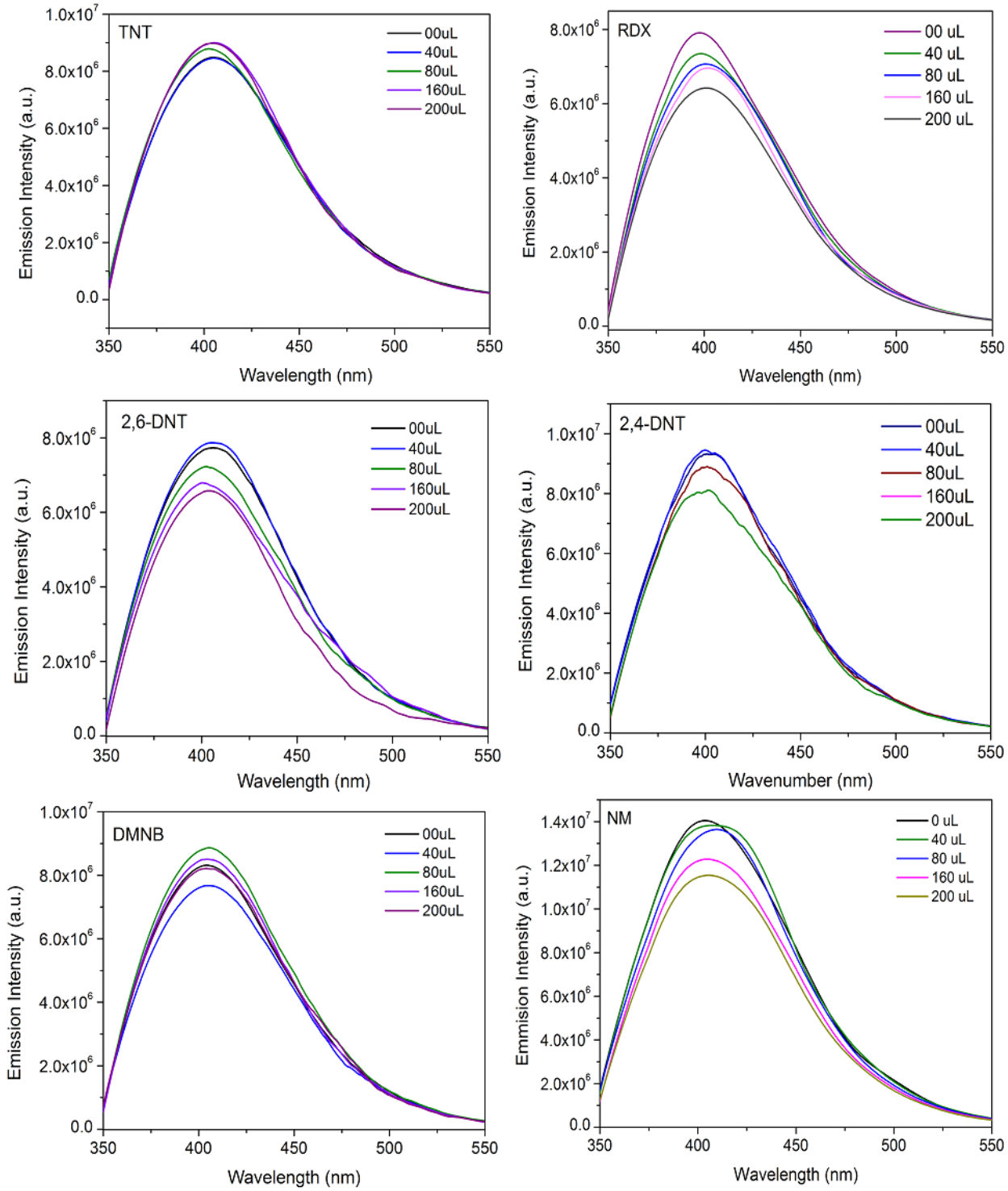

Appendix 4.3: Emission spectra of MOF (**1D**) dispersed in water, upon incremental addition of various nitro analytes solution (1mM) in water.

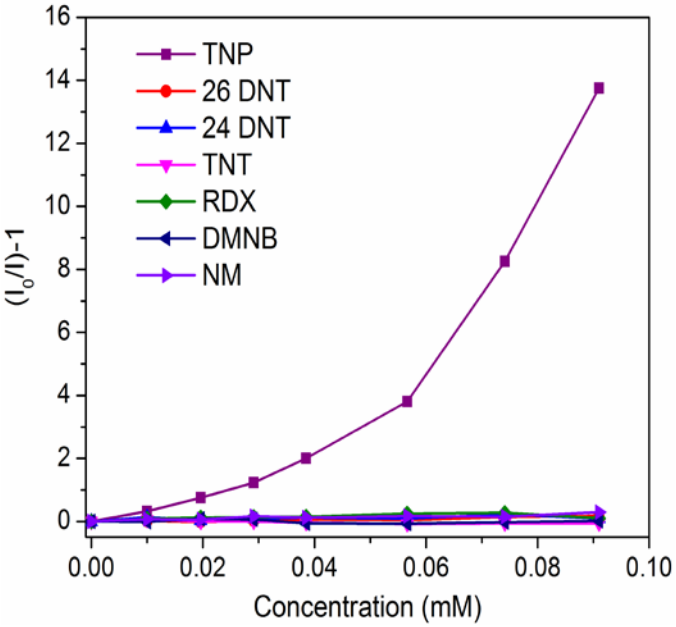

Appendix 4.4: Stern-Volmer (SV) plots for various nitro analytes in water.

Appendix 4.5: Table for HOMO and LUMO energies calculated for explosive analytes at B3LYP/6- 31G* level of theory.

Analytes	HOMO (eV)	LUMO (eV)	Band gap (eV)
NM	-8.0246	-1.8929	6.1317
DMNB	-7.7364	-1.7443	5.9921
RDX	-8.2452	-2.5634	5.6818
2,4-DNT	-8.0139	-2.9607	5.0532
2,6-DNT	-7.8588	-3.0124	4.8464
TNT	-8.3350	-3.5729	4.7621
TNP	-8.2915	-3.8750	4.4165

Appendix 4.6: Table for approximate sizes of explosive analytes.

No.	Analytes	Approximate size (D X W X L, Å)
1	NM	3.4 X 4.2 X 4.8
2	DMNB	7.1 X 7.3 X 7.7
3	RDX	5.8 X 6.3 X 8.8
4	2,4-DNT	5.6 X 7.7 X 10.1
5	2,6-DNT	5.6 X 7.7 X 9.5
6	TNT	5.6 X 7.7 X 10.2
7	TNP	5.0 X 6.2 X 7.1

5.6. Appendix:

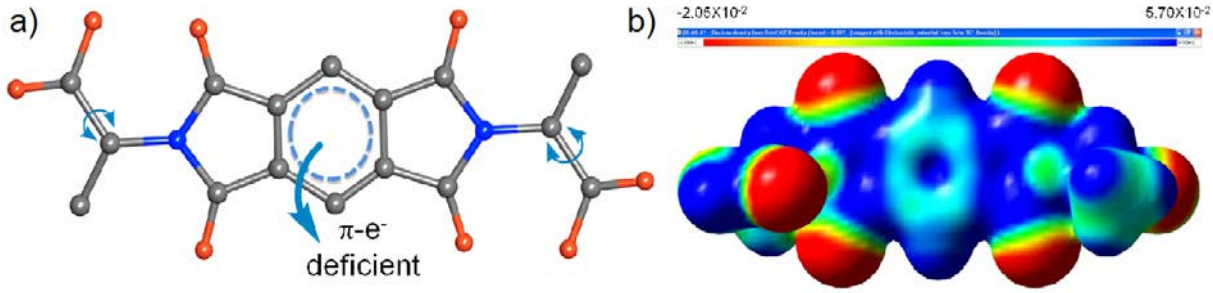

Appendix 5.1: *a) Structure of the flexible π electron-deficient ligand; b) Electrostatic potential surface for the ligand representative of the electron density map.*

Appendix 5.2: *Crystal data and structure refinement for compound **1**.*

Identification code	**Compound1**
CCDC	964583
Empirical formula	$C_{38}H_{30}N_6O_{18}Zn_2$
Formula weight	989.42
Temperature	200(2) K
Wavelength	0.71073 Å
Crystal system	Monoclinic
Space group	$P2_1$
Unit cell dimensions	a = 8.6937(7) Å b = 20.6607(18) Å β= 101.9 (2)°. c = 12.0563(11) Å
Volume	2119.0(3) $Å^3$
Z	2
Absorption coefficient	1.216 mm^{-1}
F(000)	1008
Theta range for data collection	1.73 to 27.88°.
Index ranges	-11<=h<=8, -27<=k<=27, -15<=l<=15
Reflections collected	21380
Independent reflections	9500 [R(int) = 0.0433]
Completeness to theta = 27.88°	100.0 %
Refinement method	Full-matrix least-squares on F^2
Data / restraints / parameters	9500 / 140 / 571
Goodness-of-fit on F^2	1.026
Final R indices [I>2sigma(I)]	R_1 = 0.0922, wR_2 = 0.2519
R indices (all data)	R_1 = 0.1313, wR_2 = 0.2875

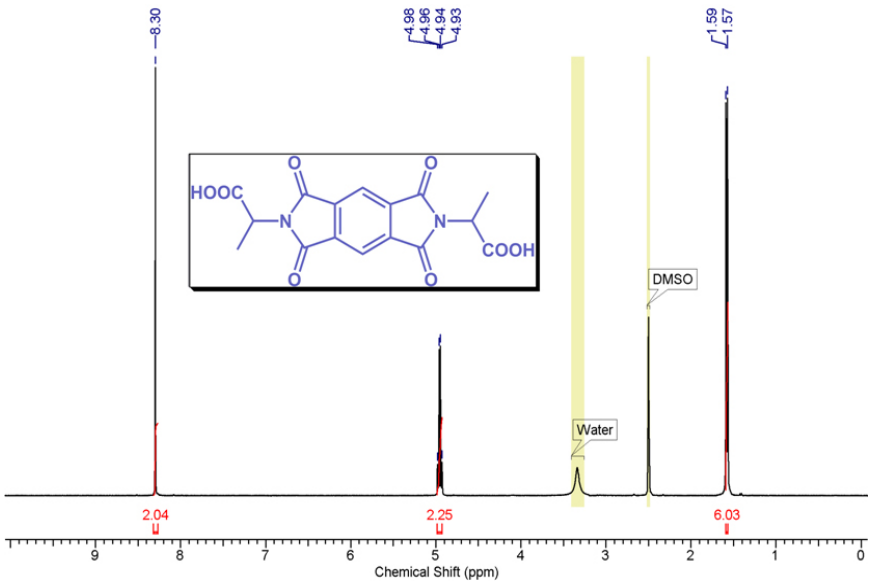

Appendix 5.3: ^{1}H NMR spectrum of Ligand LH_2.

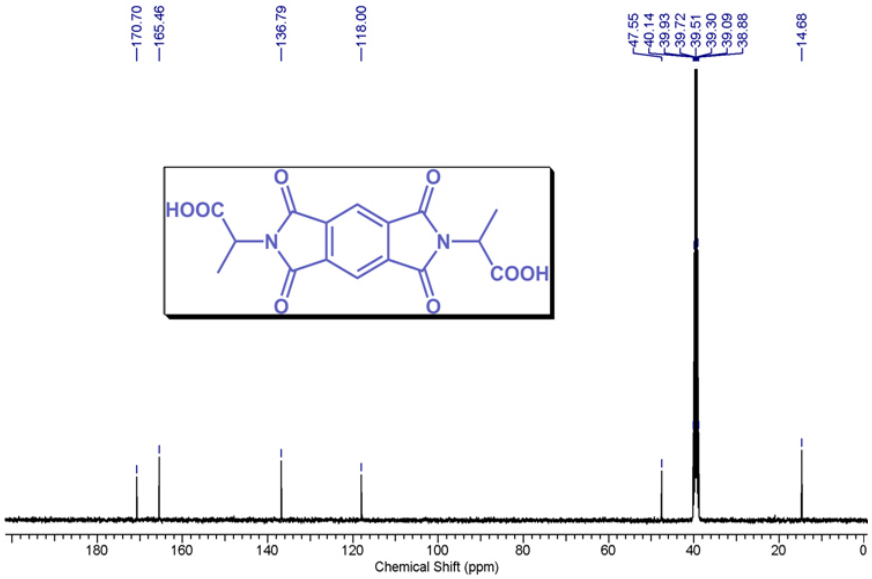

Appendix 5.4: ^{13}C NMR spectrum of Ligand LH_2.

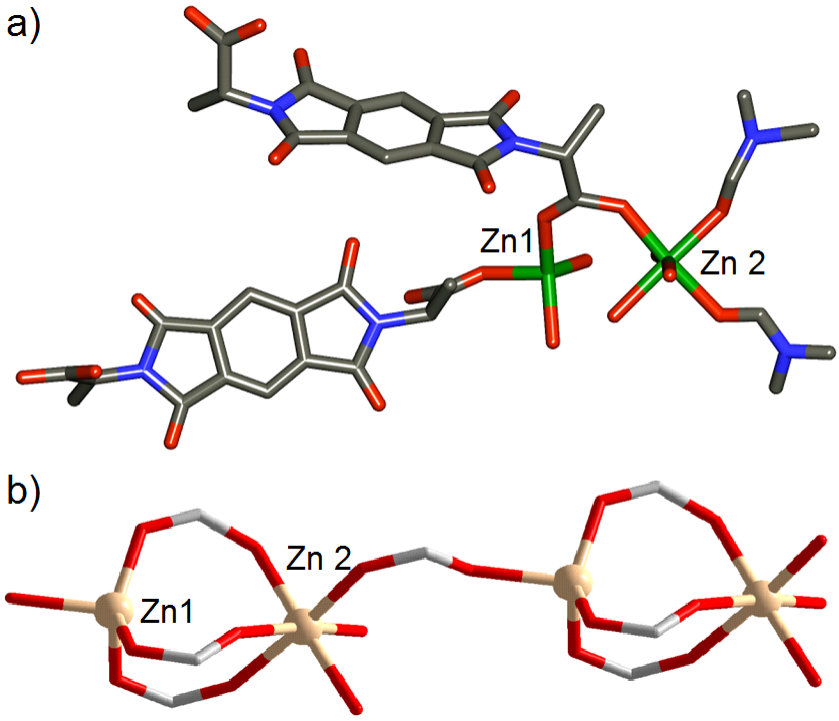

Appendix 5.5: *(a) Tetrahedral and octahedral environment of two types zinc in $[Zn_2L_2(DMF)_2]$* ***(1);*** *(b) metal carboxylate chain.*

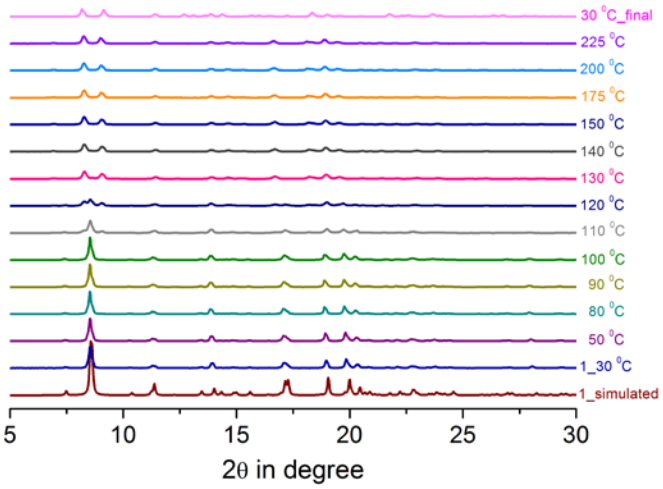

Appendix 5.6: *Variable temperature powder X-ray diffraction (PXRD) patterns of compound* ***1****.*

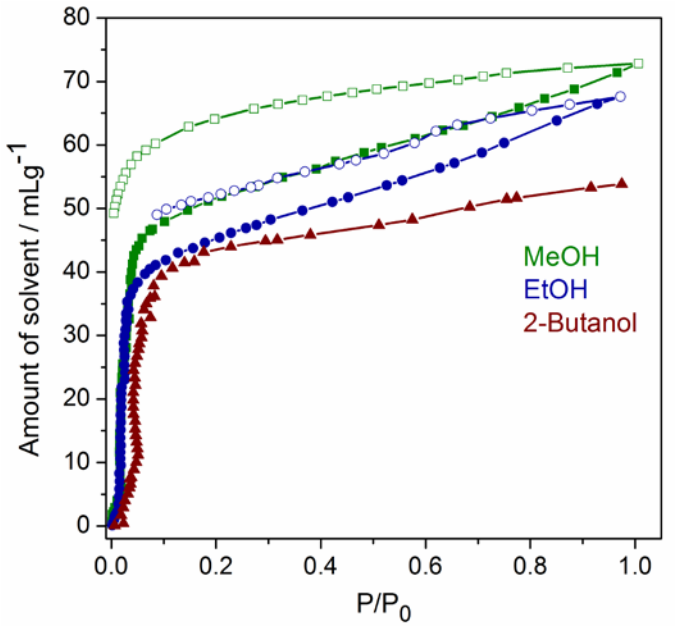

Appendix 5.7: *Solvent sorption isotherms of compound **1D** at 298K (Colour code: methanol: olive; ethanol: navy blue; 2-propanol: wine). Filled shapes = adsorption, unfilled shapes = desorption.*

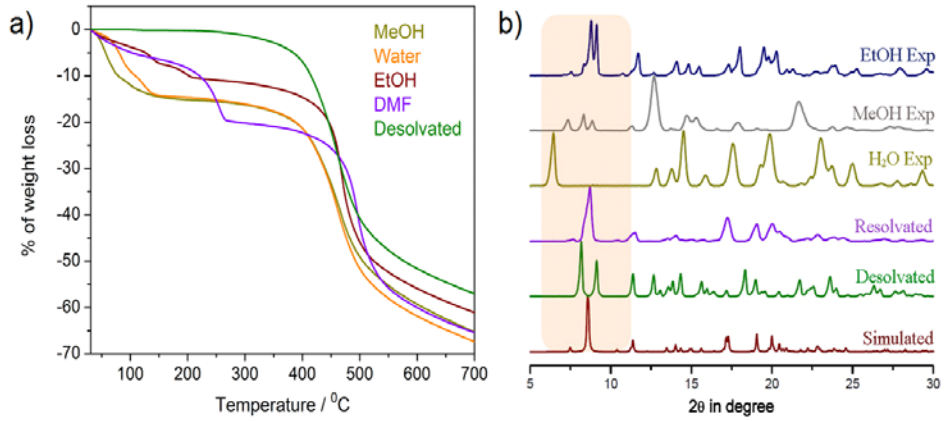

Appendix 5.8: *(a) TGA analysis of desolvated (**1D**) and exposed to vapour of some solvent (**1D** ⊃solvent); (b) PXRD pattern of simulated of **1**, desolvated (**1D**) and exposed to vapour of some solvent (**1D** ⊃solvent).*

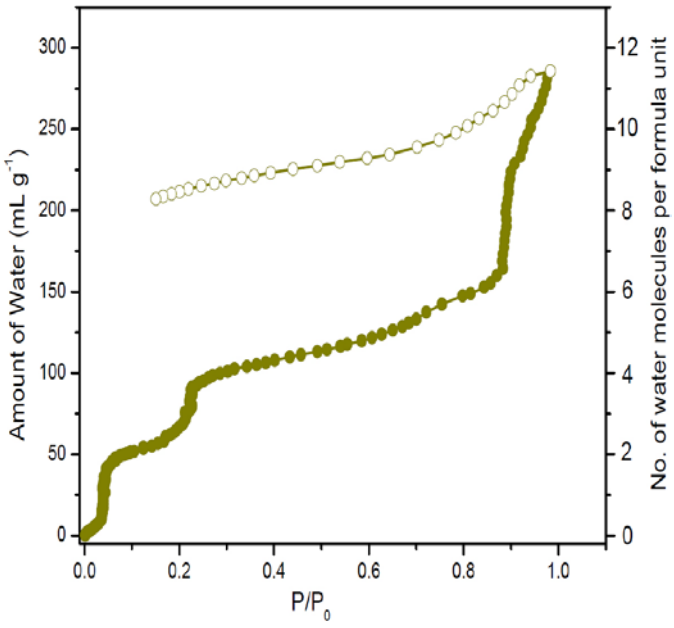

Appendix 5.9: *Water sorption isotherm of compound **1D** at 298 K.*

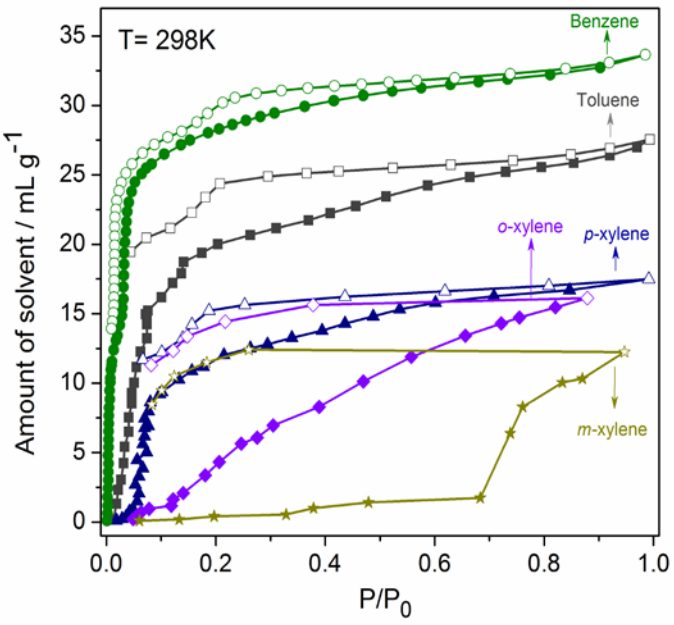

Appendix 5.10: *Sorption isotherms of π-electron rich aromatic guest within compound **1D** at 298K (Colour code: Benzene: olive; toluene: grey; p-Xylene: royal blue; o-Xylene, violet; m-Xylene, dark yellow).*

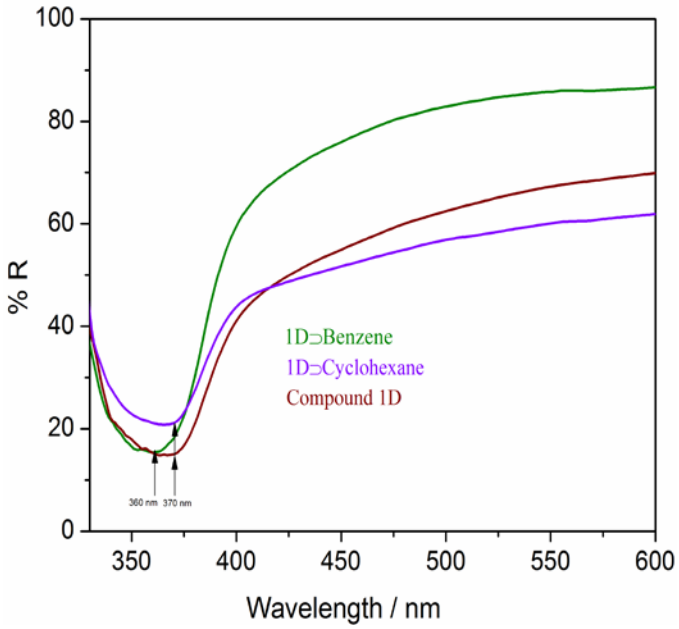

Appendix 5.11: *Solid state UV-vis spectra of compound **1D**, and solvent vapor exposed to **1D** (**1D** ⊃Benzene, **1D** ⊃Cyclohexane) at RT.*

Appendix 5.12: Table for *Solvents and their respective kinetic diameters.*

Solvent	Kinetic diameter (Å)
Benzene	5.957
Cyclohexane	6.084
Toluene	6.011
p-xylene	5.982
m-xylene	6.973
o-xylene	6.973
Dioxane*	6.114
Cyclopentane*	4.892
THF	4.874

* Kinetic diameter of dioxane and cyclopentane were estimated from molecules of similar size and chemical characteristics.

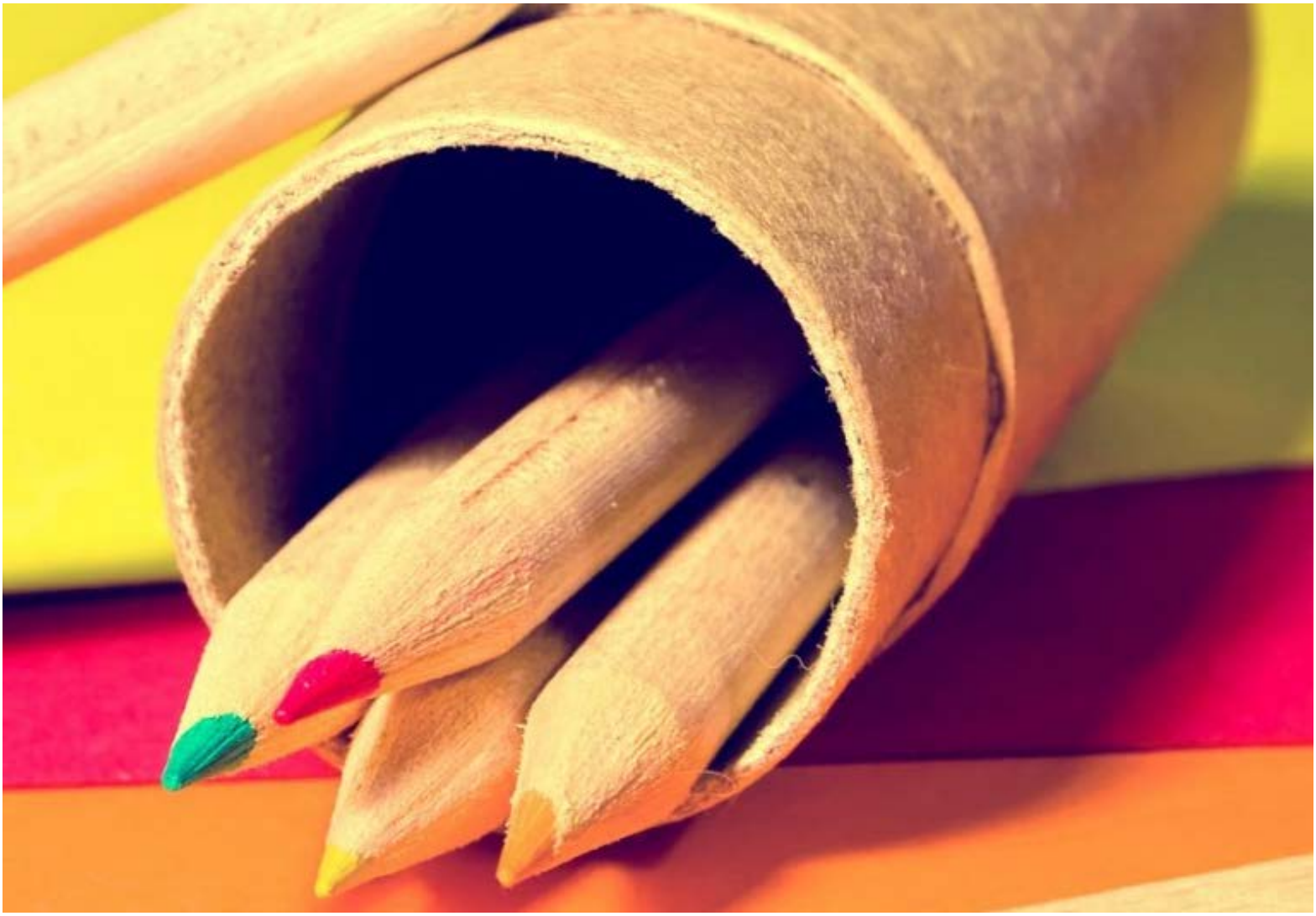

"A man may imagine things that are false, but he can only understand things that are true, for if the things be false, the apprehension of them is not understanding"

..... Sir Issac Newton

THE END